

**OPTICAL PROPERTIES PREDICTION OF NEGATIVE
DISPERSION-COMPENSATING PHOTONIC CRYSTAL
FIBER USING MACHINE LEARNING**

by

Md. Ibrahim Khalil

0419312007

MASTER OF SCIENCE
IN
INFORMATION AND COMMUNICATION TECHNOLOGY



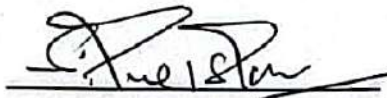
Institute of Information and Communication Technology
Bangladesh University of Engineering and Technology

Dhaka, Bangladesh

May, 2023

The thesis titled "Optical Properties Prediction of Negative Dispersion-Compensating Photonic Crystal Fiber Using Machine Learning" submitted by Md. Ibrahim Khalil, Roll No.: 0419312007, Session: April 2019, has been accepted as satisfactory in partial fulfillment of the requirement for the degree of Master of Science in Information and Communication Technology on 15th May, 2023.

BOARD OF EXAMINERS



Dr. Md. Saiful Islam
Professor
IICT, BUET, Dhaka

Chairman
(Supervisor)



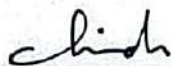
Dr. Md. Rubaiyat Hossain Mondal
Professor and Director
IICT, BUET, Dhaka

Member
(Ex- officio)



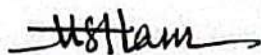
Dr. Hossen Asiful Mustafa
Associate Professor
IICT, BUET, Dhaka

Member



Dr. Md. Jarez Miah
Assistant professor
IICT, BUET, Dhaka

Member



Dr. Md. Shah Alam
Professor
EEE, BUET, Dhaka

Member
(External)

Candidate's Declaration

This is to certify that the work presented in this thesis entitled, "Optical Properties Prediction of Negative Dispersion-Compensating Photonic Crystal Fiber Using Machine Learning", is the outcome of the research carried out by Md. Ibrahim Khalil under the supervision of Dr. Md. Saiful Islam, Professor, Institute of Information and Communication Technology (IICT), Bangladesh University of Engineering and Technology (BUET), Dhaka-1000, Bangladesh.

It is also declared that neither this thesis nor any part thereof has been submitted anywhere else for the award of any degree, diploma, or other qualifications.

Signature of the Candidate

Ibrahim. 18.05.23

Md. Ibrahim Khalil

0419312007

Dedication

To my loving and inspiring wife,

Rokeya Khatun,

whose unwavering support and encouragement
carried me through the journey of my M.Sc. degree.

This achievement is as much yours as it is mine.

And to our beautiful child, **Ibnat Mayamin**

the brightest star in our lives,

born during this memorable period of our lives.

You both are my greatest motivation and joy.

Contents

Certification	ii
Candidate’s Declaration	iii
Dedication	iv
List of Figures	viii
List of Tables	xii
Acknowledgement	xiii
Abstract	xiv
1 Introduction	1
1.1 Problem Statement	2
1.2 Objectives of the Thesis	3
1.3 Thesis Outline	3
2 Literature Review	5
2.1 Chapter Summary	9
3 Basics of PCF and Machine Learning	10
3.1 Basic Principle of PCF	10
3.1.1 Origin	11
3.1.2 Structure	11
3.1.3 Modes of Operation	12
3.1.4 Guiding Light through Photonic Crystals	13
3.1.5 Solid Core Photonic Crystal Fiber	13
3.1.6 Hollow Core Photonic Crystal Fiber	14
3.1.7 Design Parameters	14
3.1.8 Application of PCF	18
3.2 Photonic Crystal Fiber Optical Attributes	18

3.2.1	Refractive Index	19
3.2.2	Confinement Loss	19
3.2.3	Chromatic Dispersion	20
3.2.4	Non-linearity	21
3.2.5	Effective Mode Area	23
3.2.6	V-Parameter	23
3.3	Full Vector Finite Element Method	24
3.3.1	Boundary and Interface Conditions	25
3.4	Machine Learning Algorithm	27
3.4.1	Linear Regression	28
3.4.2	K-Nearest Neighbors (KNN)	29
3.4.3	Decision Tree	30
3.4.4	Random Forest	30
3.4.5	Artificial Neural Network (ANN)	31
3.5	Chapter Summary	33
4	Proposed System	34
4.1	Modeling flow chart using COMSOL Multiphysics	34
4.2	New Model Creation	36
4.2.1	Model Wizard-Assisted New Model Creation	36
4.2.2	Utilizing Blank Model for Crafting a Novel Model	38
4.3	Attributes, Variables, and Extent	38
4.3.1	Global Definition	38
4.3.2	Geometry Unit	38
4.3.3	Materials Selection and Considerations	39
4.3.4	Selecting Boundaries and Addressing Geometric Factors in Design	40
4.3.5	Design Specifications for PCF Lattice Structure	41
4.4	Design of Proposed PCF Model	43
4.4.1	Mesh Analysis	45
4.4.2	Electric Field Distribution	46
4.5	Utilizing Machine Learning to Model PCF	49
4.5.1	Dataset Generation	49
4.5.2	Pre-processing of Dataset	50
4.5.3	Modelling of Machine Learning Algorithm	52
4.6	Chapter Summary	61
5	Results and Discussions	62

5.1	Analysing PCF Characteristics	62
5.1.1	Comparative Analysis of Effective Refractive Index	63
5.1.2	Comparative Analysis of Effective Area	64
5.1.3	Comparative Analysis of Confinement Loss	64
5.1.4	Comparative Analysis of Dispersion	65
5.1.5	Effect of core size on Dispersion	66
5.1.6	Impact of Cladding Air Hole Dimensions on Dispersion	67
5.2	Prediction of PCF Optical Properties using Machine learning	68
5.2.1	Prediction of Effective Refractive Index	69
5.2.2	Prediction of Effective Mode Area	70
5.2.3	Prediction of Dispersion	72
5.2.4	Prediction of Confinement Loss	73
5.2.5	Prediction of V-Parameter	74
5.3	Prediction of PCF Optical Properties using Artificial Neural Network	76
5.3.1	Layer Tuning of ANN	76
5.3.2	Neuron Tuning of ANN	80
5.3.3	Epoch Tuning of ANN	82
5.3.4	Best Artificial Neural Network Model performance	86
5.3.5	Coputational Time	90
5.4	Chapter Summary	92
6	Conclusions	93
6.1	Conclusions	93
6.2	Future Works	94
	References	95

List of Figures

3.1	Structure of basic PCF	12
3.2	Illustration of (a) solid-core PCF, (b) hollow-core PCF, and (c) typical single-mode fiber.	14
3.3	(a) Light input of fiber (b) Light output at a distance L_1 (c) Light output at a distance $L_2 > L_1$	21
3.4	Surrounding PML region of the waveguide architecture	26
3.5	Grading of PML conductivity.	27
3.6	Linear regression	28
3.7	K-Nearest Neighbor(KNN).	29
3.8	Decision Tree Classification.	30
3.9	Random Forest Tree Classification.	31
3.10	General Artificial Neural network representation	32
4.1	Flowchart for COMSOL MultiPhysics Modeling Process	35
4.2	Choosing a Space Dimension.	36
4.3	Options in physics selection.	37
4.4	Options in study selection.	37
4.5	Constructing a novel model from the basic framework.	38
4.6	Select the Geometry.	39
4.7	Material selection.	39
4.8	Mesh analysis.	40
4.9	Perform the study.	41
4.10	Cross-sectional perspective of proposed PCF for dispersion mitigation.	44
4.11	Mesh analysis of proposed structure	46
4.12	Electric field distribution of proposed structure	47
4.13	Fundamental field distribution in X-axis	48
4.14	Fundamental field distribution in Y-axis	48
4.15	Mode profile of proposed PCF	49
4.16	Analyzing the relationships between attributes using a heatmap of the correlation matrix.	51

4.17	Scatterplot matrix of features and target (effective mode index & effective area) for visualizing the structured relationship.	53
4.18	Scatterplot matrix of features and target (dispersion & confinement loss) for visualizing the structured relationship.	54
4.19	The flow diagram of an application of regression model	55
4.20	Pseudocode of the steps of the given algorithm	56
4.21	Structure of Proposed Artificial Neural Network	58
4.22	The flow chart of ANN implementation	59
5.1	Fluctuation of the effective refractive index for varying operating wavelengths for alternation of Λ from optimum($\Lambda=0.8415 \mu\text{m}$) to \pm (1 to 2%)	63
5.2	Fluctuation of the effective area for varying operating wavelengths for alternation of Λ from optimum($\Lambda=0.8415 \mu\text{m}$) to \pm (1 to 2%)	64
5.3	Fluctuation of the confinement loss for varying operating wavelengths for alternation of Λ from optimum($\Lambda=0.8415 \mu\text{m}$) to \pm (1 to 2%).	65
5.4	Fluctuation of the dispersion for varying operating wavelengths for alternation of Λ from \pm (1 to 2%).	66
5.5	Fluctuation of the dispersion for varying operating wavelengths for core diameter $d_0=0.11 \mu\text{m}$, $0.12 \mu\text{m}$ and $0.13 \mu\text{m}$	67
5.6	Fluctuation of the dispersion for varying operating wavelengths for alternation of d_1 in range of $\pm 5\%$ from optimum ($d_1=0.6 \mu\text{m}$).	68
5.7	Variation of Dispersion with different operating wavelength for alternation of d in the range of $\pm 5\%$ optimum ($d=0.8 \mu\text{m}$).	68
5.8	The scatter plot of predicted n_{eff} (y-axis) Vs actual n_{eff} (x-axis) comparing against perfect linear relationship ($y=x$).	69
5.9	Evaluating the correspondence between the simulated n_{eff} and the predicted n_{eff} across multiple algorithms with an unexplored configuration.	70
5.10	The scatter plot of predicted a_{eff} (y-axis) Vs actual a_{eff} (x-axis) comparing against perfect linear relationship ($y=x$).	71
5.11	Evaluating the correspondence between the simulated a_{eff} and the predicted a_{eff} across multiple algorithms with an unexplored configuration.	71
5.12	The scatter plot of predicted dispersion (D) (y-axis) Vs. Solid dispersion (D) (x-axis) comparing against perfect linear relationship ($y=x$).	72
5.13	Evaluating the correspondence between the simulated dispersion (D) and the predicted dispersion (D) across multiple algorithms with a new configuration.	73

5.15	Evaluating the correspondence between the simulated and predicted confinement loss across multiple algorithms with a new configuration.	74
5.14	The scatter plot of predicted confinement loss (y-axis) Vs. Actual confinement loss (x-axis) compared against perfect linear relationship (y=x).	74
5.16	The scatter plot of predicted v_{eff} Vs actual v_{eff} comparing against perfect linear relationship (y=x).	75
5.17	Evaluating the correspondence between the simulated and predicted v_{eff} across multiple algorithms with an unexplored configuration.	75
5.18	The scatter plot comparing predicted n_{eff} (y-axis) and actual n_{eff} (x-axis) for different hidden layers in the ANN against perfect linear relationship (y=x).	77
5.19	The scatter plot comparing predicted a_{eff} (y-axis) and actual a_{eff} (x-axis) for different hidden layers in the ANN against perfect linear relationship (y=x).	78
5.20	The scatter plot comparing predicted dispersion (D) (y-axis) and actual dispersion (D) (x-axis) for different hidden layers in the ANN against perfect linear relationship (y=x).	78
5.21	The scatter plot comparing predicted confinement loss(α_c) (y-axis) and actual confinement loss(α_c) (x-axis) for different hidden layers in the ANN against perfect linear relationship (y=x).	79
5.22	The scatter plot comparing predicted v_{eff} (y-axis) and actual v_{eff} (x-axis) for different hidden layers in the ANN against perfect linear relationship (y=x).	80
5.23	R-squared error for different neuron numbers for all optical properties of PCF.	81
5.24	The scatter plot comparing predicted n_{eff} (y-axis) and actual n_{eff} (x-axis) for different epochs in the ANN against perfect linear relationship (y=x).	82
5.25	The scatter plot comparing predicted a_{eff} (y-axis) and actual a_{eff} (x-axis) for different epochs in the ANN against perfect linear relationship (y=x).	83
5.26	The scatter plot comparing predicted dispersion (D) (y-axis) and actual dispersion (D) (x-axis) for different epochs in the ANN against perfect linear relationship (y=x).	84
5.27	The scatter plot comparing predicted confinement loss(α_c) (y-axis) and actual confinement loss(α_c) (x-axis) for different epochs in the ANN against perfect linear relationship (y=x).	85
5.28	The scatter plot comparing predicted v_{eff} (y-axis) and actual v_{eff} (x-axis) for different epochs in the ANN against perfect linear relationship (y=x).	85

5.29	Evaluating the correspondence between the simulated n_{eff} and the predicted n_{eff} using best ANN model with an unexplored configuration.	87
5.30	Evaluating the correspondence between the simulated a_{eff} and the predicted a_{eff} using best ANN model with an unexplored configuration.	88
5.31	Evaluating the correspondence between the simulated dispersion (D) and the predicted dispersion (D) using the best ANN model with an unexplored configuration.	89
5.32	Evaluating the correspondence between the simulated confinement loss (α_c) and the predicted confinement loss (α_c) using best ANN model with an unexplored configuration.	90
5.33	Evaluating the correspondence between the simulated v_{eff} and the predicted v_{eff} using best ANN model with an unexplored configuration.	90

List of Tables

4.1	Parameters and values in Comsol MultiPhysics	41
4.2	Properties of airs used in the model	42
4.3	Properties of silica used in the model	42
4.4	Input parameters of machine learning model	50
5.1	Average accuracy in predicting properties with different hidden layers in ANN architecture.	80
5.2	Average Accuracy of Different Neuron Counts	81
5.3	Table of Metrics for Different Epochs	86
5.4	Comparison of computational time among simulations, previous method and proposed method	91

Acknowledgement

I sincerely appreciate my thesis supervisor, Prof. Dr. Md. Saiful Islam, for constant support, guidance, enthusiasm, and motivation throughout my research endeavor. His expertise and wisdom have significantly contributed to the progress of my work and helping me grow as a researcher.

I am also immensely grateful to the members of my thesis committee, Prof. Dr. Rubaiyat Hossain Mondal, Prof. Dr. Md. Shah Alam and Dr. Hossen Asiful Mustafa, for their valuable feedback, suggestions, and constructive criticism, which have significantly contributed to the improvement of my thesis.

Special thanks go to my serving department head, Prof. Dr. Md. Azad Hossain, for their guidance and support in my academic and professional endeavours as a lecturer. His leadership and mentorship have been instrumental in my growth as an educator.

My sincere appreciation goes to my colleagues and friends in the Department of ETE, CUET for their camaraderie, stimulating discussions, and assistance during the research process. Their support and friendship have made my time a truly rewarding experience.

Last but not least, I am eternally grateful to my family, particularly my parents, my in-laws, and my partner, for their unwavering love, understanding, and support throughout my academic journey. Their belief in me has been my source of strength and motivation.

Thank you all for contributing to the completion of this thesis and for making this journey an unforgettable one.

Abstract

Dispersion in optical fiber communication causes signal degradation as light pulses spread out over distance. Dispersion compensation techniques, such as dispersion-compensating fibers, fiber Bragg gratings, and chirped fiber gratings, counteract this effect. Photonic Crystal Fibers (PCFs) offer a promising solution for dispersion compensation by counterbalancing the positive dispersion of standard fibers. PCFs have emerged to be a dynamic and adaptable solution for various applications such as encompassing spectroscopy, bio-sensing, metrology, and long-haul optical communication systems, owing to their remarkable dispersion-compensating characteristics. In this study, a novel and highly efficient Negative Dispersion-Compensating Photonic Crystal Fiber (NDC-PCF) is designed, and machine learning approaches, specifically Random Forest and Artificial Neural Network (ANN) models, are proposed for predicting output properties, including effective refractive index, dispersion, confinement loss, effective area, and V-parameter.

The machine learning models are trained and tested on input parameters within a wavelength range of 1.18–1.75 μm , pitch from 0.75–0.9 μm , core diameter, and air holes in the cladding region. Settling on a pitch value of 0.8415 μm achieving of a minimal dispersion of -1582.21 ps/(nm-km), critical for efficient optical fiber communication. Compared to conventional numerical simulations such as COMSOL Multiphysics and ANN, the proposed Random Forest model demonstrates significantly reduced computational resources and time requirements, with training in milliseconds and testing in less than one millisecond. The model achieves an impressive average accuracy of around 98%. On the other hand, the best ANN model is obtained by fine-tuning hyperparameters, such as the count of hidden layers, nodes, and training iterations, and attains an average accuracy of approximately 99.99% for all parameters, with training taking several seconds and prediction in milliseconds.

With its negative characteristics, the proposed NDC-PCF exhibits great potential for real-world applications in high-speed optical communication networks. The utilisation of machine learning approaches offers an efficient alternative to conventional numerical simulations for predicting the optical properties of NDC-PCFs, enabling faster design optimisation and cost reductions.

Chapter 1

Introduction

Within this opening chapter, the focus of the thesis study is presented on predicting the optical properties of Negative Dispersion-Compensating Photonic Crystal Fiber(PCF) using different Machine Learning approaches and analyzing the behavior of PCFs. The reason for researching this area of study is explained by summarising the current scenario of research in this field through a review of recent literature, followed by outlining the specific objectives of this study. The structure of the thesis is also outlined at the end of this chapter.

The development of optical communication systems has increased demand for high-performance fiber-optic components, including PCF with specific dispersion properties. PCFs are a unique form of optical fiber with desirable advantages making them an attractive alternative to traditional optical fibers. Negative dispersion-compensating photonic crystal fibers (NDC-PCFs) have gained particular interest due to their ability to mitigate dispersion in optical fiber transmission systems. However, the design and optimization of NDC-PCFs are complex, requiring a comprehensive understanding of the correlation between the fiber architecture and its optical features. The first part of the thesis will cover the theory of dispersion compensation and the design of DC-PCFs. This includes a review of existing DC-PCFs and their dispersion compensation properties. It involves experimental characterization of DC-PCFs, including measurements of their dispersion properties and their performance in optical communication systems. Communication systems and challenges must be overcome to realize their potential fully. The latter portion of this thesis emphasizes the application of machine learning methodologies for predicting the optical characteristics of NDC-PCFs. The aim is to create a model capable of accurately predicting the dispersion attributes of NDC-PCFs based on their structural parameters. The model will be trained using a large dataset of NDC-PCFs and will be validated using experimental data. The results of this thesis can

potentially impact the design and optimization of NDC-PCFs significantly. By providing a speedy and precise means of predicting the optical features of NDC-PCFs, this research will enable the rapid optimization of fiber structures for specific applications, leading to improved performance and reduced costs. This thesis represents a significant advancement in the field of NDC-PCFs and application of machine learning in PCF.

1.1 Problem Statement

Photonic crystal fibers (PCFs) have captured substantial prominence in optical communication due to their unique properties, such as high nonlinearity, dispersion engineering, and polarization control. PCFs can potentially improve the performance of optical communication systems by providing additional degrees of freedom for designing the fiber structure and modifying its optical properties. Such fibers are suitable for numerous purposes in communication, such as dispersion compensation, broadband light sources, and high-power fiber lasers. Therefore, studying PCFs in the context of optical communication is vital for developing new technologies and improving existing systems. These PCF characteristics demonstrate exceptional potential and enhance applications within the fiber-optic communication system [1].

Recently, micro-structured PCFs have caught the attention of scientists, researchers, and technology experts. This is due to their exceptional optical properties, which cannot be achieved using traditional optical fibers. PCF gives additional flexibility in designing the guiding characteristics such as effective index, confinement loss, propagation constant, V-parameter, dispersion, and effective mode area can be adjusted by tailoring the size, number, and arrangement of the circular air cavities [2]. Additionally, background material regulates these unique dimensions. In general, efficient modeling, analysis, and simulation of PCF structures rely on numerical processes, including the finite difference method [3] and the full Vector finite element method (FEM) [4]. One of the fundamental constraints on optical communication systems is chromatic dispersion. The bandwidth and broadening of light pulses during their journey through the optical channel are significantly impacted by dispersion. A method should be in place to reduce the positive dispersion impact in a communications system. Several strategies have been used to provide dispersion compensation, such as higher-order mode dispersion compensating multi-mode fibers [5] [6] chirped fiber Bragg gratings [7]. Another method employs dispersion mitigating fibers with a high negative dispersion [8]. A novel approach to dispersion compensation offered with substantial negative dispersion can be obtained by tailoring the geometric structure. This designing and analyzing process demands

substantial computing resources, power, and time. The quantity of input design factors is to be adjusted for optimization to determine how many iterative studies are necessary. The optimization design also requires several simulations, human interaction, computer resources, and time. However, predicting the optical properties is more appropriate per the requirements of specific applications like dispersion compensation.

1.2 Objectives of the Thesis

This research focuses on designing a PCF structure with negative dispersion to predict several properties. The primary objectives of this work will be:

- To design novel PCF architecture to obtain high negative dispersion over a wide range of wavelengths to compensate for dispersion in medium or long-haul WDM systems.
- To analyze and determine the photonic crystal fiber's various optical properties (such as dispersion, confinement loss, birefringence, effective mode index, and effective area) for creating a dataset.
- To apply several machine learning approaches for faster optical properties prediction and find the appropriate model by optimization.

The model's precision is validated through the use of a full-vector finite element method (FV-FEM) incorporating Perfectly Matched Layers (PMLs) to enable accurate simulation of Photonic Crystal Fibers (PCFs).

1.3 Thesis Outline

The subsequent sections of the thesis are arranged in the following manner:

Chapter 1 presents a brief of the research, its motivation, and objectives while emphasizing the significance and purpose of the thesis.

Chapter 2 explores dispersion-compensating photonic crystal fibers and their impact on mitigating challenges in long-haul optical communication systems. Furthermore, the review investigates the rising prominence of machine learning and artificial neural networks in this field.

Chapter 3 presents an extensive analysis of PCF with a thorough discussion and machine learning algorithms, including artificial neural networks in the prediction of optical properties of PCF.

Chapter 4 discusses the geometric model of the proposed PCF, employs the Finite Element Method (FEM) to determine fiber's optical properties, and utilizes various machine learning algorithms to predict these characteristics.

Chapter 5 focuses on the results of our research, presenting graphical depictions of the numerical findings obtained, analyzing the propagation properties of PCF, and the implementation of machine learning techniques in this particular setting.

Chapter 6 offers a concise overview of our research and outlines potential avenues for future investigation in the field.

Chapter 2

Literature Review

Before delving into the preceding discussion, providing a literature review on previous relevant research is beneficial. Photonic Crystal Fibers (PCFs) possess unique guiding characteristics closely tied to their cross-sectional air holes' geometric features and are effectively utilized in various applications. Dispersion significantly affects the bandwidth and broadening of optical pulses as they propagate through the channel.

One of the significant areas of application for PCFs is communication. The speed of communication largely depends on waveguides or communication channels. The demand for data is continuously increasing to meet consumer needs. In long-distance speedy optical communication, dispersion in the optical link is a significant challenge that reduces the data transfer rate and leads to pulse widening. It is significant to point out that an optimal optical fiber for the single-mode operation has positive dispersion within the range of about 10-20 ps/nm/km [9] [10]. A method should be in place to reduce the positive dispersion impact on the communications system. Introducing a significant negative dispersion can help compensate for the positive dispersion while lowering insertion loss and operating costs.

PCFs possess unique optical characteristics, including customized dispersion, constant single mode, strong nonlinearity, significant effective mode area, notable birefringence, confinement loss, etc. The physical structure of the PCFs significantly influences the optical characteristics mentioned earlier. Additionally, the material surrounding the PCFs also affects these unique properties. Numerous PCF designs can be designed, including rectangular [11] [12], pentagonal [13], hexagonal [14], octagonal [15], decagonal [13] elliptical [16], circular [17], spiral [18], quasi [15], kagome [14], honeycomb [19], steering [17], bow-tie [20], D-shape [21], sunflower type [22], and more. The PCFs comprise diverse crystal materials such as tellurite [23], fluoride [24], chalcogenide glasses [18], zabra [25], topas [21], zenox, BK7, and numerous others. PCFs have ver-

satellite applications, including but not limited to optical communication [21] [22], bio-sensing [16], WDM multiplexer and de-multiplexer [26], filter [27], laser & fiber amplifier [28], optical switching [29], supercontinuum generation [30], spectroscopy [31], optical coherence tomography [32], high-power technology, etc. A novel approach to dispersion compensation offered with substantial negative dispersion can be obtained by tailoring the geometric structure. Numerous researchers have developed different PCF structures to achieve more excellent negative dispersion. Liu et al. introduce a new dual slot with a rib-like shape demonstrating almost zero dispersion across a broad spectrum of wavelengths. The dispersion of the dual-slot silicon PCF is primarily governed by PCF dispersion due to the adjustment of the mode effective area, and the nonlinear coefficient and effective mode area are thoroughly investigated. By manipulating various waveguide parameters, the fiber achieved a nonlinear coefficient of 1460 m/W, and chromatic dispersion at the same time around ± 205 ps/nm/km could benefit broadband optical signal systems [33]. Tee and colleagues developed a new photonic crystal fiber (PCF) that achieves a flattened negative dispersion across communication's E, S, C, and U wavelength bands. The structure has a flattened negative dispersion of -457.4 ps/(nm-km) [34]. A new PCF-in-PCF design is analyzed numerically, providing a high average and negative dispersion range of -449 ps/nm/km to -462 ps/nm/km for the E+S+C+L+U communication waveband from 1360 nm to 1690 nm [35]. A PCF with an octagonal structure acts as a low-loss dispersion compensator for higher-order modes that can be utilized in lumped or multi-span dispersion compensation. The module loss between connectors is 3.16 dB, which can compensate for -886 ps/nm/km of dispersion, equivalent to compensating for 200 km of NZDSF [34].

PCF with five circular air channels in a ring-shaped hexagonal pattern was reported with a dispersion coefficient around -1200 to -2304 ps/(nm-km) across the 1350 nm to 1600 nm [36]. Another PCF structure was proposed in a rectangular shape with various air hole sizes with a dispersion coefficient that falls within the range of -591.3 to -2454.4 ps/nm/km across 1.55 μm [12]. Habib et al. [37] noted an octagonal PCF that exhibited negative dispersion of -850 ps/(nm-km) in the L band while maintaining a relative dispersion slope closely matching single-mode fiber (SMF) at 1550 nm of 0.0036 nm^{-1} . Additionally, the PCF achieved a birefringence around 2.53×10^{-2} at 1550 nm. The author of the same paper also presented a hexagonal structure in another publication [36]. This structure exhibited a negative -1455 ps/nm/km negative dispersion at a similar wavelength. The proposed models by Saha et al. (2018) consist of five air hole rings arranged in circular and elliptical patterns, which exhibit birefringence of 0.0275 and dispersion of -540.67 ps/nm/km at the 1.55 μm [38]. Biswas et al. introduced a new structure for a square photonic crystal fiber which offers both an

ultra-high negative dispersion around -2357.54 ps/nm/km at a 1550 nm. [36] Hasan and colleagues reported a hybrid PCF with a modified structure with a dispersion of -555.93 ps/nm/km, the nonlinearity of $40.1 \text{ W}^{-1} \text{ km}^{-1}$, and birefringence of 0.0379 at wavelength 1550 nm [39]. In a later publication, Hasan et al. proposed a single mode fiber structure having a flattened profile of -578.50 ps/nm/km [40]. In another study by M. S. Habib and colleagues (2013), an octagonal-shaped PCF was proposed, exhibiting a negative dispersion of -588.00 ps/(nm-km) [41].

So in optical communication, it is crucial to have PCF exhibiting extremely high negative dispersion to prevent pulse boarding and spread, allowing for more efficient long-distance communication. While some PCF models with negative dispersion have been reported, there is still a need to improve these models to achieve ultra-high negative dispersion. Meeting this demand for ultra-high negative dispersion is crucial for achieving optimal dispersion profiles in optical communication. Prediction of the optical properties is more appropriate per the requirements of specific applications like dispersion compensation.

Precise simulation and enhancement of photonic crystal structures typically depend on numerical methods, such as the finite difference method [3], finite element method (FEM) [4], block-iterative frequency-domain method [42], and plane wave expansion method [43] [44]. Nevertheless, these approaches necessitate substantial computational resources when handling complex photonic crystal structures; multiple simulations are necessary to achieve an optimized design. The quantity of input design attributes needing optimization also affects these iterative analyses. In recent years, Machine learning strategies have attracted widespread attention and been applied in different fields, including computer vision, automation, image processing, natural language processing, different classification or regression problems, and more. In photonics, researchers have also begun to explore the potential applications of these techniques. They have used machine learning in a variety of areas, such as multi-mode fibers [45], plasmonics [46], meta-materials [47], bio-sensing [48], meta-surface design [49] [25], networking [50], and optical communications [51]. Kiarashinejad et al. [52] developed a deep learning approach employing the dimensionality reduction approach to comprehending electromagnetic wave-matter interactions in nanostructures. Another study used a geometric deep learning approach to analyze nanophotonics structures [53]. Additionally, in 2018, Dispersion relations [54] were calculated, and Q-factors [55] were optimized in photonic crystals using extreme learning and deep learning techniques.

The first study applying deep learning methods for determining the optical properties of a PCF has been done on only solid cores using Artificial Neural Network (ANN) parameters, including wavelength ($0.5\text{-}1.8 \mu\text{m}$), pitch ($0.8\text{-}2.0 \mu\text{m}$), diameter to pitch ratio

(0.6-0.9), and several rings (4-5) for a silica solid-core PCF [56]. The evaluation metric of the proposed model is expressed by Mean-Square Error (MSE) and varies around 0.00065 for different optical parameters. The same writer proposed another study applying Machine Learning Regression Techniques to Nanophotonic Waveguide Studies. An absolute percentage error of under 5% was achieved when predicting outputs for slot, strip, and directional waveguide coupler [56].

Another related work combines solid, hollow, and multi-core PCF to calculate the optical characteristics using ANN, achieving the minor MSE 0.001 [57]. The computational time was also compared with the simulation time. Training the model takes time in the second range, and for testing, ms amount of time is required [56]. Das et al. proposed a study on applying algorithms like Linear regression, decision trees, and random forest trees in predicting the optical properties of PCF [58]. The maximum R squared value is 0.995 with minimum MSE 2.78×10^{-10} .

Another broad study applied ANN and SVM as machine learning models to predict optical properties. The Mean absolute percentage errors using ANN and SVM were recorded at 0.032% and 0.014%, respectively [59]. Vyas et al. suggested a revised photonic crystal fiber (PCF) measuring a negative dispersion of approximately -3126 ps/nm/km at the $1.55 \mu\text{m}$ [60]. Accurate computation of design parameters contributes to enhancing the desired outcome. The paper uses an extreme learning machine to predict the negative dispersion coefficient of the modified PCF.

In recent years, there has been significant research on photonic crystal fibers (PCFs) and their unique optical properties, including customized dispersion, single-mode behavior, strong nonlinearity, and notable birefringence. Various PCF designs and materials have been proposed and analyzed to achieve specific optical properties, such as negative dispersion for compensation in optical communication systems. Despite the development of PCFs with negative dispersion, there remains a need to improve these models to achieve ultra-high negative dispersion for optimal dispersion profiles in optical communication. Traditional numerical methods for simulating and optimizing photonic crystal structures, such as the finite difference method, finite element method, and plane wave expansion method, require substantial computational resources and multiple iterations, particularly when handling complex structures. Machine learning techniques have recently emerged as an alternative approach for analyzing and predicting the optical properties of PCFs, offering advantages in terms of computational efficiency and accuracy.

Although some studies have applied machine learning techniques like artificial neural networks (ANNs) and support vector machines (SVMs) to predict the optical properties

of solid-core, hollow, and multi-core PCFs, there is still room for further exploration of machine learning-based techniques for predicting the optical properties of negative dispersion-compensating PCFs. Developing accurate and efficient machine learning models for predicting ultra-high negative dispersion in PCFs could contribute to the advancement of long-distance optical communication systems and other applications requiring dispersion compensation.

2.1 Chapter Summary

Photonic crystal fibers (PCFs) exhibit unique optical properties, with negative dispersion being essential for compensation in optical communication systems. Despite progress in PCF designs, achieving ultra-high negative dispersion remains a challenge. Traditional numerical methods for simulating and optimizing PCFs require substantial computational resources and multiple iterations. Machine learning techniques have recently emerged as an alternative, offering computational efficiency and accuracy in predicting optical properties. Further exploration of machine learning-based techniques for predicting negative dispersion-compensating PCFs can contribute to advancements in long-distance optical communication systems.

Chapter 3

Basics of PCF and Machine Learning

The chapter offers a theoretical exploration of the essential principles underlying PCF and Machine Learning Algorithms. In addition, different optical characteristics of PCF, including effective index, confinement loss, propagation constant, V-parameter, dispersion, and effective mode, are also briefly explained. The basic machine learning techniques (Linear regression, K-Nearest Neighbors, Decision tree, Random forest tree) and Artificial Neural Networks (ANN) are described briefly.

3.1 Basic Principle of PCF

Photonic Crystal Fiber (PCF) is a specific variety of optical fibers with unique properties, making them an appealing choice to traditional optical fibers. The fundamental concept of PCFs relies on establishing a cyclical modification in the refractive index within the fiber core concerning cladding. The photonic crystal structure significantly controls light propagation within the fiber, leading to unique properties not found in traditional optical fibers.

An extraordinary property of PCF is their proficiency in guiding light by total internal reflection, which occurs when the light is guided in the core section as a result of the refractive index variation compared to cladding. The photonic crystal structure can produce various modes of propagation, leading to the properties of the guided light, such as its dispersion, nonlinearity, and confinement. Another essential property of PCFs is their capacity to regulate the dispersion of light. Dispersion represents an occurrence in optical fibers where varying wavelengths of light propagate at distinct velocities, spreading an optical pulse over time. In traditional optical fibers, the dispersion is mainly due to material dispersion due to the variation of refractive indices among core

and cladding materials. In PCFs, the structure of photonic crystals can be customized. To introduce negative dispersion, which counteracts the positive dispersion in traditional optical fibers. This leads to a reduction in pulse widening and enables high data rate transmission over longer distances. PCFs also have a range of other distinct characteristics that make them attractive for various applications. For example, PCFs can have very low nonlinearities, which makes them suitable for high-speed optical communication systems. PCFs can also have a high degree of confinement, which reduces sensitivity to bending and torsion, making them ideal for use in harsh environments.

3.1.1 Origin

The origin of Photonic Crystal Fibers (PCFs) can be traced back to the mid-1980s when researchers first started to explore the idea of creating periodic variations in the refractive mode index of optical fibers. The concept of photonic crystals, characterized by periodic refractive index alternation in the refractive index, had already been established in solid-state physics. Researchers began considering the possibility of creating photonic crystal structures in optical fibers. One of the earliest proposed appeals for PCFs was to create optical fibers with low loss and high dispersion, which would suit high-speed optical communication systems. In 1986, Yablonovitch proposed the concept of photonic bandgap fibers, which would have a photonic crystal structure that could confine light within the fiber. This concept formed the basis of much of the early research on PCFs [61]. Over the following years, researchers continued to explore the potential of PCFs and developed new techniques for fabricating PCFs with more complex structures. One of the critical breakthroughs in the field came in the late 1990s when researchers at the University of Southampton demonstrated that PCFs could be used to create fibers with negative dispersion, which could be used to mitigate the positive dispersion in traditional optical fibers. Since then, PCFs have become an active research domain, continually expanding and transforming. Today, PCFs are used in various applications, including speedy optical communication systems, medical imaging, and sensing. The development of PCFs has profoundly impacted optics and paved the way for new and exciting technologies previously impossible with traditional optical fibers.

3.1.2 Structure

The configuration of a PCF entails a core enveloped by a cladding exhibiting a reduced refractive index marked in Figure 3.1. The core and cladding comprise a specific ar-

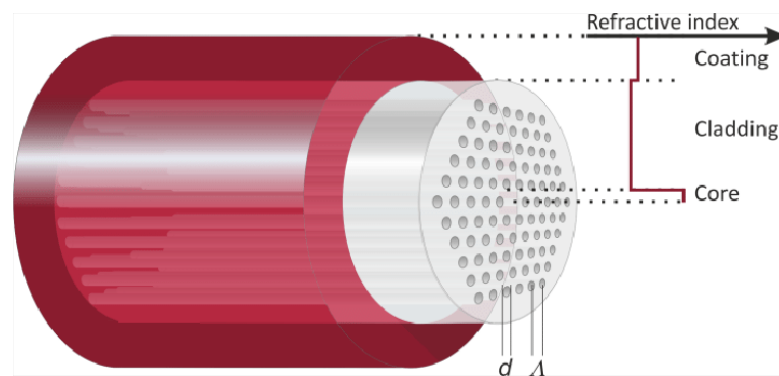


Figure 3.1: Structure of basic PCF

arrangement of air holes or "defects" along the fiber axis, forming a photonic crystal. The air cavities are usually oriented in a regular lattice pattern and are surrounded by the core material. The air medium's size, shape, and arrangement determine the properties of the PCF. A PCF's core comprises a recurring pattern of air holes extending along the fiber's length and surrounded by a glass cladding. The periodicity of the air cavities creates a photonic crystal structure that modulates the fiber's refractive index and allows the fiber to control the flow of light in new and innovative ways. The structure of a PCF is typically described in terms of the air hole size, orientation, and distance of one hole from another. The air holes (circular or elliptical), size, and pitch of the air holes can be tailored to create fibers with specific optical properties. For example, PCFs can be designed to have a high or low nonlinearity, to exhibit negative or zero dispersion, or to have a high or low confinement loss.

3.1.3 Modes of Operation

Based on the confinement approach, there are two distinct modes of PCF operation, the index-guiding principle and the photonic bandgap principle.

The Index Guiding Principle is a fundamental concept that explains how light is confined and guided within a Photonic Crystal Fiber (PCF). The index guiding principle states that a PCF's core can hold the light of a PCF if the core's average refractive index is greater than the cladding's. The refractive index of a material determines the speed at which light propagates along that material. In traditional optical fibers, the fiber's core has a greater refractive index than the cladding, which causes light to be restricted within the core. However, in PCFs, the regular distribution of air holes influences the fiber's refractive index. It creates a photonic crystal structure that confines light in a new and innovative way. The index guiding principle is critical to the functioning of PCFs because it allows the fibers to confine light in a way that is different

from traditional optical fibers. This allows PCFs to exhibit various optical characteristics like negative or zero dispersion, high confinement loss, and high nonlinearity.

The Photonic Bandgap Principle is a fundamental concept that explains how light is guided and confined within a PCF [62]. A photonic bandgap signifies a frequency spectrum where light is unable to transmit through a substance. The photonic bandgap configuration in a PCF enables light to be restricted within the core by preventing it from propagating. The air holes' size, shape, and periodicity can be controlled to create a photonic bandgap structure that matches the wavelength of the light transmitted through the fiber. This enables the PCF to confine light in a way that is different from traditional optical fibers, which use total internal reflection to preserve light containment. The photonic bandgap principle is critical to the functioning of PCFs because it allows the fibers to confine light differently from typical optical fibers. These properties make PCFs desirable for numerous applications, ranging from high-speed optical communication systems to medical imaging and sensing technologies.

3.1.4 Guiding Light through Photonic Crystals

Guiding light in photonic crystal fiber refers to the confinement and propagation of light within a structure. Photonic crystal fibers are optical fibers with a photonic bandgap structure, which confines light within the fiber and prevents it from propagating. The arrangement of photonic crystal fiber is formed by incorporating air holes in the fiber's cladding, generating a cyclic configuration of materials with varying refractive indices [61] [62]. This periodic arrangement creates a photonic band-gap structure that confines light within the fiber's core and prevents it from propagating out of the structure. By adjusting the dimensions, shape, and periodicity of the air holes, as well as the refractive indices of the materials, the characteristics of photonic crystal fibers can be manipulated. This allows photonic crystal fibers to exhibit various optical properties, including negative or flat dispersion, high confinement loss, and nonlinearity.

3.1.5 Solid Core Photonic Crystal Fiber

A Solid Core Photonic Crystal Fiber (SC-PCF) is a distinct type of PCF featuring a solid core encased by a photonic bandgap architecture. The fiber's core comprises a material with a high refractive index with respect to cladding index material. The cladding contains a regular pattern of air holes, forming a photonic bandgap structure that traps light within the solid core. SC-PCFs differ from traditional optical fibers because they have a photonic bandgap structure allowing high-light confinement within the core. This high

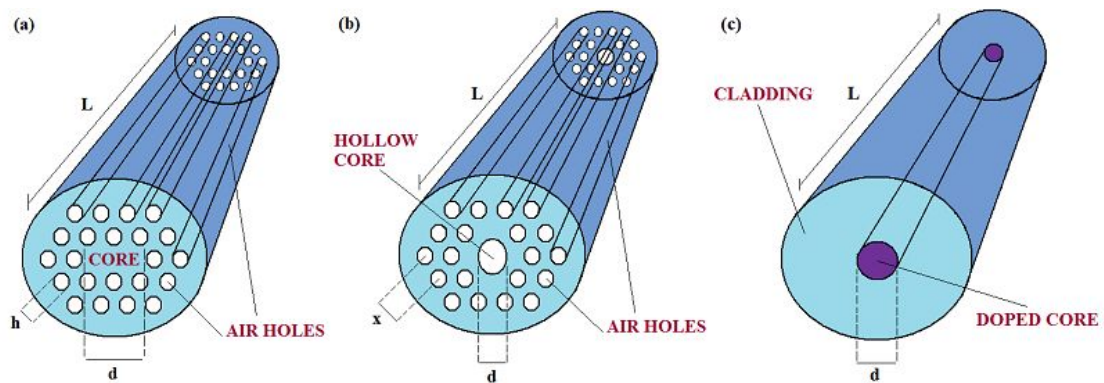


Figure 3.2: Illustration of (a) solid-core PCF, (b) hollow-core PCF, and (c) typical single-mode fiber.

confinement results in a large effective area, which can be helpful in various applications, including nonlinear optics, high-power fiber lasers, and fiber sensors.

3.1.6 Hollow Core Photonic Crystal Fiber

Hollow core photonic crystal fiber (HC-PCF) is a specific kind of photonic crystal configuration fiber with a hollow core surrounded by a photonic bandgap structure. The fiber's hollow core is made of air. HC-PCFs differ from traditional optical fibers because they have a photonic bandgap structure allowing high-light confinement within the hollow core.

Figure 3.2 displays a model of the core of micro-structured PCFs, in which L indicates the length of the fiber, d indicates the diameter of the core, and h indicates the pitch of the air hole. Including Figure 3.2 simplifies the representation and avoids unnecessary complexity [63].

3.1.7 Design Parameters

The parameters of a PCF refer to the various design and manufacturing aspects that determine its optical properties and performance. These parameters can be adjusted during the design and fabrication to achieve desired performance characteristics, including high confinement, low loss, effective mode area, effective refractive index, or specific dispersion properties.

3.1.7.1 Core Diameter

The core diameter determines the size of the region in which light is confined and guided and is a significant factor affecting the fiber's optical performance. A smaller core diameter leads to higher confinement and nonlinearity, as more light is confined within a smaller region. However, a smaller core diameter also makes the fiber more sensitive to bends and other mechanical perturbations, which can cause increased loss and reduced performance. On the other hand, a larger core diameter provides excellent mechanical stability and lower loss but reduces the fiber's nonlinearity and confinement.

Therefore, the choice of core diameter is a trade-off between different performance characteristics and must be optimized for a specific application. Smaller core diameters are generally favored for high-nonlinearity applications, while larger ones are favored for low-loss, high-stability applications.

3.1.7.2 Hole Size and Spacing

The air hole diameter and spacing between them in a PCF cladding region are the most critical design parameters determining the fiber's optical properties and performance. The air cavities in the cladding region form a periodic array, or photonic crystal, that acts as a bandgap structure that restricts the propagation of specific wavelengths of light. The air holes' diameter and spacing determine the bandgap's size and shape and, thus, the fiber's dispersion and confinement properties. A smaller hole diameter leads to a narrower bandgap, which can result in a higher level of confinement. However, a smaller hole diameter makes the fiber more susceptible to fabrication errors, resulting in increased loss and reduced performance. On the other hand, a larger hole diameter provides greater tolerance to fabrication errors and increased mechanical stability but also leads to a broader bandgap and reduced confinement. The spacing between the air holes is another critical factor that affects the fiber's optical properties. A smaller spacing leads to a narrower bandgap and increased confinement but also increases the complexity of the fiber's fabrication. The choice of hole diameter and spacing is a trade-off between different performance characteristics and must be optimized for a specific application. In general, smaller hole diameters and spacing are favored for high-confinement applications, while larger hole diameters and spacing are favored for low-loss, high-stability applications.

3.1.7.3 Refractive Index Contrast

The refractive index contrast of a Photonic Crystal Fiber (PCF) refers to the difference between the refractive indices of the core and cladding regions of the fiber. This difference is one of the key parameters determining the fiber's guiding properties and plays a critical role in the confinement and transmission of light within the fiber. A high refractive contrast results in a robust guiding mechanism, enabling the light to be directed within the core even if the core's diameter is minimal. This results in a high level of confinement and low loss for the guided mode. On the other hand, a low refractive index contrast leads to weaker guiding and larger core diameter, which can result in reduced confinement and increased loss for the guided mode. Refractive index contrast is a trade-off between performance characteristics and must be optimized for a specific application. High refractive index contrast is generally favored for low-loss, high-confinement applications, while low refractive index contrast is favored for low-complexity, low-cost applications. It is significant to highlight that the refractive index contrast of PCFs can be adjusted through various materials and fabrication techniques, including using glass or polymer materials with different refractive indices and core-cladding designs with different structural asymmetry. These techniques allow tailoring the fiber's optical properties to meet specific application requirements.

3.1.7.4 Air Fraction

The air fraction of a Photonic Crystal Fiber (PCF) refers to the fraction of the cladding region occupied by air holes. It is a crucial parameter determining the fiber's optical properties and performance. It is directly associated with the variation in refractive index between the fiber's center and cladding. An elevated air fraction causes a reduced refractive index contrast between the core and the cladding, resulting in less practical guidance and higher loss for the transmitted mode. Nevertheless, a higher air fraction simplifies the fiber's production process and lowers costs.

Besides, a low air fraction results in a high refractive index contrast and strong guiding, which leads to high confinement and low loss for the guided mode. However, a low air fraction makes fiber more difficult and expensive. And its susceptibility to fabrication errors and mechanical perturbations. The choice of air fraction is a trade-off between different performance characteristics and must be optimized for a specific application. High air fraction is generally favored for low-complexity, low-cost applications, while low air fraction is favored for high-confinement, low-loss applications. It is significant to point out that the air fraction can be modified by varying the dimension, spacing, and

orientation of the hollow cavities in the cladding region and using different materials and fabrication techniques to create the core and cladding regions. These techniques allow tailoring the fiber's optical properties to meet specific application requirements.

3.1.7.5 Fiber Geometry and Structural Asymmetry

Fiber geometry refers to the structure and scale of the fiber's core and cladding sections. It comprises factors like the diameter of the core, the size and spacing of the holes within the cladding section, and the positioning of the air holes within the cladding region. These parameters determine the fiber's dispersion and confinement properties and play a critical role in guiding light within the fiber. The structural asymmetry of the fiber refers to the distinctions in structure between the core and cladding regions, like the variations in dimensions and organization of the air holes within the cladding area. This dissimilarity in refractive index values between the core and cladding sections thus affects the fiber's guiding properties and optical performance. The choice of fiber geometry and structural asymmetry is a trade-off between different performance characteristics and must be optimized for a specific application. For example, small core diameters and high structural asymmetry are favored for high-confinement, low-loss applications. Low-complexity, low-cost applications favor a large core diameter and low structural asymmetry. The fiber geometry and structural asymmetry can be adjusted using different materials and fabrication techniques, such as glass or polymer materials and core-cladding designs. These techniques allow tailoring the fiber's optical properties to meet specific application requirements.

3.1.7.6 Material Composition

The material composition of a Photonic Crystal Fiber (PCF) refers to the material used to create the core and cladding regions of the fiber. This parameter is critical in the fiber's optical properties and performance, as different materials have different refractive indices and other optical properties. In particular, silica glass is often selected for PCF fabrication because of its impressive transparency, reduced loss, and exceptional mechanical stability, which makes it well-adapted for high-performance scenarios. Besides, polymer materials offer low cost, ease of processing, and a wide range of refractive index values, making them well-suited for low-complexity, low-cost applications. The material composition can be adjusted using different fabrication techniques, such as different glass or polymer materials and various doping or index-modifying techniques. These techniques allow tailoring the fiber's optical properties to meet specific

application requirements.

3.1.8 Application of PCF

Due to their distinctive optical properties, photonic crystal fibers have a wide variety of applications. Some of the critical applications of PCFs include nonlinear optics, the high confinement of light within the core of PCFs, combined with their large effective area, makes them ideal for nonlinear optical tasks, including supercontinuum generation and frequency transformation.

1. Nonlinear item optics: The high confinement of light within the core of PCFs, combined with their large effective area, makes them ideal for nonlinear optical applications and frequency conversion.
2. High-power fiber lasers: The high nonlinearity of PCFs allows for generating high-power fiber lasers with improved beam quality and stability.
3. Fiber sensors: PCFs have high sensitivity to changes in the surrounding environment, making them useful for sensing applications, pressure sensing, and strain sensing.
4. Telecommunication: PCFs are used in telecommunication systems for long-haul and metropolitan area networks. They offer high bandwidth and low dispersion, making them ideal for high-speed data transmission.
5. Bio-medical applications: PCFs can be used in biomedical applications such as in vitro diagnostics, endoscopy, and optical coherence tomography due to their ability to guide light through biological tissues without damaging them.
6. Optical spectroscopy: The high confinement of light in the core of PCFs allows for improved optical spectroscopy, suitable for gas sensing and environmental monitoring applications.

3.2 Photonic Crystal Fiber Optical Attributes

Photonic Crystal Fibers (PCFs) are optical fibers that have a microstructured cladding region with a periodic orientation of air holes. The unique structure of PCFs gives them distinct optical properties than standard optical fibers, allowing for diverse applications.

3.2.1 Refractive Index

The effective refractive index signifies the overall refractive index of the light that is transmitted within the fiber. It is a complex number, with both real and imaginary components, and is decided by the structure of the fiber and frequency of light. The effective refractive index is a crucial property of PCFs, as it determines the guided modes' dispersion, confinement, and loss properties. The real component of the effective refractive index determines the speed of light in the fiber and the magnitude of the confinement. In contrast, the imaginary part determines the loss of the guided mode. The calculation of the refractive index for the fused silica material in the proposed configuration is represented by Sellmeier's equation 3.1 in ref [12],

$$n^2(\lambda) = 1 + \frac{X_1\lambda^2}{\lambda^2 - Y_1} + \frac{X_2\lambda^2}{\lambda^2 - Y_2} + \frac{X_3\lambda^2}{\lambda^2 - Y_3} \quad (3.1)$$

Here 'n' indicates the refractive index, a function of operating wavelength ' λ '. At the Standard temperature, the Sellmeier coefficients of fused silica can be quantified as $X_1=0.6961663$, $X_2=0.4079426$, $X_3= 0.8974794$ and $Y_1=0.0046914826 \mu\text{m}^2$, $Y_2=0.0135120631 \mu\text{m}^2$ and $Y_3=97.9340025 \mu\text{m}^2$.

The fiber geometry and structural asymmetry, the material composition, and the wavelength of the light influence the effective refractive index. The fiber geometry and structural asymmetry determine the variation in refractive index between the core and the surrounding cladding regions. In contrast, the material composition determines the overall refractive index of the fiber. The wavelength of the light determines the effective refractive index through the dispersion properties of the fiber.

3.2.2 Confinement Loss

The confinement property of a Photonic Crystal Fiber (PCF) refers to the fiber's ability to restrict light within its core. The core is encircled by a regularly spaced arrangement of air holes in PCFs, creating a photonic bandgap that restricts light propagation. By controlling the air holes' size, shape, and spacing, the photonic bandgap can guide light in the fiber's core, even for wavelengths that would otherwise propagate in the cladding.

The degree of light confinement in a PCF's core is related to the difference in refractive indices between the core and cladding materials. A high refractive index contrast leads to strong confinement and a minor mode field diameter. In contrast, a low refractive index contrast leads to weaker confinement and a larger mode field diameter. Some light may have escaped from the PCF core into the cladding region. Confinement loss

(L_c) decides how much light escapes from the core area. It can be derived using the imaginary portion of the fundamental refractive index and denoted by [12],.

$$L_c\left(\frac{dB}{m}\right) = 8.686 \times k_0 \text{Im}[n_{\text{eff}}] \quad (3.2)$$

Where, $\text{Im}[n_{\text{eff}}]$ represents the imaginary portion of the refractive index, and k_0 illustrates free space wave numbers. In addition, the confinement property of a PCF is also affected by the fiber geometry and the wavelength of light being guided. As an example, a PCF with a smaller core diameter and a higher number of air holes will exhibit superior confinement properties compared to one with a larger core diameter and a lower number of air holes.

3.2.3 Chromatic Dispersion

The dispersion property of a Photonic Crystal Fiber (PCF) refers to the wavelength-dependent alternation of the propagation speed of light within the fiber. In general, the dispersion of light in a PCF is caused by the differences in the effective refractive index for different wavelengths of light.

Dispersion values may range from positive to negative based on the fiber design and the wavelength of light. Positive dispersion occurs when longer wavelengths travel slower than shorter wavelengths, while negative dispersion occurs when longer wavelengths travel faster than shorter wavelengths. Positive dispersion is often called normal dispersion, while negative dispersion is called anomalous dispersion. In a conventional optical fiber, light pulses travel along the channel, and dispersion mechanisms within the fiber lead to their broadening. The scenario is demonstrated in Figure 3.3, where one may observe that as each pulse expands, it overlaps with neighboring pulses, making them indistinguishable when reaching the receiver input. The fiber geometry and the refractive index profile in PCFs can control the dispersion property. In contrast, a PCF with a larger core diameter and a lower refractive index contrast will have a lower dispersion property. Dispersion is the time-domain expansion or widening of transmitting pulses through an optical fiber. Changes easily influence pitch (\wedge), diameter, and shape of different holes within the cladding region. So, chromatic dispersion (D) is quantified by [12]

$$D(\lambda) = -\frac{\lambda}{c} \frac{d^2 \text{Re}(n_{\text{eff}})}{d\lambda^2} \quad (3.3)$$

Here, λ represents the wavelength, c defines the maximum speed of light, $\text{Re}(n_{\text{eff}})$ expresses the actual portion of the refractive index calculated from (1). In addition to the

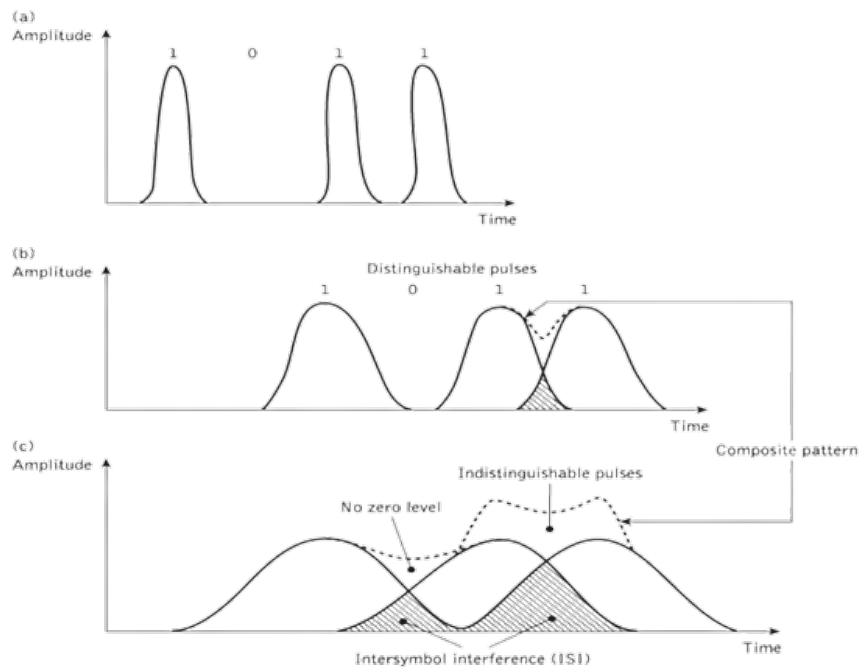


Figure 3.3: (a) Light input of fiber (b) Light output at a distance L_1 (c) Light output at a distance $L_2 > L_1$

dispersion property, the dispersion slope, the degree to which dispersion varies with frequency, is also an essential parameter in PCFs. The dispersion slope can be either positive or negative, determining the amount of chromatic dispersion or the spreading of light pulses in the fiber.

3.2.4 Non-linearity

The nonlinear property of a Photonic Crystal Fiber (PCF) refers to how the fiber's refractive index changes in response to changes in optical intensity. Nonlinear effects are essential in PCFs because they can cause significant distortions of optical signals and limit the fiber's performance in specific applications.

The most common type of nonlinear effect in PCFs is self-phase modulation (SPM), which occurs when changes in the optical intensity cause variations in the phase of the optical wave. SPM can lead to spectral broadening and distortion of optical signals, mainly when the optical intensity is high. The calculation of the coefficient of non-linearity, which is linked to the rate of dispersion and can enhance data capacity and transmission capabilities, is performed using equation (4) in reference [12]

$$\gamma_c = \frac{2\pi}{\lambda} \frac{n_2}{A_{\text{eff}}} \quad (3.4)$$

Another significant nonlinear effect in PCFs is four-wave mixing (FWM), which happens when two optical pulses combine to generate new waves with different frequencies. FWM can cause significant crosstalk between optical signals and limit the fiber's performance in speedy optical communication systems. The nonlinear characteristic of a PCF is directly related to the effective nonlinear coefficient, representing the intensity of the nonlinear impact. The fiber's material composition, geometry, and refractive index profile affect the effective nonlinear coefficient. Here are some key nonlinear effects to consider:

Kerr Effect: The Kerr effect is a fundamental nonlinear optical phenomenon observed in various optical materials, including PCFs. It refers to the change in refractive index of a material in response to the intensity of light passing through it. In PCFs, the Kerr effect can lead to self-phase modulation (SPM) and cross-phase modulation (XPM), which can impact signal propagation and nonlinear interactions.

Self-Phase Modulation (SPM): SPM is a nonlinear effect caused by the intensity-dependent refractive index change in the fiber. It results in spectral broadening of optical pulses as they propagate through the PCF. This broadening can introduce distortions and affect the overall transmission characteristics of the fiber.

Cross-Phase Modulation (XPM): XPM occurs when two or more optical signals with different wavelengths interact in a nonlinear medium, such as PCF. The intensity of one signal can induce a phase shift in the other signal, leading to wavelength-dependent phase modulation. XPM can cause crosstalk and nonlinear interference effects in PCF-based optical communication systems.

Four-Wave Mixing (FWM): FWM is a nonlinear process that occurs when multiple optical signals interact in a nonlinear medium. It involves the mixing of different frequencies, resulting in the generation of new frequencies. FWM can cause spectral distortion, signal degradation, and interference in PCF-based systems.

Raman Scattering: Raman scattering is a nonlinear process where light interacts with molecular vibrations in the fiber material. It leads to energy transfer between the interacting photons, resulting in wavelength conversion and amplification. Raman scattering can impact signal propagation and may require compensation techniques in PCF-based systems.

3.2.5 Effective Mode Area

The Effective Mode Area (EMA) property of a Photonic Crystal Fiber (PCF) refers to the area of the cross-section of the optical mode that effectively guides light in the fiber. The EMA is an essential parameter in PCFs because it determines the fiber's nonlinearity and ability to transmit high-power optical signals. A larger EMA generally results in a lower nonlinearity and a higher tolerance to optical power. In comparison, a smaller EMA results in a higher nonlinearity and a lower tolerance to optical power. The EMA has a direct relationship with the core diameter squared and an inverse relationship with the refractive index contrast.

In PCFs, the EMA can be controlled by the fiber geometry and the refractive index profile. For example, a PCF with a larger core diameter and a lower refractive index contrast will have a larger EMA. In comparison, a PCF with a lower core size and a higher refractive index contrast will have a smaller EMA. The effective area is the core portion that actively transmits the optical wave straight within the material. The effective mode area is determined using equation (3.5) from reference [12].

$$A_{\text{eff}} = \frac{(\int_{-\infty}^{\infty} |E|^2 dx dy)^2}{\int_{-\infty}^{\infty} |E|^4 dx dy} \quad (3.5)$$

In addition to the EMA, confinement loss, which is the loss of light caused by the finite size of the core, is also a significant parameter in PCFs. The confinement loss is proportional to the difference between the refractive index of the core and the cladding. It determines the optical power that can be transmitted through the fiber.

3.2.6 V-Parameter

The V-parameter, also known as the normalized frequency, is a parameter used to describe the guiding properties of a Photonic Crystal Fiber (PCF). The V-parameter is related to the waveguide dispersion and the effective refractive index of the fiber. The V-parameter can be calculated as the normalized frequency of the waveguide, and it is given by the equation (3.6) in [12]:

$$v_{\text{eff}} = \frac{2\pi a}{\lambda} \sqrt{n_{\text{co}}^2 - n_{\text{cl}}^2} \quad (3.6)$$

Where a is the core radius of the fiber, and λ represents the wavelength of the light being guided.

The V-parameter is an essential parameter in PCFs because it determines the waveguide dispersion, which is dependent on the group velocity of light on its frequency. A larger V-parameter generally results in a more significant waveguide dispersion, and a smaller V-parameter results in a smaller waveguide dispersion. The fiber geometry and the refractive index profile can control the V-parameter. For example, a PCF with a larger core radius and a lower refractive index contrast will have a larger V-parameter. A PCF with a smaller core radius and a higher refractive index contrast will have a smaller V-parameter.

3.3 Full Vector Finite Element Method

The Full Vector Finite Element Method (FVFEM) is a computational technique for modeling and analyzing the behavior of optical fibers, including PCF. It is a powerful tool for simulating PCFs' complex optical and geometrical properties, including traversal in the fiber, the interplay between light and the photonic crystal structure, and the effect of fabrication imperfections. FVFEM utilizes the finite element method as its foundation. This numerical technique divides the geometry of the fiber into small elements and solves the equations governing the system using these elements. In the FVFEM, the optical field is represented by a vector rather than a scalar, which allows for the simulation of both the magnitude and direction of the field. This provides a more complete and accurate representation of the optical field, which is particularly important in PCFs due to their complex geometries and optical properties.

The FVFEM can simulate various optical phenomena in PCFs, including dispersion, confinement, and nonlinearities. It can also analyze the effects of fabrication imperfections on the fiber's optical attributes, such as hole size, shape variations, and PCF fabrication for specific applications. The optical mode analysis is carried out on a cross-section, with the wave propagating in the z-direction and presenting a particular form.

$$\overline{H}(x, y, z, t) = \overline{H}(x, y)e^{j(\omega t - \beta z)} \quad (3.7)$$

In this case, β is the propagation constant, and ω represents the angular frequency. An eigenvalue equation for the magnetic field, \overline{H} , is obtained from the Helmholtz equation.

$$\nabla \times (n_2 \nabla \times \overline{H}) - k_0^2 \overline{H} = 0 \quad (3.8)$$

Which is solved for the eigenvalue $\lambda = -j\beta$. The magnetic field is set to zero as a boundary

condition on the cladding's exterior. Given that the field amplitude decays quickly with respect to the cladding radius, this boundary condition is appropriate.

3.3.1 Boundary and Interface Conditions

Boundary and interface conditions are essential for modeling photonic crystal fibers (PCFs). They determine how light travels through the fiber and interact with the photonic crystal structure.

Boundary conditions refer to the conditions that are imposed on the optical field at its surface. In PCFs, the boundary conditions determine how light enters and exits the fiber and interacts with the air holes and the cladding material. Common boundary conditions include the perfectly matched layer (PML) and the Dirichlet boundary conditions, which specify the behavior of the optical field at the fiber's surface. Interface conditions refer to the conditions that are imposed at the interface between two different materials in the fiber. In PCFs, the interface conditions determine how light passes from one material to another and how it is affected by the refractive index contrast at the interface. Common interface conditions include the Fresnel reflection and transmission conditions, which describe the behavior of light when it encounters the boundary between two materials having distinct refractive indices. The choice of boundary and interface conditions is important for the accuracy of the simulation results. For example, the PML boundary condition is a common choice for PCF simulations because it provides a stable and accurate representation of the optical field at the fiber surface. Similarly, the Fresnel reflection and transmission conditions are commonly used at the junction of the air holes and the cladding material, as they offer a more precise representation of the optical field.

3.3.1.1 Perfect Matched Layer

The Perfect Matched Layer (PML) is a commonly used boundary condition in modeling photonic crystal fibers (PCFs). The PML is a mathematical layer that is added to the boundary of the simulation domain to absorb outgoing waves and prevent reflections. The PML was initially introduced by J. P. Berenger in 1994 [64].

The PML boundary condition is an artificial layer that absorbs outgoing waves and prevents reflections. It works by modifying the wave equation at the boundary to absorb outgoing waves and not reflect them into the simulation domain. This allows for more accurate simulations and reduces the effects of reflections on the results. Undoubt-

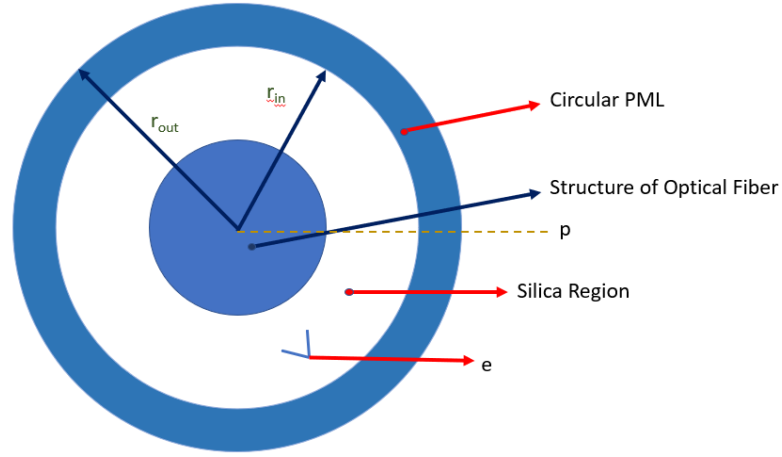


Figure 3.4: Surrounding PML region of the waveguide architecture

edly, the most effective PML formulation currently is the Convolutional-PML (CPML). CPML forms the PML using an anisotropic, dispersive substance. Implementing CPML is relatively simple, as it does not necessitate splitting the fields. The PML region can be regarded as a flawless absorber with a specific level of conductivity. However, the optimized conductivity is derived from particular equation sets. In our research, we utilized the cylindrical PML provided in commercial software.

After thorough analysis, wave equations can be formulated within the PML region.

$$\bar{n} \times \bar{H} = j\omega n_2 s \bar{E} \quad (3.9)$$

$$\bar{n} \times \bar{E} = -j\omega \mu \bar{H} \quad (3.10)$$

$$s = 1 - j \frac{\sigma_e}{\omega n^2 \epsilon_0} = 1 - j \frac{\sigma_m}{\omega \mu_0} \quad (3.11)$$

Where,

E: Electric Field

H: Magnetic Field

σ_e and σ_m : The ideal thickness 'e' for the PML layer is proportional to the operating wavelength's multiples. To prevent numerical reflection, the conductivity within the PML region is gradually increased to its maximum value instead of an abrupt change, as illustrated in figure 3.5.

To achieve a perfectly matched condition that ensures no Reflection occurs at the junction, the following can be stated:

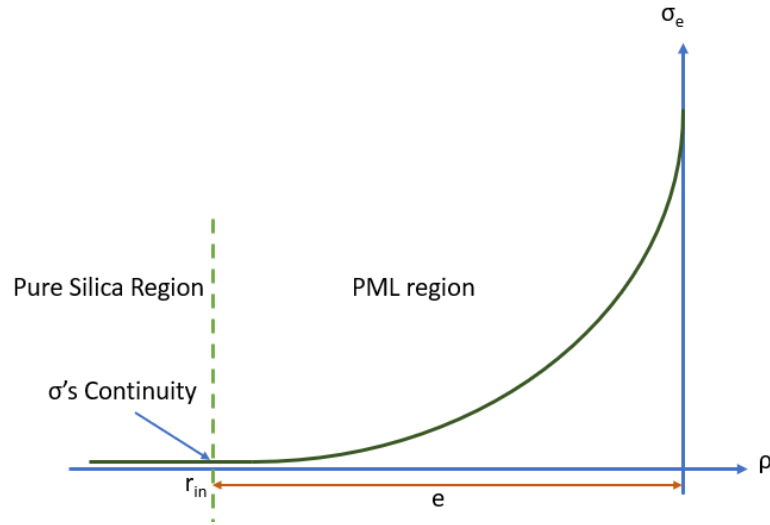


Figure 3.5: Grading of PML conductivity.

$$\frac{\sigma_e}{\epsilon_0 n^2} = \frac{\sigma_m}{\mu_0} \quad (3.12)$$

Here, the Reflection coefficient can be represented by

$$R = \exp\left[-2 \frac{\sigma_{\max}}{\epsilon_0 c n} \int_0^d \left(\frac{\rho}{d}\right) d\rho\right] \quad (3.13)$$

Based on this, the maximum conductivity is determined as follows:

$$\rho_{\max} = \frac{m+1}{2} \frac{\epsilon_0 c n}{d} \ln\left(\frac{1}{R}\right) \quad (3.14)$$

Here, m represents the polynomial order for grading conductivity. The equations convey that the lowest reflection occurs when the conductivity is at its maximum. Nonetheless, due to numerical error factors, there is a preferred reflection amount for precisely calculating the propagation constant. An enduring complex effective index value can be achieved by altering the PML's thickness and position relative to the PCF's center.

3.4 Machine Learning Algorithm

Machine learning is a subset of artificial intelligence that enables computers to learn and adapt from data without explicit programming. Its significance lies in its ability to analyze vast amounts of data, identify patterns, and make predictions, leading to improved decision-making and automation. Machine learning has revolutionized various fields,

including computer vision, natural language processing, and healthcare, by providing innovative solutions and enhancing existing technologies. It also enables the development of personalized services and products, ultimately improving user experiences. As computational power and data availability increase, machine learning will continue to play a vital role in advancing scientific research and driving technological innovation.

3.4.1 Linear Regression

Linear regression is a supervised machine learning algorithm for regression problems. This approach depicts the link between a dependent variable (the target variable) and one or several independent variables (the input variables). The purpose of linear regression is to discover the ideal linear link between the dependent and independent variables so that we can estimate the value of the dependent variable based on a series of values for the independent variables [65]. Consider the below image of Figure 3.6.

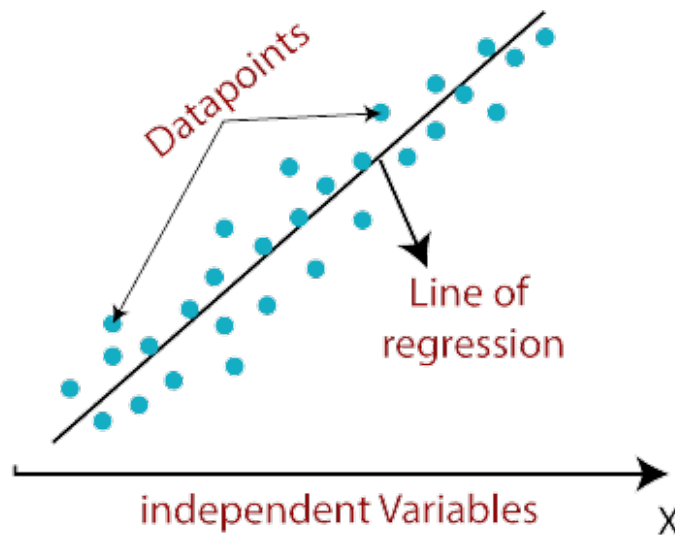


Figure 3.6: Linear regression

We assume the association between the dependent and independent variables is linear in linear regression. Mathematically, linear regression can be represented as [66].

$$y = a_0 + a_1x + \epsilon \quad (3.15)$$

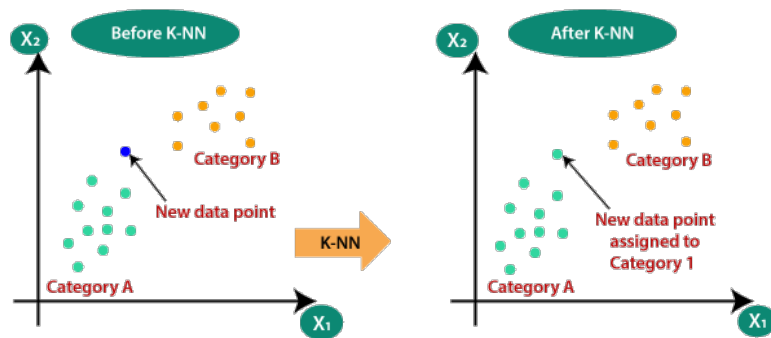


Figure 3.7: K-Nearest Neighbor(KNN).

Here, y represents the dependent (target) variable, while x is the independent (predictor) variable. The term a_0 denotes the line's intercept, providing an additional degree of freedom, and a_1 is the linear regression coefficient, which serves as the scale factor for each input data point. ϵ represents random error. Several methods for solving linear regression include the ordinary least squares (OLS) method, gradient descent, and the standard equation method [67]. The choice of method depends on the size and complexity of the data, as well as the computational resources available. Linear regression is a simple and widely used algorithm well-suited for many regression problems. However, it has some limitations, including the assumption of a linear relationship between the dependent and independent variables, which may not be accurate in some cases. More complex models, such as polynomial or non-linear regression, may be more appropriate. Section text.

3.4.2 K-Nearest Neighbors (KNN)

The K-Nearest Neighbors (KNN) algorithm is a method in machine learning used to classify data and regression problems [68]. It is based on the closeness of data points in the feature space and using them to make predictions. The KNN algorithm records all existing instances and determines the classification of new instances based on the majority decision of its closest neighbors. The algorithm is simple, effective, and has relatively low computational costs [68]. In a KNN algorithm, the K value is a hyperparameter determined before the algorithm is run. When K is assigned a value of 1, the algorithm is referred to as the nearest neighbor algorithm. If K is set to a higher value, the algorithm becomes more robust to noise in the data. The KNN algorithm makes predictions based on the majority class of its nearest neighbors [67]. This algorithm can handle both binary and multi-class classification issues.

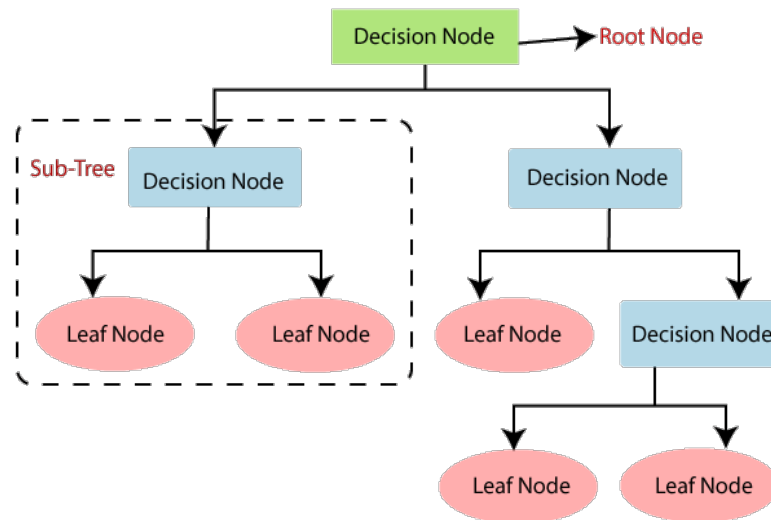


Figure 3.8: Decision Tree Classification.

3.4.3 Decision Tree

A Decision Tree is a popular machine-learning algorithm for our desired regression problems [67]. A tree-based algorithm divides the input feature space into smaller regions based on certain conditions. Each node in the tree represents a test on an attribute, and the branches represent the possible outcomes of that test. The final leaves of the tree represent the prediction of the target variable. The prediction is based on most of the target values of the nearest data points in the region represented by that leaf [69].

The Decision Tree algorithm recursively builds the tree, starting from the root and then splitting the data into subsets based on the test at each node. The attribute that results in the best split is chosen for each node until a stopping criterion is met, for example, The peak tree depth or a minimum quantity of samples present in a zone. The Decision Tree algorithm can be predicted by starting from the root and then traversing down the tree based on the test conditions at each node until a leaf is reached. The prediction for the new data point is then given by the target value associated with the leaf.

3.4.4 Random Forest

Random Forest is an ensemble learning method for regression in machine learning. It is a type of decision tree algorithm that creates a forest of decision trees and combines the prediction of each tree to arrive at the final prediction [67].

In a Random Forest, multiple decision trees are created from random data set samples. The samples are selected with replacement, known as bootstrapping, and the features

are also selected randomly at each split in the decision tree. This means that each decision tree in the forest has a different combination of data points and features, leading to diversity in the trees and improved prediction accuracy.

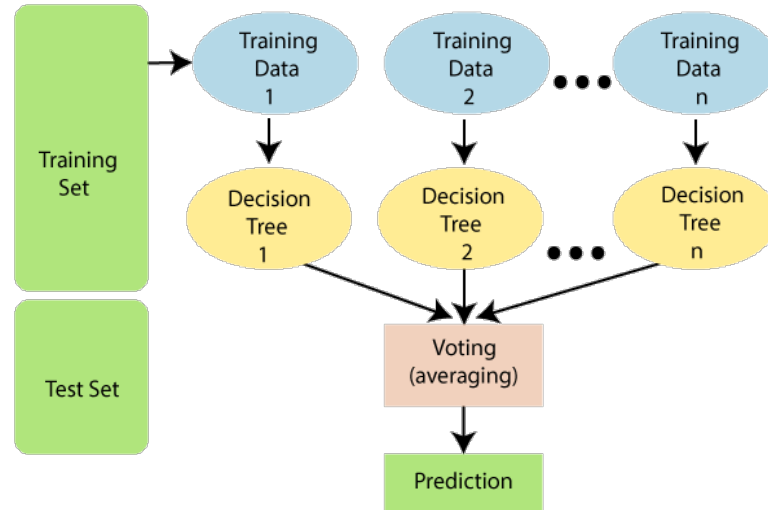


Figure 3.9: Random Forest Tree Classification.

Finally, the trees' predictions in the forest are combined using majority voting or taking the average, depending on whether the problem is a classification or regression task. Random Forest is a robust algorithm that can handle missing values and outliers in the data and is less prone to overfitting than a single decision tree. It is widely used for classification, regression, feature selection, and outlier detection tasks.

3.4.5 Artificial Neural Network (ANN)

Artificial Neural Network (ANN) is based on the human brain's structure and function designed to mimic its complex interconnected neurons to process and learn from input data. It is a complex network of artificial neurons (also known as artificial nodes) connected to form an extensive, interconnected system. ANNs can be used to perform a variety of tasks, including pattern recognition, decision-making, and data classification [70].

An artificial neuron is a simple processing unit that takes input from one or more sources, performs a computation on that input, and produces a single output. These outputs are then used as inputs to other neurons in the network, allowing the information to be processed and analyzed in multiple stages. The inputs to an ANN are typically numerical values representing an object's or data point's characteristics. Each neuron in the network is connected to one or more input neurons, and the strength of these

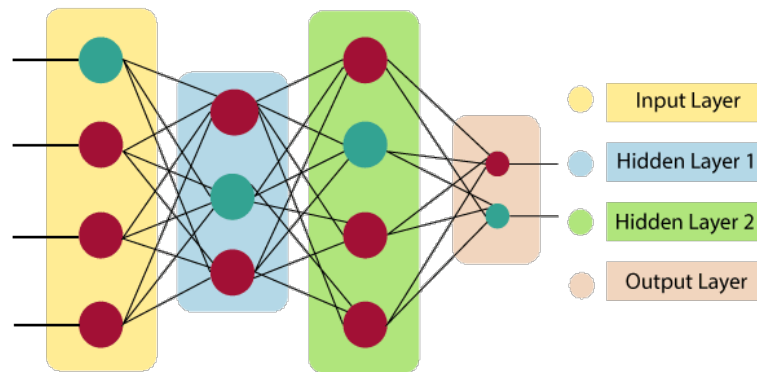


Figure 3.10: General Artificial Neural network representation

connections is determined by the weights assigned to them [71]. The weight of each connection is adjusted during the learning process so that the network can learn to make accurate predictions.

The most critical component of an ANN is its activation function. The activation function converts the inputs and weights into a single output value [72].

Typical activation functions comprise the sigmoid function, the hyperbolic tangent function, and the rectified linear unit (ReLU) function, which is defined as follows: [73] [74] [75]

$$\text{Sigmoid} : \sigma(z) = \frac{1}{1 + e^{-z}} \quad (3.16)$$

$$\text{HyperbolicTangent}(\text{Tanh}) : \sigma(z) = \frac{e^z - e^{-z}}{e^z + e^{-z}} \quad (3.17)$$

$$\text{RectifiedLinearUnit}(\text{ReLU}) : \sigma(z) = \max(0, z) \quad (3.18)$$

Once the input values have been transformed into outputs by the activation function, they are used as inputs to other neurons in the network.

This process continues until the final output layer is reached, at which point the network has produced a prediction for the input data. The learning procedure within an ANN involves fine-tuning the connection weights among the neurons present in the network. This is typically carried out using optimization techniques like gradient descent, which adapt the weights depending on the difference between the network's predicted outcomes and the actual target values.

Several types of ANNs include feedforward networks, recurrent networks, and convolutional neural networks. Feedforward networks are the simplest type of ANN, in which the data flows through the network in a single direction from input to output.

On the other hand, Recurrent networks allow information to flow in loops, allowing the network to retain information from previous time steps. One of the critical benefits of ANNs is their ability to learn from large amounts of data. This makes them well-suited for various applications, including image recognition [76], natural language processing [77], and financial forecasting [78]. They can also be used for non-linear regression, which involves fitting a curve to data that does not follow a straight line. Another advantage of ANNs is their ability to learn and make predictions despite multiple inputs and outputs. This makes them well-suited for complex tasks such as speech recognition, where the output is a sequence of words, and the inputs are audio signals.

3.5 Chapter Summary

In this background chapter, we have explored the optical properties of photonic crystal fibers (PCFs) and the application of machine learning algorithms in their analysis. We discussed the unique characteristics of PCFs, such as customized dispersion, strong nonlinearity, and significant effective mode area, and their importance in various applications, including optical communication and dispersion compensation. Furthermore, we delved into the role of machine learning algorithms. Emphasizing the growing significance of machine learning techniques in fields like photonics, we highlighted their application in studying and predicting the optical properties of PCFs with greater accuracy and efficiency, overcoming the limitations of traditional numerical methods that require substantial computational resources. By summarizing this background chapter, we have showcased the interplay between the optical properties of PCFs and the potential of machine learning algorithms to enhance their analysis. This foundation sets the stage for our main research question and methodology, which aims to predict the optical properties of negative dispersion-compensating PCFs using machine learning techniques.

Chapter 4

Proposed System

This chapter focuses on designing and modeling Photonic Crystal Fiber (PCF) structures and their effectiveness in mitigating dispersion in the context of optical communication systems. The goal is to create and analyze PCF lattice structures to determine their efficiency in compensating for dispersion. The design process uses the latest COMSOL Multiphysics software, version 5.0. The software provides a comprehensive platform for analyzing various optical and mechanical properties of the PCF structures. The outcome of this study will contribute to the advancement of optical communication systems and provide insights into the design of efficient PCF structures for dispersion compensation.

4.1 Modeling flow chart using COMSOL Multiphysics

Modeling Photonic Crystal Fiber (PCF) structures using COMSOL Multiphysics software typically involves several steps.

- The geometry of the PCF, including the core and cladding regions, the arrangement of holes, and the size and spacing of the holes, is defined.
- The appropriate materials for the core and cladding regions are chosen.
- The simulation parameters, such as the type of analysis (e.g., eigenvalue, time-domain), wavelength range, boundary conditions, and mesh density, are set up.
- The necessary boundary conditions, such as the effective index of the core and cladding regions and the refractive index of the surrounding material, are applied to the simulation.

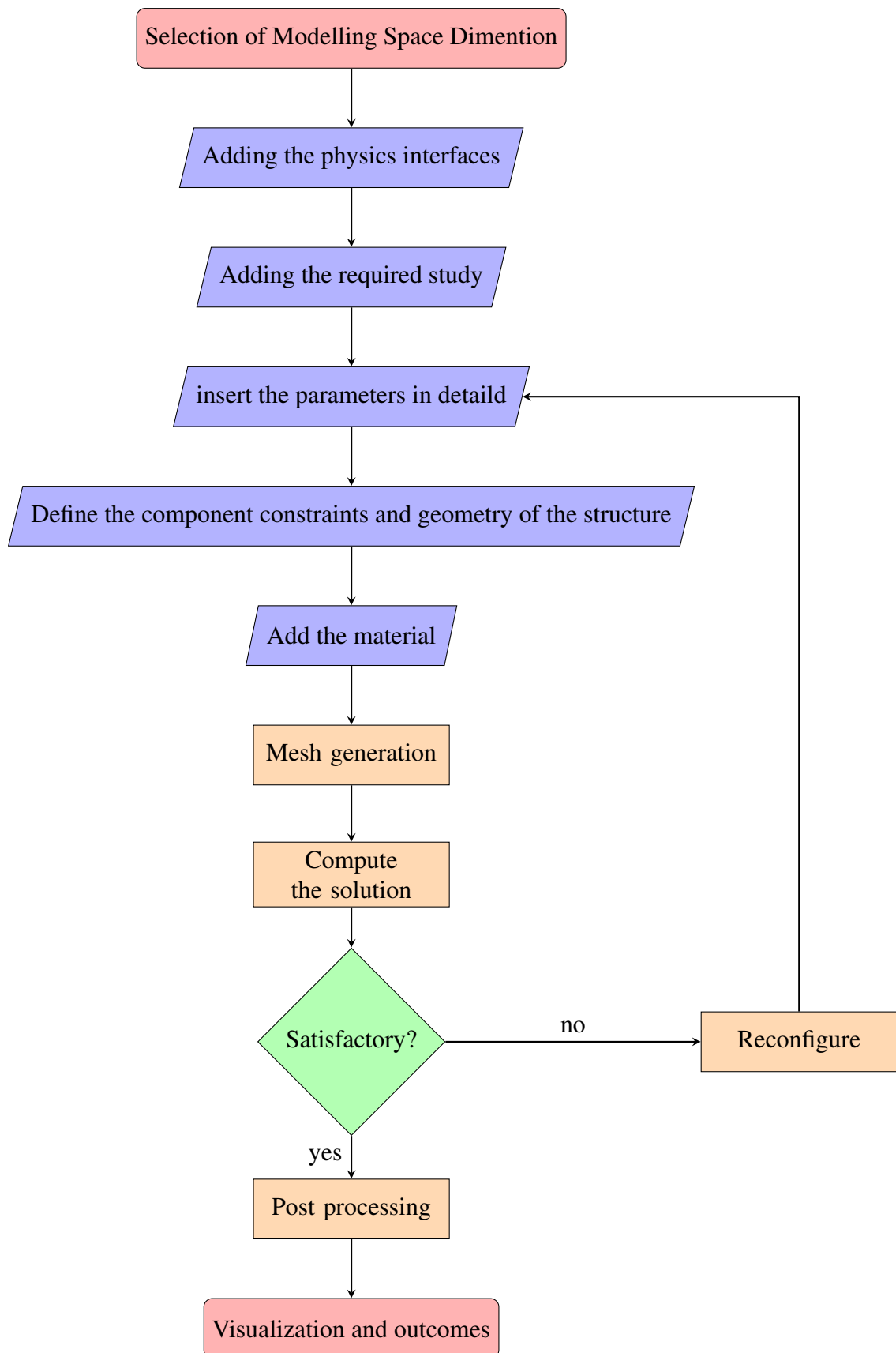


Figure 4.1: Flowchart for COMSOL MultiPhysics Modeling Process

- The eigenmodes of the PCF are solved using the finite element method.
- The dispersion characteristics of the PCF, such as the effective index, mode area, and confinement loss, are extracted.
- The results are analyzed to assess the performance of the PCF design, and any necessary changes to the geometry or material properties are made.
- The simulation and analysis process is repeated until the desired performance criteria are met.
- The final design is saved, and the relevant results are exported for further analysis and optimization. These are the general steps in designing a Photonic Crystal Fiber using COMSOL. The exact details and complexity of each step will depend on the specific requirements of the PCF design and the user's experience. The modeling steps are depicted in Figure 4.1 as a flow chart.

4.2 New Model Creation

One has the option of either choosing a model from the Model Wizard or creating one from scratch using a Blank Model.

4.2.1 Model Wizard-Assisted New Model Creation

The steps involved in selecting the space dimension, physics, and study process within Model Wizard are:

step-1: Choose from the available spatial dimensions, including 3D, 2D Axisymmetric, 2D, 1D Axisymmetric, 1D, or 0D, as shown in the figure 4.2.

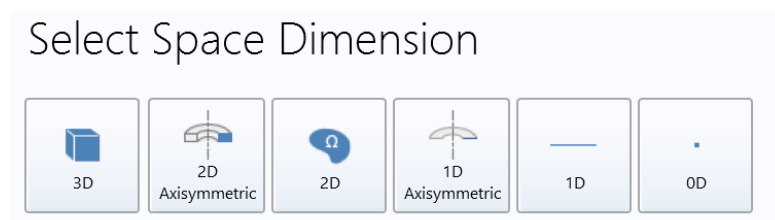


Figure 4.2: Choosing a Space Dimension.

Step-2: Choose one or multiple physics from the categorized Physics block as section in the figure 4.3.

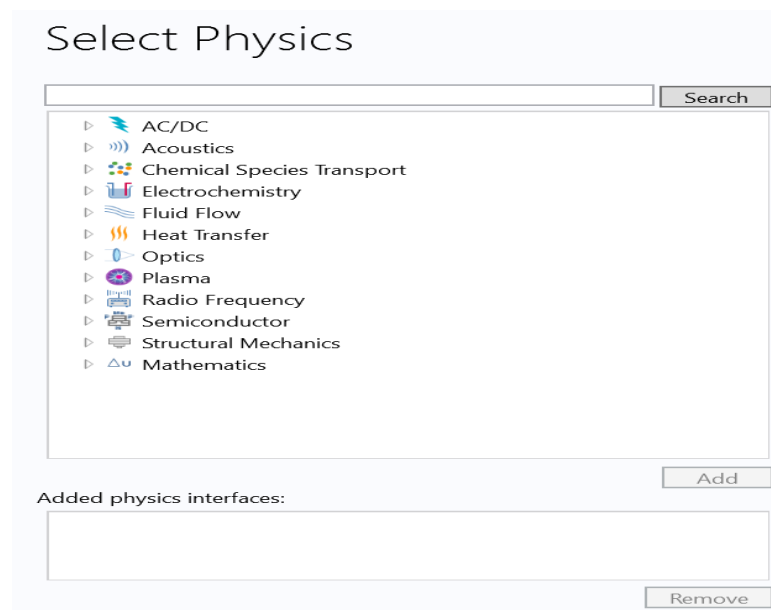


Figure 4.3: Options in physics selection.

Step-3: Choose a Study from the Study section, then click "Done." This will display a blank model on the desktop.

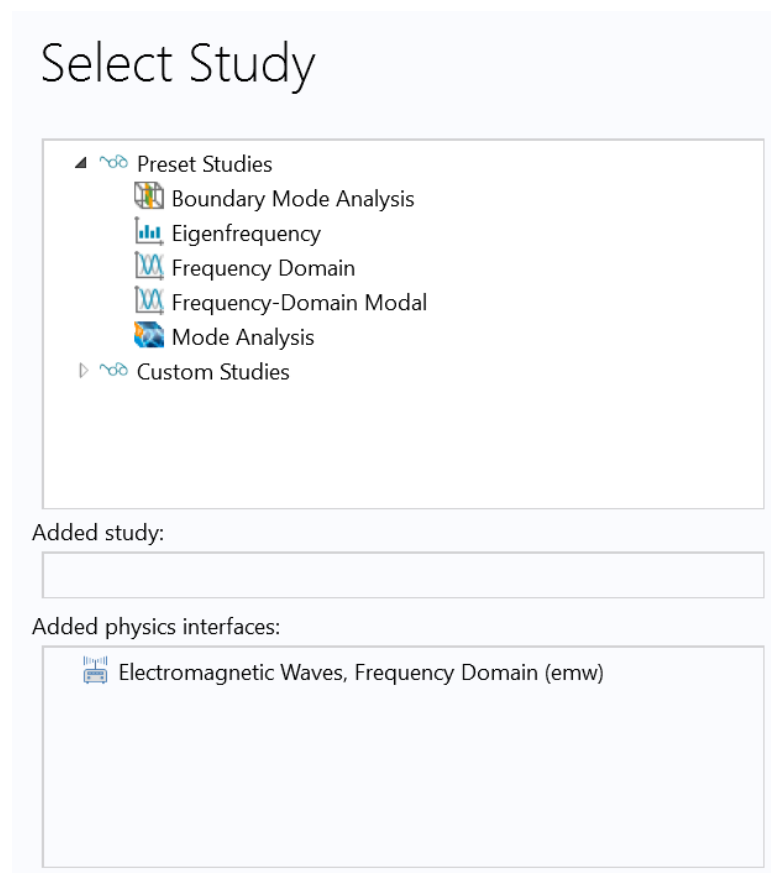


Figure 4.4: Options in study selection.

4.2.2 Utilizing Blank Model for Crafting a Novel Model

It's possible to skip the Model Wizard steps and directly create a blank model by can choose a model from the Model Wizard or create.

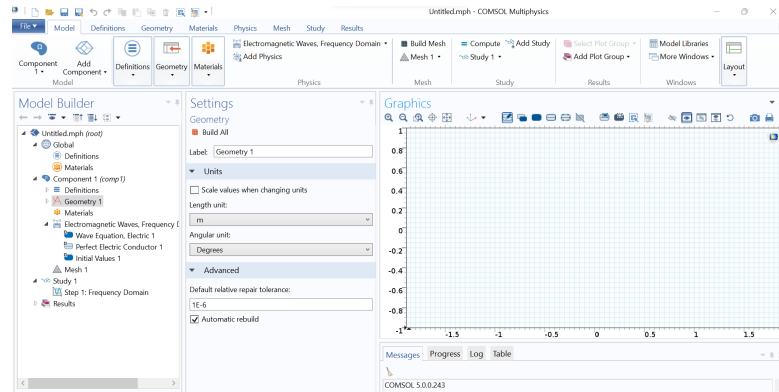


Figure 4.5: Constructing a novel model from the basic framework.

4.3 Attributes, Variables, and Extent

4.3.1 Global Definition

The Global Definition section allows the user to specify their parameters by defining the name, expression, and value of the parameters.

4.3.2 Geometry Unit

The user can choose the geometrical structure in the geometry section by right-clicking on the mouse. The size and shape of the object can also be defined easily in this section. The directory of a user file path for the windows operating system is: C:\ProgramData\Microsoft\Windows\Start Menu\Programs\COMSOL Multiphysics 5.0

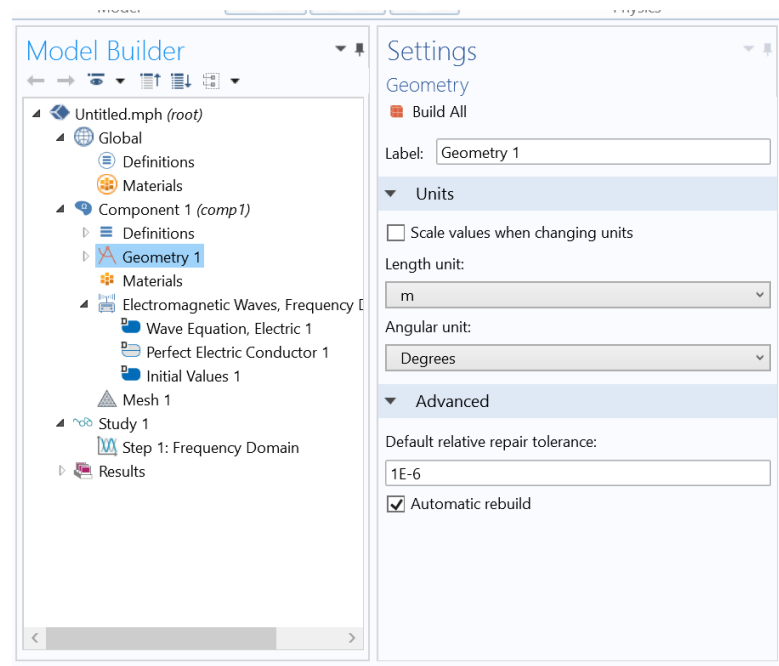


Figure 4.6: Select the Geometry.

4.3.3 Materials Selection and Considerations

Choose a material from the materials library, which can be found in the component or node block, as depicted in figure 4.7.

Choose the "Add Materials" block. Materials can be added in a two-step process:

Step-1: Select the Home tab from the ribbon and click "add material."

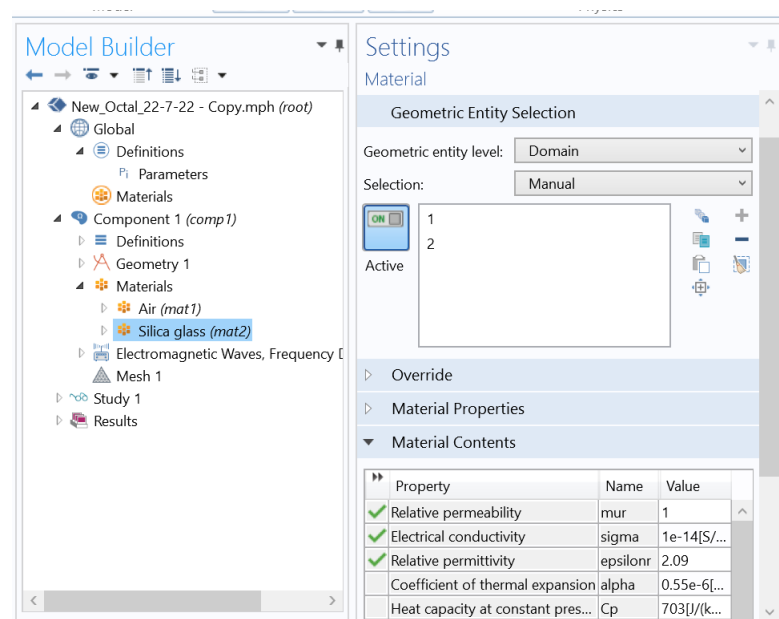


Figure 4.7: Material selection.

Step-2: In the Model Builder, right-click on "Comp. 1_Materials" and choose "Add Material."

4.3.4 Selecting Boundaries and Addressing Geometric Factors in Design

One can choose a boundary from the "electromagnetic waves frequency domain." If a boundary is not chosen, its color will usually be 'gray'. If a boundary is chosen, it will appear 'blue'. To select the boundary condition, choose the electromagnetic waves frequency domain first, then right-click and select the 'boundary'. This is illustrated in figure 4.7.

4.3.4.1 Executing mesh condition

The mesh selection specifies the element size and sequence type, as demonstrated in Figure 4.8.

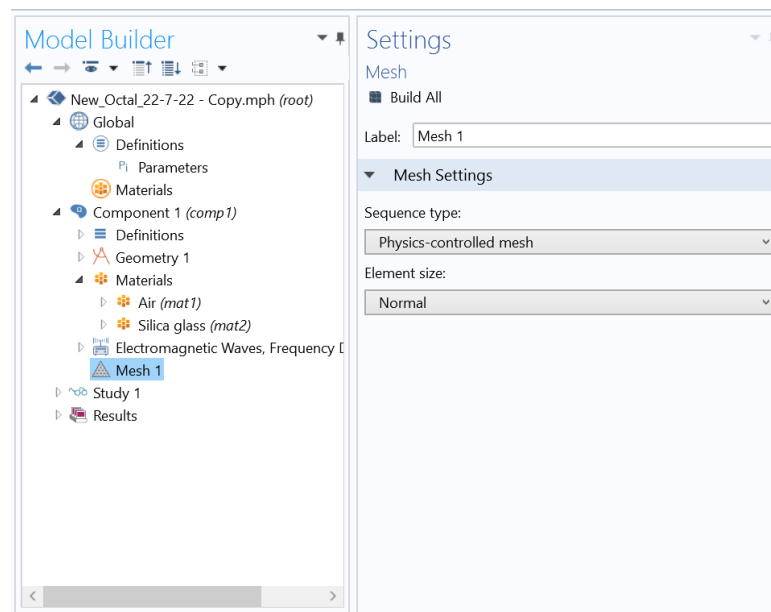


Figure 4.8: Mesh analysis.

4.3.4.2 Executing the study condition

The final step involves specifying the conditions for analysis, such as the mode frequency and number, displayed in figure 4.9.

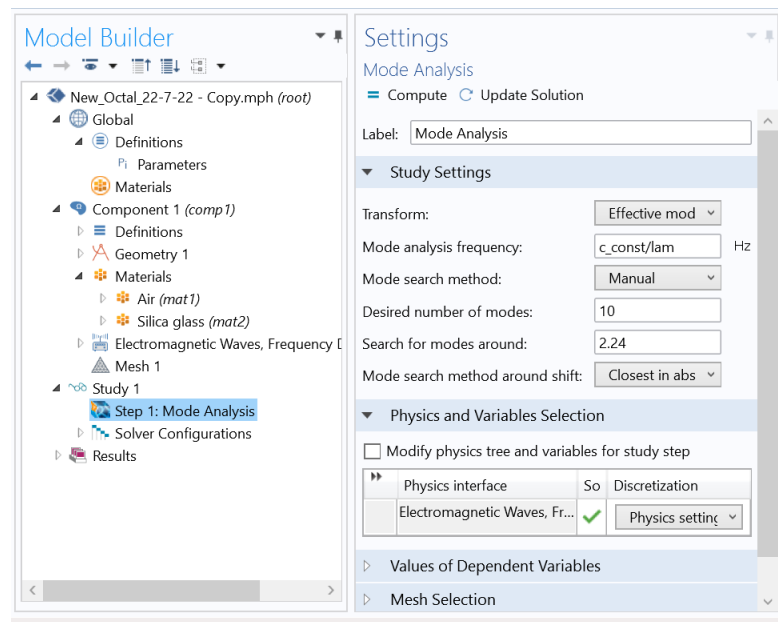


Figure 4.9: Perform the study.

4.3.5 Design Specifications for PCF Lattice Structure

The table shows the values of different parameters used in Comsol MultiPhysics software.

Table 4.1: Parameters and values in Comsol MultiPhysics

Parameter	Value
Pressure	1 atm
Boundary thickness	0.01 m
Temperature	293.15 K
Boundary condition	Transition Boundary Condition
Material-1	Silica Glass
Material-2	Air

4.3.5.1 Label: Material properties

4.3.5.2 Label: Frequency domain analysis of electromagnetic waves

The effective mode index (EMI) measures how the waveguide’s propagation constant compares to the free space propagation constant. In other words, it quantifies how much the waveguide affects the speed of light compared to free space. The effective index can vary depending on the specific excited mode in the waveguide, and multiple effective indices can exist for a single waveguide system. The wave equation for effective mode

Table 4.2: Properties of airs used in the model

Property	Name	Value	Unit	Property group
✓ Relative permeability	mur	1	1	Basic
✓ Relative permittivity	epsilon _{nr}	1	1	Basic
✓ Electrical conductivity	sigma	0[S/m]	S/m	Basic
Dynamic viscosity	mu	eta([1/K])[Pa*s]	Pa*s	Basic
Ratio of specific heats	gamma	1.4	1	Basic
Heat capacity at constant pressure	C _p	C _p (T[1/K])[J/(kg*...]	J/(kg*K)	Basic
Density	rho	rho(pA[1/Pa],T[1...]	kg/m ³	Basic
Thermal conductivity	k	k(T[1/K])[W/(m*K)]	W/(m-K)	Basic
Speed of sound	c	cs(T[1/K])[m/s]	m/s	Basic
Refractive index	n	1	1	Refractive index
Refractive index, imaginary part	ki	0	1	Refractive index

Table 4.3: Properties of silica used in the model

Property	Name	Value	Unit	Property group
✓ Relative permeability	mur	1	1	Basic
✓ Electrical conductivity	sigma	1e-14[S/m]	S/m	Basic
✓ Relative permittivity	epsilon _{nr}	2.09	1	Basic
Coefficient of thermal expansion	alpha	0.55e-6[1/K]	1/K	Basic
Heat capacity at constant pressure	C _p	703[J/(kg*K)]	J/(kg*K)	Basic
Density	rho	2203[kg/m^3]	kg/m ³	Basic
Thermal conductivity	k	1.38[W/(m*K)]	W/(m-K)	Basic
Young's modulus	E	73.1e9[Pa]	Pa	Young's modulus and Poisson's ratio
Poisson's ratio	nu	0.17	1	Young's modulus and Poisson's ratio
Refractive index	n	1.47	1	Refractive index
Refractive index, imaginary part	ki	0	1	Refractive index

analysis is the Helmholtz equation. It is a partial differential equation describing electromagnetic or acoustic wave propagation in a homogeneous, isotropic medium. The equation is given by:

$$\nabla^2 \phi(r, t) + k_0^2 \phi(r, t) = 0 \quad (4.1)$$

where $\phi(r,t)$ is the wave field, k_0 is the wavenumber, and ∇^2 is the Laplacian operator. This equation can be solved in the frequency domain to find the effective mode indices of the waveguide. The effective mode indices can then be used to calculate the dispersion properties of the waveguide, such as group velocity and chromatic dispersion.

4.3.5.3 Label: Mesh and Mode Analysis

In mesh analysis, the PCF structure is divided into a grid of small cells, and numerical methods like the finite difference method (FDM), finite element method (FEM), or the beam propagation method (BPM) are used to solve the electromagnetic equations that govern the traveling of light through the PCF. Mode analysis of photonic crystal fiber (PCF) includes the study of the modes of electromagnetic wave propagation in the fiber structure. PCFs have a unique cross-sectional geometry with air holes arranged periodically, resulting in a photonic bandgap prohibiting the propagation of specific frequencies.

Physics controlled Mesh.

Element size: Finer

Mode Analysis Frequency: variable GHz

Mode search method: Manual

Desired Number of Modes: 10

4.3.5.4 Label: Eigenvalue Solver

In the context of photonic crystal fibers (PCFs), eigenvalue solvers are used to calculate the propagation constants and modes of light inside the fiber. Several numerical techniques are employed by these solvers to solve Maxwell's equations governing the electromagnetic field inside the PCF. The eigenvalue solvers can handle complex PCF structures, including non-uniform and anisotropic fibers, and provide accurate and efficient solutions for the propagation constants and modes of the fiber.

Relative solver: $1 \times e^{-6}$

Eigenvalue Transformation: Effective mode index

Desired number Eigenvalues: 6

4.3.5.5 Mode analysis solver

Mode analysis solver is a numerical method used to determine the mode characteristics of photonic crystal fibers (PCFs). It involves solving Maxwell's equations in a periodic structure of the PCF using numerical techniques. Mode analysis solver is a numerical method to model photonic crystal fibers (PCF) characteristics. It involves solving Maxwell's equations in a periodic structure of the PCF using numerical techniques.

4.4 Design of Proposed PCF Model

Electromagnetic mode analysis studies the behavior of electromagnetic waves in a photonic crystal fiber (PCF) structure. It involves calculating the waveguide's effective mode index (EMI) and determining the wave equation that describes the propagation of the waves in the PCF. This analysis requires a fine mesh to capture the electromagnetic field distribution in the structure accurately. The analysis can be performed using a high-performance solver capable of solving large sparse linear equations. The results of this analysis can provide valuable information about the transmission and confinement properties of PCF structures and can be used to optimize their design for specific

applications.

Structure

Figure 4.10 illustrates the proposed PCF structure. This innovative proposed design is characterized by air holes (depicted in white) that are strategically embedded within a silica material (shown in maroon). The figure also includes a sky-blue-colored region, which represents the Perfectly Matched Layer (PML) of the PCF. The design highlights a cladding region that comprises six rectangular air cavities and one hexagonal air cavity. These air chambers, which are all circular, play a critical role in the PCF's overall design and performance. The primary design considerations for this PCF are the diameters and pitches of the air holes, as they significantly impact the fiber's optical properties. The proposed structure was modeled using a widely available simulation tool COMSOL Multiphysics 5.0.

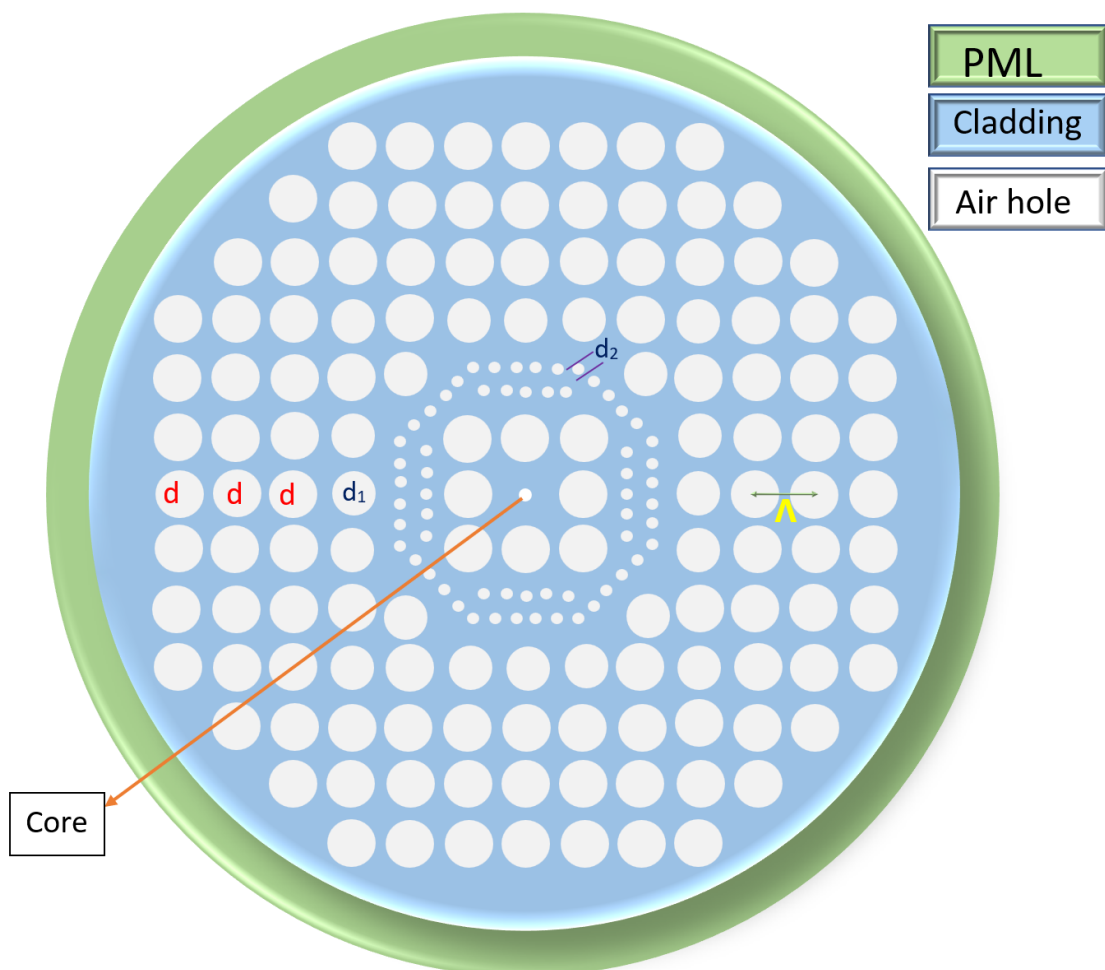


Figure 4.10: Cross-sectional perspective of proposed PCF for dispersion mitigation.

Design Parameters

In the context of Photonic Crystal Fiber (PCF) design, the term "pitch" (denoted by Λ) refers to the distance between two air cavities situated within the same layer or ring of the fiber. This parameter plays a vital role in determining the optical properties and performance of the PCF. The proposed design has two types of air cavities with distinct pitches: rectangular and hexagonal. For the rectangular air holes in the cladding region, the pitch is $\Lambda = 0.8415 \mu\text{m}$. On the other hand, the hexagonal air cavities have a smaller pitch of $\Lambda = 0.225 \mu\text{m}$. These differences in pitch values contribute to the unique configuration of the fiber, resulting in specific optical characteristics. In addition to pitch, the diameter of the air holes is another crucial design aspect. The rectangular air holes have a diameter of $d = 0.8 \mu\text{m}$, while six are slightly smaller, with a diameter of $d_1 = 0.6 \mu\text{m}$. The hexagonal air holes possess a diameter of $d_2 = 0.225 \mu\text{m}$. Furthermore, the PCF features a core diameter of $d_0 = 0.12 \mu\text{m}$, a critical parameter for controlling the fiber's guiding properties. The pitch and diameter values of the air cavities in the proposed PCF design are essential parameters that directly impact the fiber's optical performance. Optimizing these values allows the PCF to meet specific requirements in various optical communication applications.

Perfectly matched layer (PML) To minimize nonphysical scattering, the PCF structure incorporates an asymmetric circular PML with a thickness that is 6% less than the outer layer. The inner and outer radii of the PML are $6.2 \mu\text{m}$ and $6.6 \mu\text{m}$, respectively. The PML enhances the PCF's performance by reducing scattering effects.

Background Material The background material for the proposed PCF structure was selected as silica due to its exceptional optical transmittance. Using silica ensures that the PCF can efficiently transmit light over a broad wavelength spectrum, making it suitable for various applications in optical communication systems.

4.4.1 Mesh Analysis

The finite element method (FEM) and adaptive meshing techniques are employed in this study to solve Maxwell's equations and control errors in the analysis of the proposed Photonic Crystal Fiber (PCF) structure. By focusing on a frequency range from 1340 to 1700 nm, the study aims to determine the effective refractive index of the PCF for various wavelengths within this range. The FEM analysis is carried out for each triangle-shaped section of the mesh, allowing more accurate calculations of the fiber's optical properties.

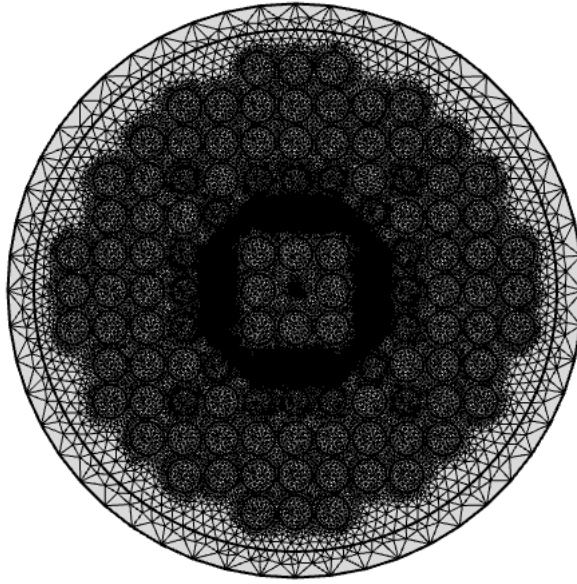


Figure 4.11: Mesh analysis of proposed structure

Scattering boundary conditions are applied to the cladding region of the PCF to prevent leaky mode reflections from entering the fiber's core, ensuring more accurate results in the simulation. The finalized geometry of the PCF consists of 195 domains, 784 boundaries, and 784 vertices. The full mesh comprises 53,866 triangular domain elements and 5,696 boundary elements. The mesh's characteristics include a total element area ratio of 4.72×10^{-4} , a minimum element quality of 0.6603, an average element quality of 0.9407, and a mesh area of $1.367 \times 10^{10} \text{ m}^2$. These mesh properties ensure the accuracy and precision of the FEM analysis.

The proposed PCF structure offers significant improvements over previous designs regarding optical properties. The cladding region of the fiber is made of solid silica materials with a higher refractive index (RI) than the core. This design choice enhances the guiding properties of the fiber and results in better overall performance. The finite element method and adaptive meshing techniques effectively analyze the proposed PCF structure, enabling a more accurate understanding of its optical properties. The resulting design offers substantial improvements over previous PCF designs and demonstrates the potential for enhanced performance in various optical communication applications.

4.4.2 Electric Field Distribution

The electric field distribution, E , is obtained by solving an eigenvalue problem derived from Maxwell's equations. It is well-established that light is primarily confined within the central core region in the optimal ray-passing model, meaning that the highest mag-

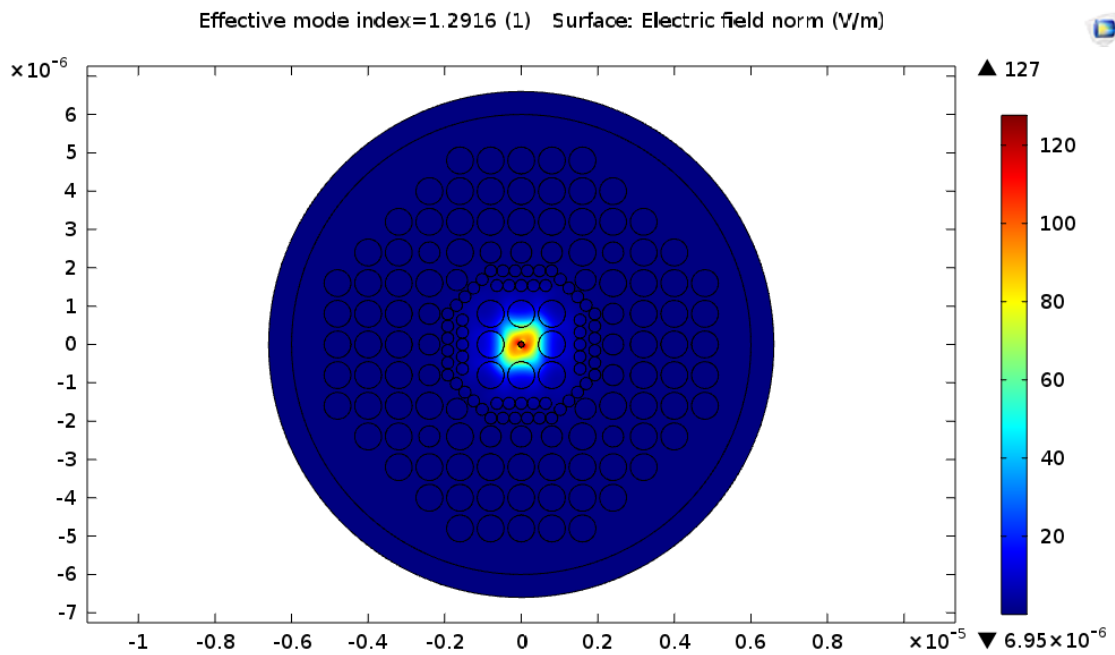


Figure 4.12: Electric field distribution of proposed structure

netic field density is present in the core for a specific model. The effective mode index is altered for a given wavelength to achieve the best possible outcome, identifying the configuration that allows the most light to pass through the central region. This process determines the desired value of the compelling mode index for any given wavelength. COMSOL Multiphysics software offers a numerical approach for simulating the electric field using the finite element method (FEM) [4]. Through FEM calculations, the electric field intensity and distribution can be visualized, considering the practical dimensions and material properties of the electro-spinning setup.

Figures 4.13 and 4.14 illustrates the fundamental mode distribution along the X and Y axes at an operating wavelength of $1.5\mu\text{ m}$. These visual representations indicate that the X-polarized and Y-polarized mode fields are effectively confined within the fiber's core. This effective confinement is primarily attributed to the higher core index than the cladding region.

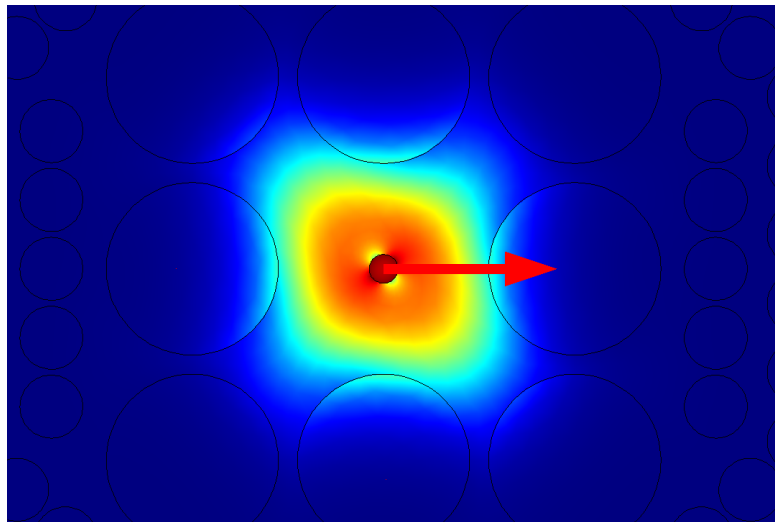


Figure 4.13: Fundamental field distribution in X-axis

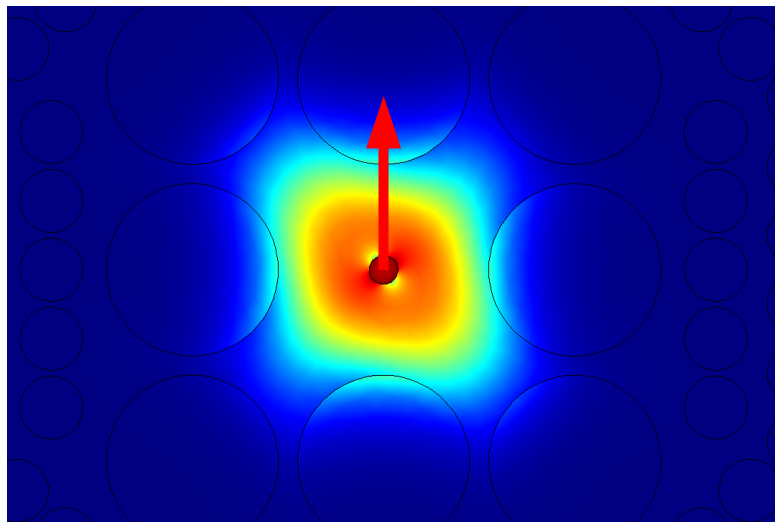


Figure 4.14: Fundamental field distribution in Y-axis

The proposed PCF design exhibits a strong dependence of dispersion on several factors, including the pitch, size, and location of the air channels within the fiber structure. By carefully adjusting these parameters, the optical properties and performance of the PCF can be optimized for various applications in optical communication systems. This highlights the importance of understanding the interplay between these factors when designing PCFs to ensure optimal performance and desired characteristics.

Figure 4.15 displays the three-dimensional electric field distribution, also known as power intensity profiles, for the PCF at a wavelength of $1.55 \mu\text{m}$. The analysis reveals that the peak intensity value is located at the core's center, suggesting that the electric field is effectively confined within the core region of the PCF. This observation indicates

that the PCFs are designed to ensure strong electric field confinement to the core, which is crucial for efficient optical communication systems. The plot also provides insights into the power flow for the proposed PCF.

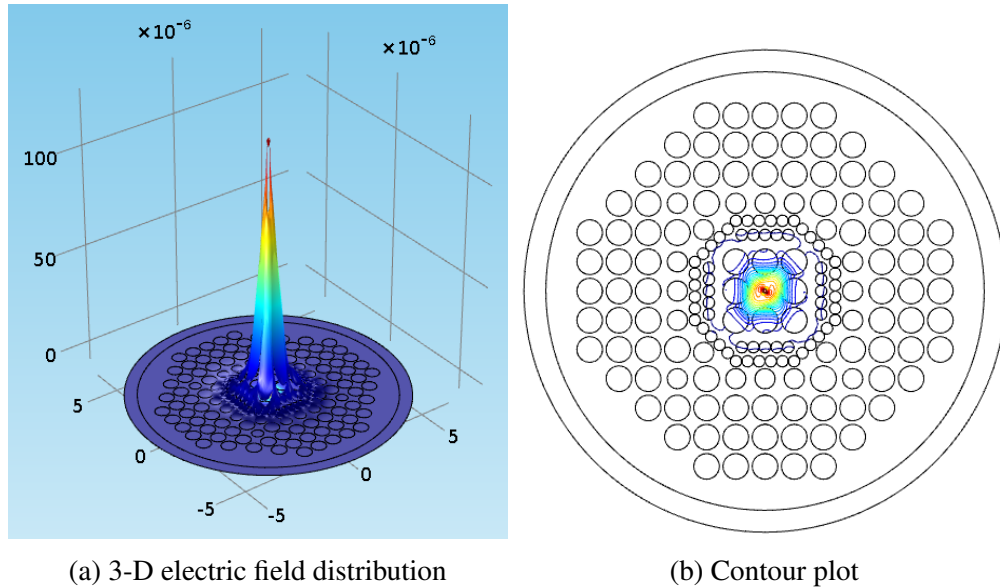


Figure 4.15: Mode profile of proposed PCF

4.5 Utilizing Machine Learning to Model PCF

The proposed research requires quantitative information, which calls for creating a dataset. Several simulation steps were taken to generate this dataset, and specific preprocessing steps, such as handling noisy or inconsistent data and assessing the correlation between different variables. These steps ensure the dataset is clean, reliable, and suitable for further analysis or application of various techniques, such as machine learning algorithms, to extract valuable insights and make accurate predictions. Proper data preprocessing is crucial for the success of any data-driven research or modeling, as it directly impacts the results' quality.

4.5.1 Dataset Generation

The designed Photonic Crystal Fiber (PCF) undergoes simulation to generate a finite and accurate dataset. The effectiveness of machine learning models is highly dependent on the data's quality, type, and correlation. This dataset consists of 454 rows and 11 column values, which are used for further processing. For predicting output properties such as effective mode index (n_{eff}), dispersion (D), V-parameters (V_{eff}), effective mode

area (a_{eff} , and confinement loss, input design parameters like pitch, wavelength, size of core air holes, and diameters of holes (in both circular and hexagonal patterns) within the silica region are adjusted. The machine learning models can optimize the PCF design based on the provided dataset. The input design parameters are modified in the following manner:

Table 4.4: Input parameters of machine learning model

Parameter	Range	Step
Pitch	0.75-0.88 μm	0.01
Diameter of core	0.067-0.15 μm	Random
Diameter of octagonal pattern air hole	0.3-0.39 μm	Random
Diameter of closely attached air hole	0.68-0.96 μm	Random
Diameter of rectangular pattern air hole	0.63-0.88 μm	Random
Wavelength	1.18-1.75 μm	0.03

4.5.2 Pre-processing of Dataset

The relationship between two quantitative attributes can be visualized using a correlation matrix heatmap, as depicted in Figure 4.16. Examining the correlation matrix helps identify six significant, unique input features that correlate more with the PCF output optical features. These features include input design parameters like pitch, wavelength, size of core air holes, and diameters of holes (in both circular and hexagonal patterns). Figure 4.16 demonstrates that attributes with a strong relationship yield a high correlation value, while those with a weak relationship exhibit a low correlation value. The process involves randomizing the dataset and standardizing its features. The dataset contains features with different value ranges, which can be problematic for neural network modeling. To address this issue, we applied MinMax normalization, which scales the data to fit within a [0,1] range. This enhances the model's precision and shortens training time [33]. Furthermore, categorical attributes, such as PCF types with text values, are converted to integers using label encoding. Randomizing the dataset: It is shuffled or randomized to avoid any biases. This ensures the data points are in random order and not arranged to favor any particular set of values. This is important because biases in the data could lead to a machine-learning model that doesn't generalize well to new, unseen data. Eliminating the mean: This step involves calculating the mean (average) value for each feature in the dataset and subtracting the mean from each data point. This process is also known as "centering" the data. This gives the features a mean of zero, which helps ensure that the features are on a comparable scale and that no single feature dominates the learning process. Scaling to unit variance: After centering the data, the next step is to scale the features to have a standard deviation (or

variance) of 1. This is achieved by dividing each data point by the standard deviation of the corresponding feature. This step is known as "normalizing" or "standardizing" the data. Scaling the features to unit variance ensures that all features have the same importance in the learning process and that the model is not biased toward features with larger magnitudes.

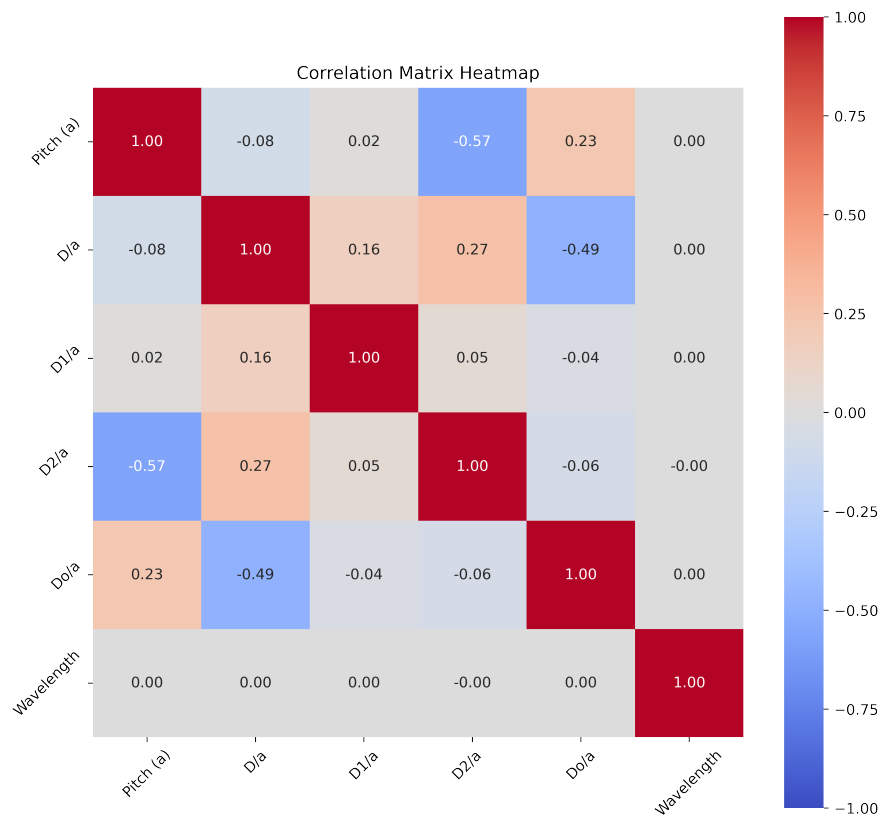


Figure 4.16: Analyzing the relationships between attributes using a heatmap of the correlation matrix.

By following these preprocessing steps, the dataset will have more uniform and comparable features, which is essential for many machine learning algorithms to work effectively. This helps to improve the performance and generalization of the resulting model. In this scenario, the data is divided into three distinct sets: training, validation, and test sets. These sets are used to build, fine-tune, and evaluate the model's performance. The data is distributed in proportions of 80%, 10%, and 10%, respectively, meaning 80% is used for training, while the remaining 20% is evenly split between validation and testing.

4.5.2.1 Scatterplot Matrix of Features and Target Variables

This scatterplot 4.17 and 4.18 matrix displays the pairwise relationships between the feature variable and the five target variables. Each scatterplot depicts the relationship between one feature variable and one target variable, allowing us to visually inspect the dependence of the target variables on the features. From all of the figure, it is clear that all output feature has a linear relation with the diameter of core, air holes of cladding region and pitch. But all of them follow a polynomial relationship with respect to the wavelength. The optical output properties greatly depend on the air hole size of the closely attached rectangle formation. The impact of input features is also analyzed from this where pitch has lower impact with respect to the air hole size or core size.

We can assess the data's correlations, trends, and potential outliers by examining the scatterplots. The plots can help us identify whether linear, quadratic, or more complex relationships exist between the features and targets. Furthermore, the scatterplot matrix can help us determine if there are any interactions between the features or the targets, which could have implications for our modeling efforts.

4.5.3 Modelling of Machine Learning Algorithm

Using Regression Model

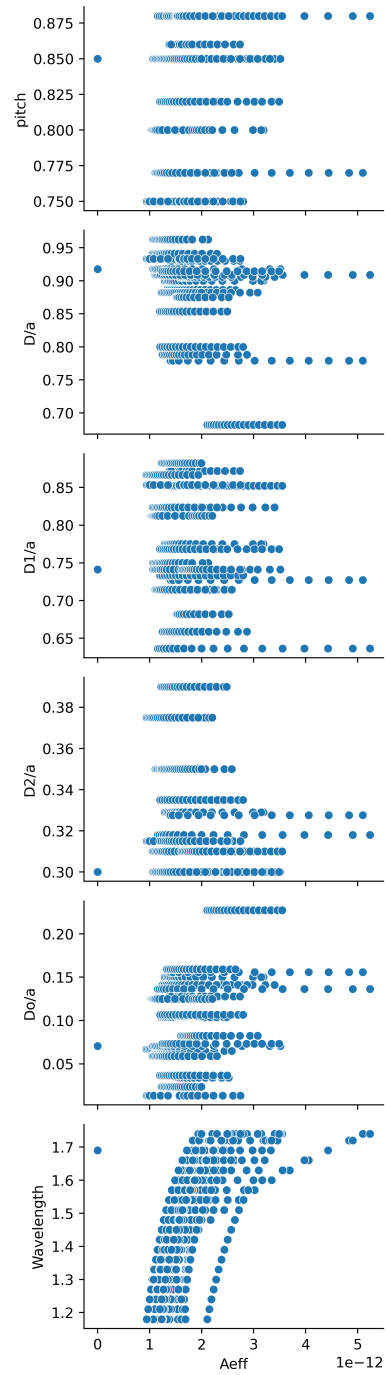
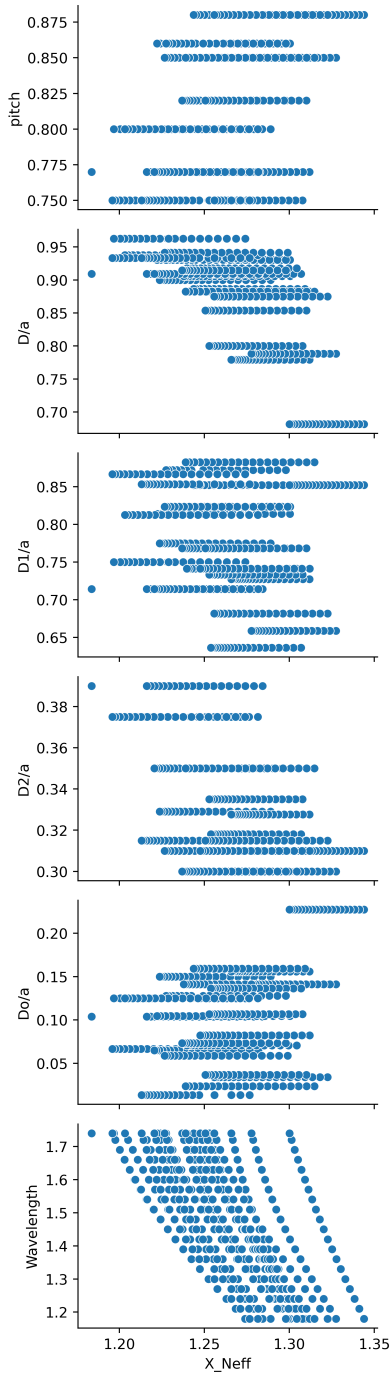
Firstly, the database trains four different regression models on the provided training data and saves them as files for later use. Four different regression models, Linear regression (LR), K-nearest neighbor (KNN), Decision Tree (DT), and Random Forest Tree (RT), are used to evaluate the optical properties of the proposed PCF. Various machine learning algorithms, including Linear Regression (LR), K-Nearest Neighbor (KNN), Decision Tree, and Random Forest Tree, have been utilized to predict optical properties. In the case of linear regression, the fit-intercept option is set to 'True' during construction. The KNN algorithm is designed with five neighbors and uses the Minkowski Distance Metric. A uniform weight is also applied to ensure equal weighting for all points within each neighborhood. The decision tree algorithm chooses the optimal splitting strategy at each node. The squared-error criterion is employed to evaluate the quality of each split. As for the Random Forest Tree, it is built using 100 trees and adopts a criterion similar to that of the Decision Tree.

The entire process is illustrated in figure 4.19. For each of the four models, the following steps are executed:

Instantiate the model: A new instance of the model is created by calling its class con-

Scatterplot Matrix of Next Target vs Features

Scatterplot Matrix of Next Target vs Features



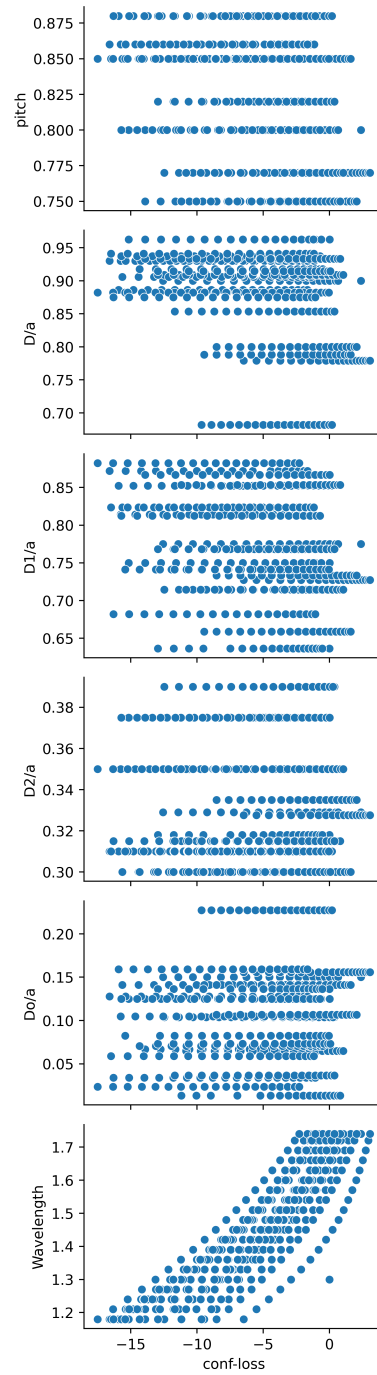
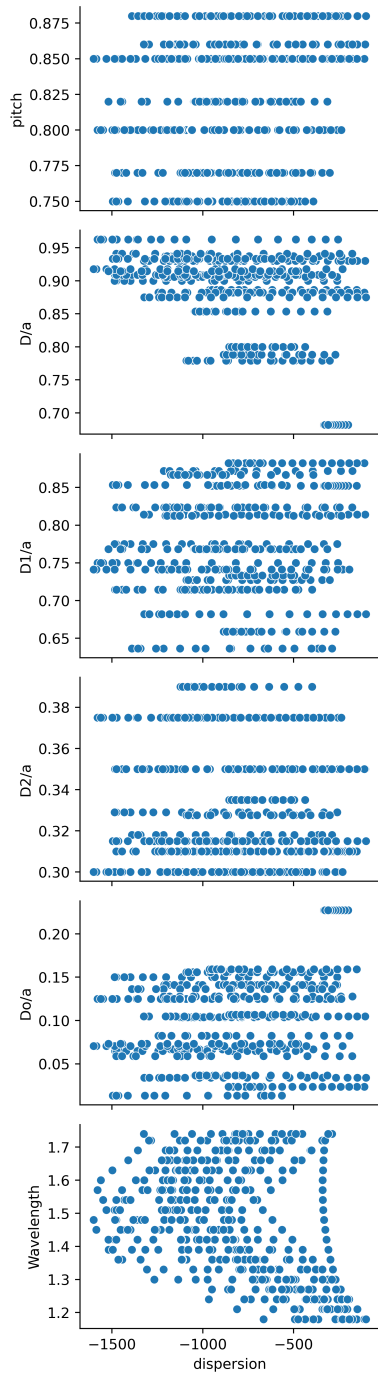
(a) Scatterplot Matrix of n_{eff} vs features

(b) Scatterplot Matrix of a_{eff} vs features

Figure 4.17: Scatterplot matrix of features and target (effective mode index & effective area) for visualizing the structured relationship.

Scatterplot Matrix of Next Target vs Features

Scatterplot Matrix of Next Target vs Features



(a) Scatterplot Matrix of D vs features

(b) Scatterplot Matrix of α_c vs features

Figure 4.18: Scatterplot matrix of features and target (dispersion & confinement loss) for visualizing the structured relationship.

structor (e.g., `LinearRegression()`, `KNeighborsRegressor()`, `DecisionTreeRegressor()`, or `RandomForestRegressor()`).

Train the model: The model is trained on the provided training data (`X_train`, `y_train`) using the `fit()` method.

Save the model: The trained model is saved to a file on disk using the `pickle.dump()` function. The file path is created by concatenating the path variable with the model's corresponding filename (e.g., `'lr.pkl'`, `'knn.pkl'`, `'dt.pkl'`, or `'rf.pkl'`).

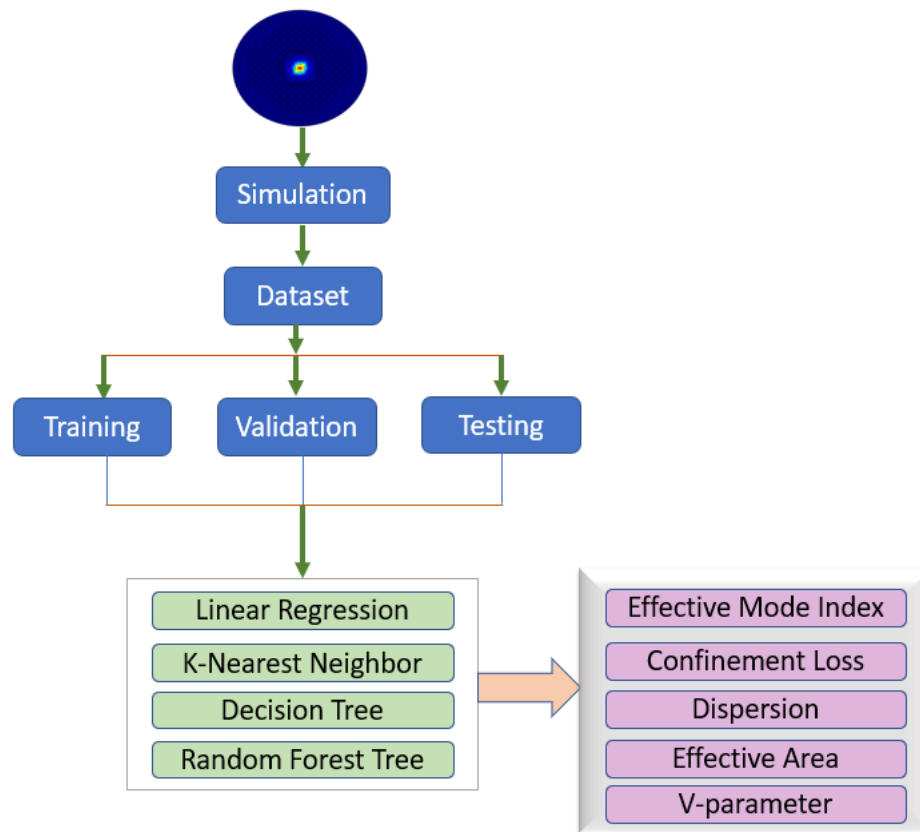


Figure 4.19: The flow diagram of an application of regression model

We load four trained regression models from disk and evaluate their performance on a test set using the R2 score metric. **Load the models:** The previously saved models (Linear Regression, K-Nearest Neighbors, Decision Tree, and Random Forest) are loaded using the `pickle.load()` function. The model instances are stored in separate variables (`lr_model`, `knn_model`, `dt_model`, `rf_model`).

Create a list of models and model names: The loaded models are placed in a model list, and their corresponding names are placed in a separate list called model names.

Print the performance on the test set: The R2 score for each model's predictions on the test set (`X_test`) is printed. The R2 score is a commonly used metric for evaluating the

```

BEGIN
1. LOAD dataset
2. CHECK for null values in dataset
3. SEPARATE dataset into features and target
4. NORMALIZE features and target using StandardScaler
5. SPLIT dataset into training and test sets using train_test_split
6. TRAIN regression models on training set:
   - Linear Regression
   - K-Nearest Neighbors Regression
   - Decision Tree Regression
   - Random Forest Regression
7. SAVE each trained model to a file using pickle.dump
8. LOAD the saved models using pickle.load
9. LOOP through each model:
   a. MAKE predictions on test set
   b. CALCULATE R2 score for each model
   c. PRINT the R2 score along with the model name
END

```

Figure 4.20: Pseudocode of the steps of the given algorithm

performance of regression models, with values ranging from 0 to 1. Higher R2 scores indicate better model performance.

Loop through the models: The `enumerate()` function is used to loop through the models in the model list and their corresponding names in the model names. For each model:

Make predictions: The model's `predict()` method is called on the test set (`X_test`) to generate predictions (`y_pred`).

Calculate the R2 score: The R2 score is computed with the help of the `r2_score` function from `sci-kit-learn` by comparing the actual target values (`y_test`) and the predicted values (`y_pred`).

Print the R2 score: The R2 score for each model is printed with its corresponding name from the model names list. Figure 4.20 explain the steps taken using regression algorithm, which is described briefly.

Using Artificial Neural Network

In supervised machine learning, algorithms are trained using a labeled dataset, where each input example has a corresponding output or target value. The goal is to learn the

underlying relationship between inputs and outputs so that the model can make accurate predictions on new, unseen data. Artificial Neural Networks (ANNs) are machine learning models that have proven highly effective in various supervised learning tasks, including regression and classification problems. They are particularly well-suited for handling complex, non-linear patterns and features in the data, which is one of the reasons they are considered one of the best techniques for supervised learning. The architecture of a neural network consists of interconnected layers of nodes or neurons. Each neuron in a layer receives input from the previous layer, processes it, and passes the result to the next layer. The first layer, the input layer, takes in the raw data, while the last layer, called the output layer, produces the final prediction. Between the input and output layers, one or more hidden layers can help the network learn intricate relationships within the data.

In the context of this study, the goal is to predict the optical properties of Photonic Crystal Fibers (PCFs) using a regression model. PCFs are optical fibers with unique light-guiding properties, making them valuable in various applications, such as telecommunications and sensing. The neural network is trained on a dataset containing various input features related to the PCF's structure, such as its components' size, shape, and arrangement. The output or target variable is the optical properties of the PCF. During the training process, the network learns the relationship between the input features and the target variable. Once trained, the ANN can then be used to predict the optical properties of new, untested PCFs based on their input features.

Network Structure

An Artificial Neural Network (ANN) comprises interconnected nodes, often called neurons. The ANN serves as a framework for processing complex data inputs and learning from specific input data without relying on pre-programmed, task-specific rules. A widely used type of ANN is the Multilayer Perceptron (MLP). An MLP comprises three or more layers, as depicted in Fig. 4.21, which includes an input layer, two hidden layers, and an output layer. These layers function as fully connected layers, meaning that each node in one layer connects to every node in the subsequent layer. Each node possesses an assigned variable weight as input, which are linearly combined (or summed) and passed through an activation function to produce the output for that specific node.

Network Algorithm

The algorithm begins with the collection of simulation or experimental data, which serves as the foundation for the machine learning model by providing a sample of the real-world relationships between input features and target outputs. The training procedure is illustrated in Fig. 4.22. Pitch(\wedge), Diameter of core(d_0), Diameter of octagonal

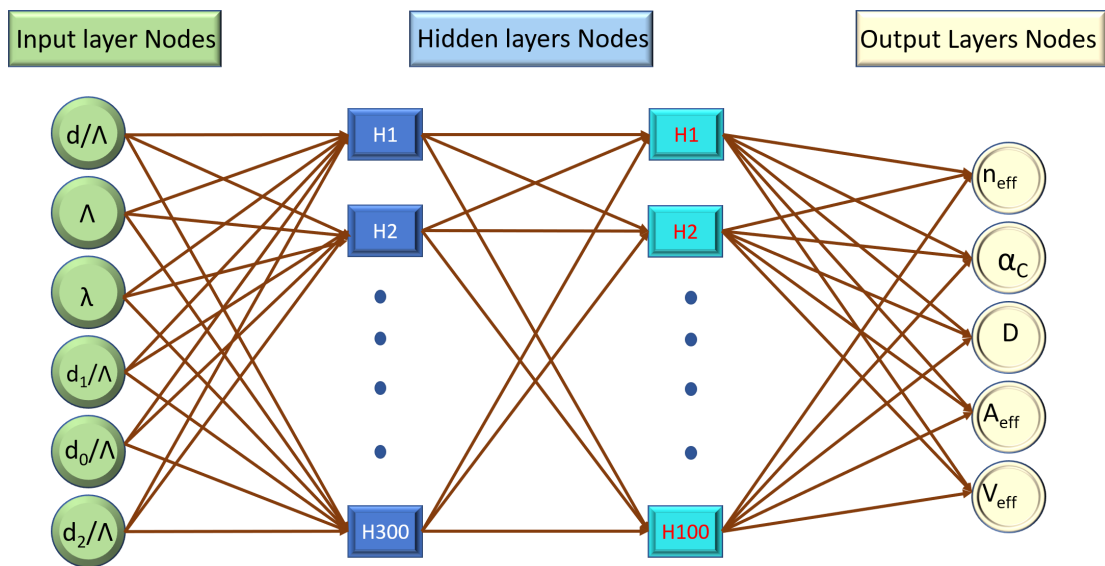


Figure 4.21: Structure of Proposed Artificial Neural Network

pattern air hole (d_1 , Diameter of closely attached air hole (d) and Diameter of rectangular pattern air hole (d_2) are the physical input parameters. Before feeding the data into the model, it undergoes preprocessing, including normalization and shuffling. Normalization scales the features to a uniform range, typically between 0 and 1, or to a standard distribution with mean 0 and variance 1, ensuring that no single feature dominates the learning process. Shuffling randomizes the order of the data points, reducing potential biases and ensuring the model generalizes well to unseen data.

Once preprocessed, the data is split into three subsets: training(80%), validation(10%), and testing(10%) datasets. The training set is used to teach the model, while the validation set helps fine-tune the model's hyperparameters and evaluate its performance during training. The testing dataset assesses the final model's performance on unseen data, estimating how well it will perform in real-world applications.

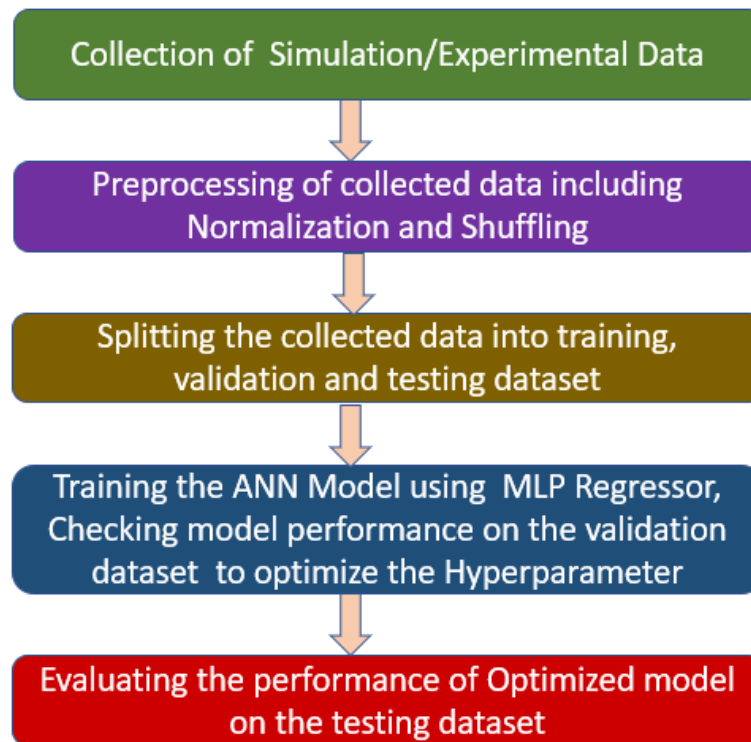


Figure 4.22: The flow chart of ANN implementation

An Artificial Neural Network (ANN) model is then trained using the Multi-Layer Perceptron (MLP) Regressor. The ANN architecture consists of multiple input, hidden, and output layers. The model is trained on the training dataset, and its performance is evaluated using the validation dataset. This feedback loop helps optimize the hyperparameters, such as the learning rate and the number of hidden layers, to achieve the best possible performance.

Finally, after the ANN model is trained and its hyperparameters are optimized, its performance is evaluated on the testing dataset. For prediction of output properties like effective mode index (n_{eff}), dispersion (D), V-parameters (V_{eff}), effective mode area (A_{eff}) and confinement loss, the input design parameters such as pitch, wavelength, number of air holes, and diameter of holes (circular and hexagonal pattern) in the silica region will be tailored. This step is crucial for assessing how well the model has generalized to unseen data and estimating its real-world performance. The evaluation metrics, such as R-squared error, quantify the model's accuracy and effectiveness in predicting the target outputs.

Activation Functions:

ANN bridges inputs and outputs by utilizing a collection of nonlinear functions estimated by applying nonlinear activation functions. Sigmoid, Tanh (hyperbolic tangent),

and ReLU (rectified linear unit) are some of the frequently employed activation functions [79]. ReLU is often preferred, enabling models to train significantly faster than the Tanh function.

Optimization Solver:

Optimizing weight values during machine learning training is an essential step, and various solvers can be employed to achieve this. Three notable solvers include Limited-memory Broyden-Fletcher-Goldfarb-Shanno (LBFGS), Stochastic Gradient Descent (SGD), and Adaptive Moment Estimation (Adam) [80]. Each solver has advantages and drawbacks, but the Adam optimizer is often preferred for various reasons. The Adam optimizer works well on relatively large datasets, which makes it suitable for handling complex problems that involve a substantial amount of data. It combines the best aspects of the momentum-based SGD and the adaptive learning rate methods, offering an efficient and robust optimization approach. This results in faster convergence of the learning process, improved accuracy, and overall better performance.

Hidden Layers and Nodes:

When designing an Artificial Neural Network (ANN), one of the crucial aspects to consider is the architecture of the network, which includes the number of layers and the number of nodes (or neurons) in each layer. Determining the optimal structure for an ANN is challenging, as there is no definitive rule or formula to pre-determine the ideal configuration for a given problem. This particular neural network architecture comprises one input layer, two hidden layers, and one output layer. The two hidden layers consist of 500 and 100 neurons, respectively. The choice of the number of layers and nodes in each layer is often based on experimentation and prior experience with similar problems. This process typically involves trial and error, where various architectures are tested, and their performances are compared to find the most suitable one for the problem.

Epochs:

An epoch is a single pass through the entire dataset during training, which consists of multiple iterations depending on the batch size. In this specific case, 5000 epochs are specified for the training process. The appropriate number of epochs is essential to avoid overfitting or underfitting the model. Ideally, the number of epochs should be chosen when the R Squared score converges to an acceptable limit, indicating that the model has learned the underlying patterns in the data.

4.6 Chapter Summary

In the proposed methodology, we utilize machine learning techniques to predict the optical properties of negative dispersion-compensating photonic crystal fibers (PCFs) effectively and efficiently. By integrating a suitable machine learning algorithm with a comprehensive dataset of PCF designs and their corresponding optical properties, we aim to create a predictive model capable of accurately estimating the performance of novel PCF structures. This approach streamlines the design and optimization process for PCFs, enabling the development of tailored dispersion-compensating fibers with improved performance in optical communication systems.

Chapter 5

Results and Discussions

COMSOL Multiphysics 5.0 is employed to design the proposed PCFs using the finite element method to determine the electric field distribution and fundamental mode properties. The effective refractive index (n_{eff}) is obtained using Perfectly Matched Layer (PML) boundary conditions. The modal refractive indices are then utilized to compute the (a_{eff}), Dispersion (D), confinement loss (α_c), and V-parameter (v_{eff}) through numerical calculations. Secondly, Machine learning algorithms such as linear regression(LR), k-nearest neighbor (KNN), Decision tree(DT), and random forest tree(RFT) are used to predict the optical properties of the proposed method regardless of the numerical solution. Another study has been done to expect the same properties using the Artificial neural network(ANN). The hyperparameters (Number of hidden layers, number of neurons in each layer, and epoch in training) have been optimized to get better rest for predicting properties more accurately than previous. The machine learning models, including the ANN model, are designed using the python language, the Keras library, and part of the TensorFlow framework. The code is a Python script that uses the matplotlib library to generate different types of plots.

5.1 Analysing PCF Characteristics

This section analyzes Photonic Crystal Fiber (PCF) characteristics by adjusting their geometrical structure. Modifying parameters such as air hole size, pitch, and core diameter can enhance PCF performance in various applications, including optical communication systems. The study aims to understand the impact of these structural adjustments on properties like effective refractive index, dispersion, confinement loss, and more. This research can contribute to developing more efficient and versatile PCFs,

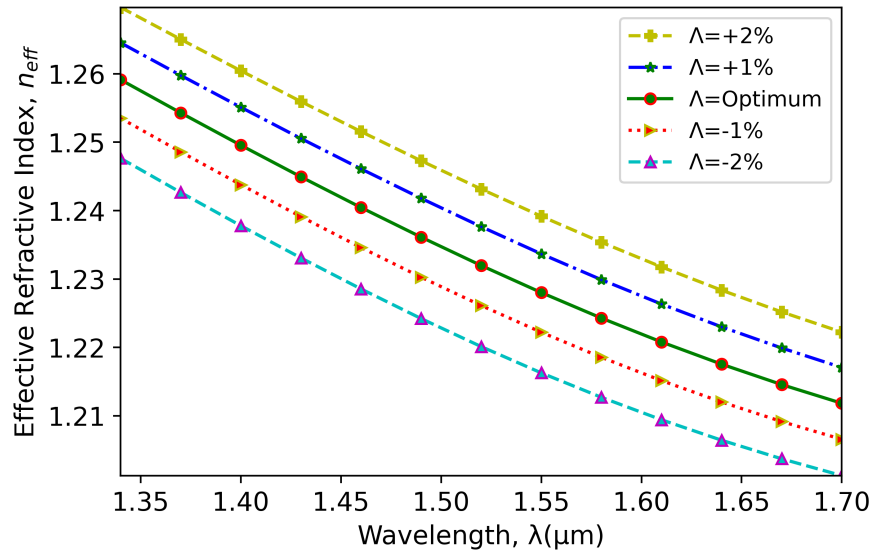


Figure 5.1: Fluctuation of the effective refractive index for varying operating wavelengths for alternation of Λ from optimum ($\Lambda = 0.8415 \mu\text{m}$) to \pm (1 to 2%)

providing valuable insights for designing next-generation optical devices.

5.1.1 Comparative Analysis of Effective Refractive Index

Figure 5.1 displays the relationship between the wavelength and the effective refractive index for a Photonic Crystal Fiber (PCF). The effective refractive index is a complex value composed of real and imaginary parts. Still, in this case, the plot focuses on the fundamental part of the refractive index as it varies concerning the wavelength. Figure 5.1 demonstrates this relationship for different pitch values, which are varied from $\pm 1\%$ and $\pm 2\%$ from the optimum value of $\Lambda = 0.8415 \mu\text{m}$. From the figure, it can be observed that the effective refractive index varies linearly with the wavelength for each pitch value. This linear behavior can be attributed to high-frequency electromagnetic waves being well confined within the core of the PCF. In contrast, low-frequency waves tend to spread out into the cladding region. PCF The pitch value directly influences the amount of air present in the cladding region. A higher pitch indicates reduced air in the cladding, increasing the effective refractive index. This trend can be observed in the plot, where the effective refractive index increases with an increasing pitch value. By visualizing these relationships, the code enables users to gain valuable insights into the behavior of the effective refractive index and its dependence on the wavelength and pitch of a PCF.

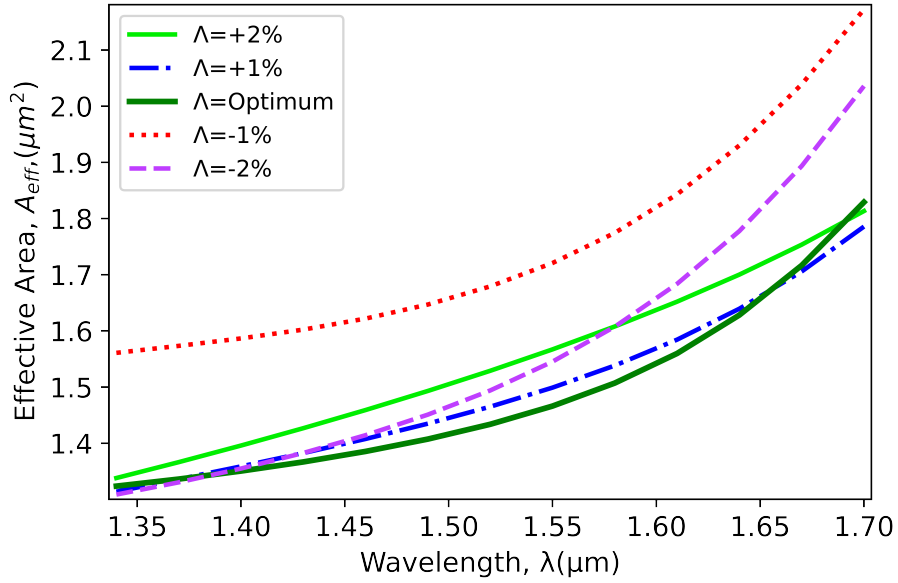


Figure 5.2: Fluctuation of the effective area for varying operating wavelengths for alternation of Λ from optimum ($\Lambda = 0.8415 \mu\text{m}$) to \pm (1 to 2%)

5.1.2 Comparative Analysis of Effective Area

Figure 5.2 displays the relationship between the wavelength and the effective area (A_{eff}) for a Photonic Crystal Fiber (PCF). The effective area is an essential parameter in optical fiber design, as it significantly impacts the fiber's performance in terms of nonlinearity and signal confinement. The plot in Figure 5.2 demonstrates this relationship for different pitch values, which are varied from $\pm 1\%$ and $\pm 2\%$ from the optimum value of $\Lambda = 0.8415 \mu\text{m}$. From the plot, it can be observed that the effective area exhibits distinct trends concerning the wavelength for each pitch value. These trends can be attributed to the varying geometric structure of the PCF, as the pitch value affects the arrangement and size of the air holes in the cladding region.

5.1.3 Comparative Analysis of Confinement Loss

Figure 5.3 presents a graphical representation of the confinement loss in a Photonic Crystal Fiber (PCF) plotted on a logarithmic scale as a function of wavelength. Confinement loss is an essential parameter in fiber optics, as it determines how effectively light is confined within the fiber's core, directly impacting signal transmission efficiency. The figure also represents the confinement loss in the logarithm scale concerning wavelength. Confinement loss is related to wavelength and increases as wavelength increases. The logarithm value of confinement loss decreases with the increased pitch value. The figure highlights the relationship between confinement loss and wavelength,

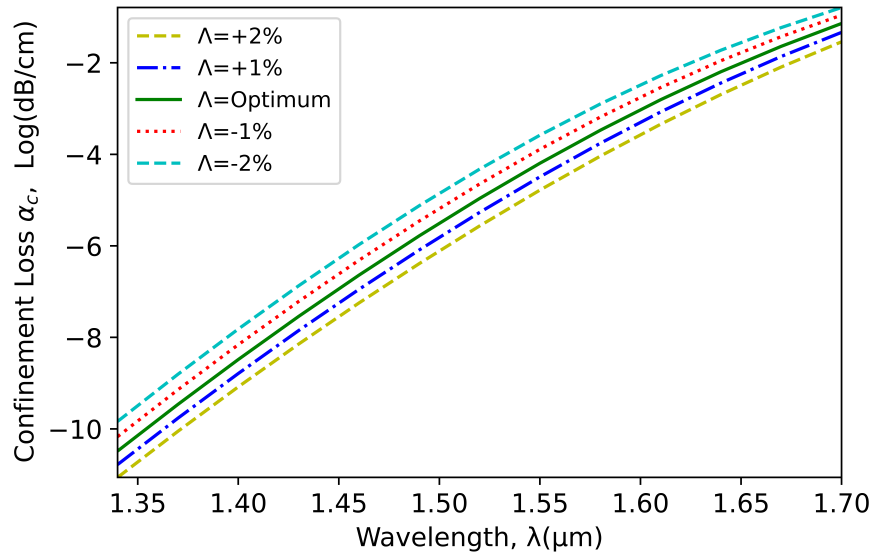


Figure 5.3: Fluctuation of the confinement loss for varying operating wavelengths for alternation of Λ from optimum ($\Lambda=0.8415 \mu\text{m}$) to \pm (1 to 2%).

showing that the confinement loss also increases as the wavelength increases. This implies that the light is less effectively confined within the fiber's core for longer wavelengths, leading to increased signal power loss. Additionally, the figure illustrates the impact of pitch values on confinement loss. Pitch refers to the spacing between the air holes in the cladding region of a PCF. The logarithm value of confinement loss decreases when the pitch value increases. This trend suggests that increasing the pitch value improves the confinement of light within the fiber, resulting in a lower confinement loss.

5.1.4 Comparative Analysis of Dispersion

Figure 5.4 demonstrates the relationship between the wavelength (λ) and dispersion in a Photonic Crystal Fiber (PCF) with varying pitch values. Specifically, it illustrates how the dispersion changes as the wavelength and pitch values are adjusted. If the pitch values become more minor concerning the other value, it shows the highest dispersion at a specific wavelength. And then, the value of dispersion rises again. With the consideration of the minimum and steady value of negative dispersion in the optical fiber communication window, pitch $\Lambda=0.8415 \mu\text{m}$ is chosen to obtain minimum dispersion $-1582.21 \text{ ps}/(\text{nm}\cdot\text{km})$

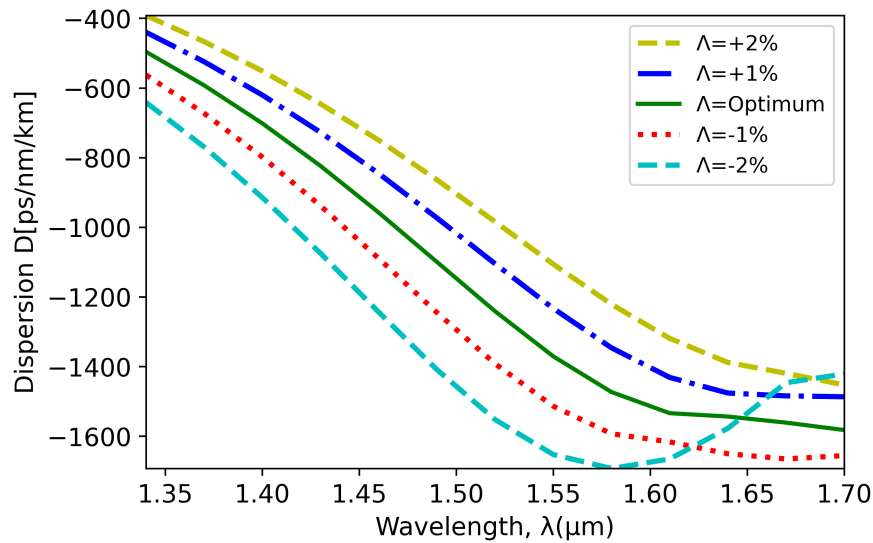


Figure 5.4: Fluctuation of the dispersion for varying operating wavelengths for alternation of Λ from $\pm(1$ to 2%).

5.1.5 Effect of core size on Dispersion

Figure 5.5 exhibits the dispersion as a function of wavelength with different core air hole diameters. The core size of a photonic crystal fiber (PCF) has a significant impact on its dispersion properties. As the core size increases, the effective mode area also increases, leading to a decrease in the fiber's confinement of light. This results in a lower modal overlap with the core material and, consequently, a reduction in the material dispersion. As the core with a bigger diameter than optimum $d_0=0.12 \mu\text{m}$ has the solid capacity for confine light, the dispersion is lesser for it. The maximum dispersion obtained in this observation is $-1604.2 \text{ ps}/(\text{nm}\cdot\text{km})$. The inversely proportional relationship between the diameter of the core and dispersion is demonstrated in Figure 5.5.

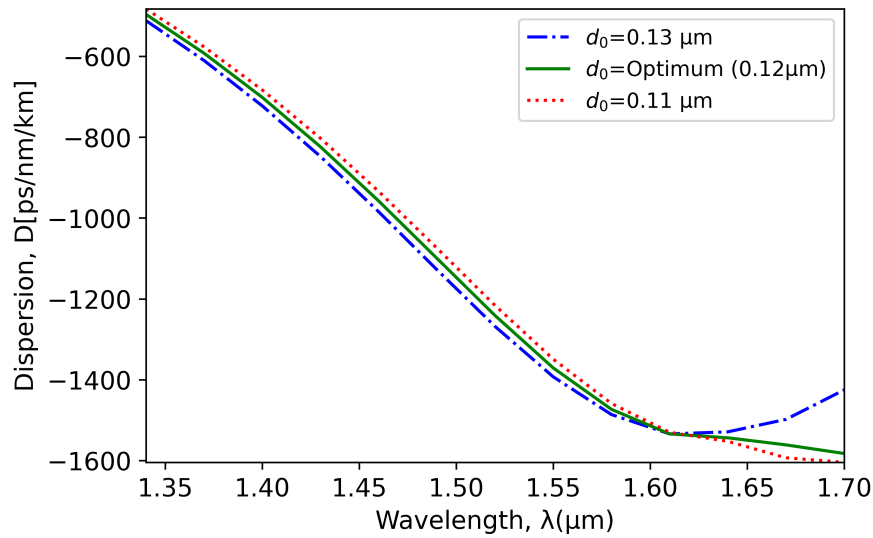


Figure 5.5: Fluctuation of the dispersion for varying operating wavelengths for core diameter $d_0=0.11 \mu\text{m}$, $0.12 \mu\text{m}$ and $0.13 \mu\text{m}$.

5.1.6 Impact of Cladding Air Hole Dimensions on Dispersion

The dimensions of the cladding air holes in a photonic crystal fiber (PCF) have a significant impact on its dispersion properties. Altering the size, shape, and arrangement of air holes in the cladding can lead to changes in both the waveguide dispersion and the effective refractive index of the fiber. As the size of the air holes increases, the refractive index contrast between the core and the cladding becomes more pronounced, resulting in a stronger confinement of light within the core. This can lead to an increase in the waveguide dispersion, which can either enhance or counteract the material dispersion depending on the specific PCF design. Figure 5.6 shows the variation of dispersion along with wavelength where all other parameters are constant. The air holes with optimum diameter $d=0.8 \mu\text{m}$ are closely shielded in the core region, so the light is bounded into the core. With a more central air hole, the dispersion becomes more negative. The maximum negative dispersion $-2065.2 \text{ ps}/(\text{nm}\cdot\text{km})$ is obtained at $\lambda=1550 \text{ nm}$.

Whenever the diameter of air holes situated after one square ring increases, the dispersion also increases concerning the wavelength. This is shown in Figure 5.7. In this case, the air holes aren't near the core. The light confinement strength in the core doesn't linearly depend on it. The maximum dispersion with optimum $d_1=0.6 \mu\text{m}$ is $-1582.21 \text{ ps}/(\text{nm}\cdot\text{km})$ but with $d_1=0.57 \mu\text{m}$, it is $-1626.8 \text{ ps}/(\text{nm}\cdot\text{km})$.

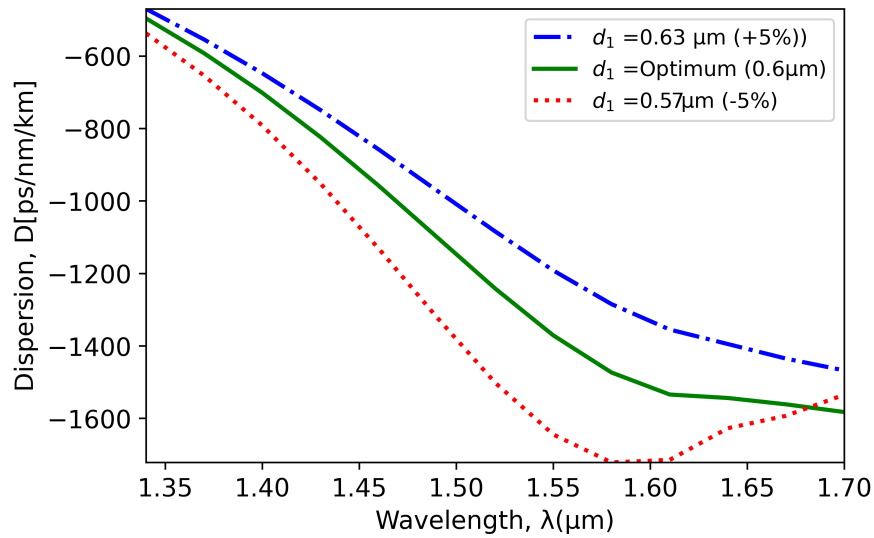


Figure 5.6: Fluctuation of the dispersion for varying operating wavelengths for alternation of d_1 in range of $\pm 5\%$ from optimum ($d_1 = 0.6 \mu\text{m}$).

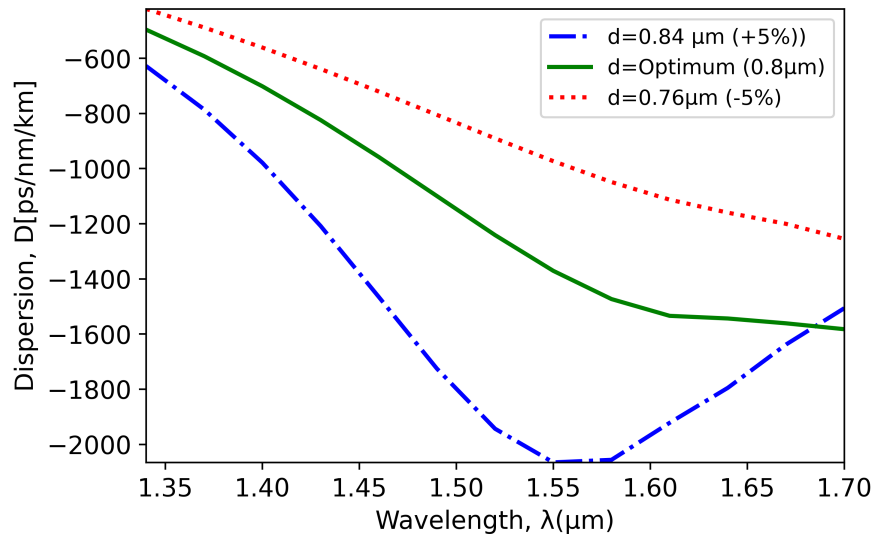


Figure 5.7: Variation of Dispersion with different operating wavelength for alternation of d in the range of $\pm 5\%$ optimum ($d = 0.8 \mu\text{m}$).

5.2 Prediction of PCF Optical Properties using Machine learning

Predicting the optical properties of photonic crystal fibers (PCFs) using machine learning involves creating a model that can learn from a dataset of known PCF properties and use this knowledge to predict the properties of new, unseen PCFs. This study uses four

machine learning algorithms (Linear regression, K-nearest neighbor, Decision Trees, and Random forest tree).

5.2.1 Prediction of Effective Refractive Index

Figure 5.8 shows the scatter plot of predicted vs. effective refractive index (n_{eff}). The solid black line ($y = x$) indicates the ideal linear model response. The blue, orange, green, and red circles refer to the data points of linear regression, KNN, Decision Tree, and Random Forest Tree, respectively. The r-square value is considered an evaluation metric. The blue data points of linear regression are comparatively far from the solid line, which indicates the lower r-square value of 0.96. The data points of KNN are more scattered in the region of n_{eff} between 1.28 and 1.30. Hence has the lowest r-square value at 0.95. Most of the Decision Tree and Random Forest Tree data points touch the solid black line. This gives about a 99% r-square value.

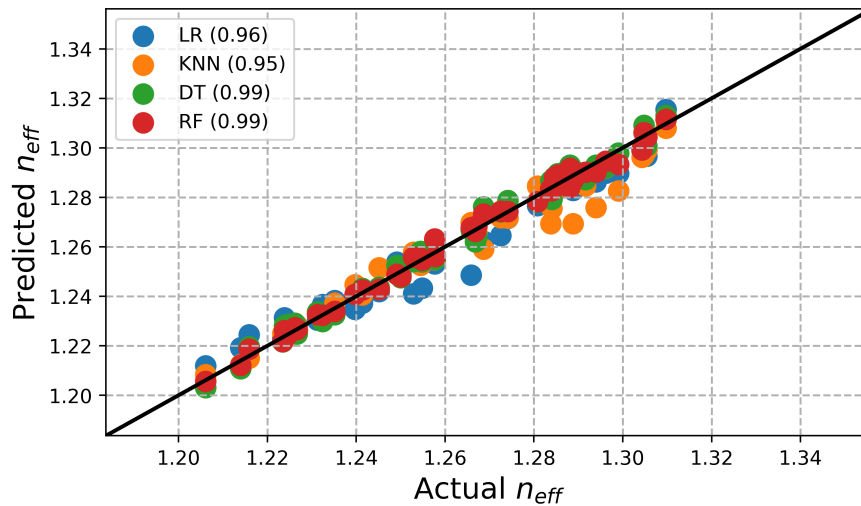


Figure 5.8: The scatter plot of predicted n_{eff} (y-axis) Vs actual n_{eff} (x-axis) comparing against perfect linear relationship ($y=x$).

This trained linear regression model was then used to predict the effective refractive index (n_{eff}) values at unknown PCF parameters, $\Lambda = 0.875 \mu\text{m}$, $d/\Lambda = 0.08536$, $d_1/\Lambda = 0.7885$, $d_2/\Lambda = 0.3$ and $d_0/\Lambda = 0.0914$ as shown in Figure 5.9 n_{eff} data corresponding to these parameters was never recorded or provided during the training of the model. The solid line with circle markers shows the actual values of n_{eff} . In contrast, different line styles and markers represent the predicted values from four different regression models (linear regression, k-nearest neighbors, decision tree, and random forest). A dashed-dotted line with hexagon markers represents the linear regression model predictions, a

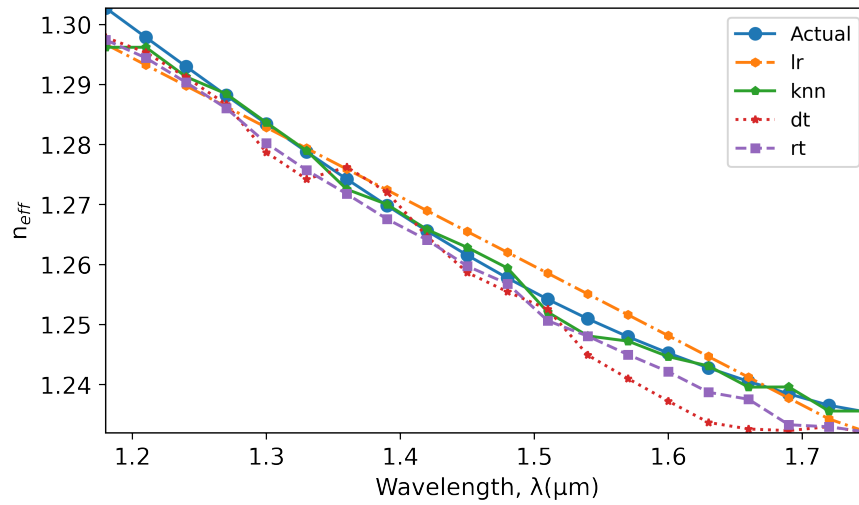


Figure 5.9: Evaluating the correspondence between the simulated n_{eff} and the predicted n_{eff} across multiple algorithms with an unexplored configuration.

solid line with pentagon markers shows the k-nearest neighbors model predictions, a dotted line with star markers displays the decision tree model predictions, and a dashed line with square markers depicts the random forest model predictions. It can be observed that all regression models exhibit varying degrees of agreement with the actual values, demonstrating their ability to predict the effective refractive index at different wavelengths. This comparison allows users to assess the performance of each model in estimating n_{eff} for a PCF, providing valuable insights into the effectiveness of different machine-learning approaches for this particular application. KNN gives more significant fluctuation compared to another model because of lower accuracy.

5.2.2 Prediction of Effective Mode Area

Figure 5.10 represents how well the tested data points of effective mode area (A_{eff}) are fitted compared to the ideal model. The data points around $5\mu m^2$ are not close to the ideal model for every model. Because there are very few data points in the 3.5 to $5\mu m^2$, the algorithm couldn't learn well with these fewer data. However, the data points of the Decision Tree and Random Forest Tree are much closer than the other machine learning models, and hence the r-square value is 96% and 97%, respectively. The linear regression model gives the lowest r-square value of 0.65.

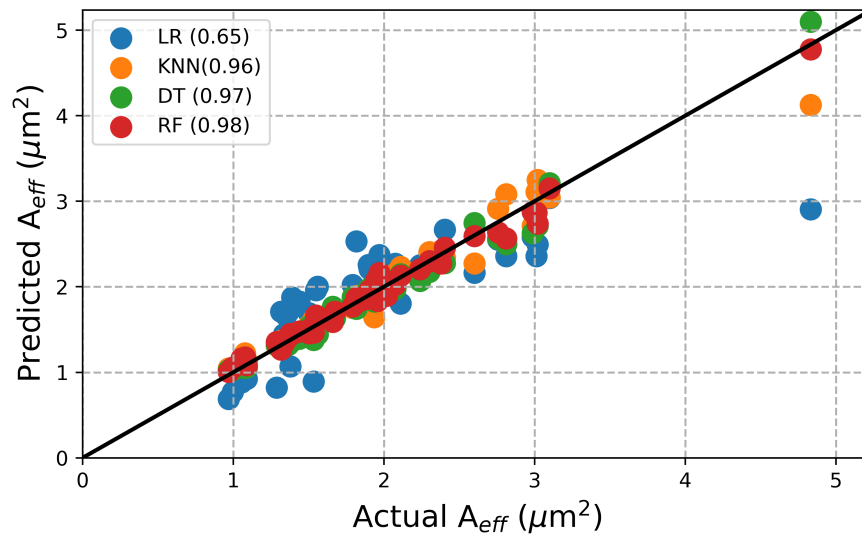


Figure 5.10: The scatter plot of predicted a_{eff} (y-axis) Vs actual a_{eff} (x-axis) comparing against perfect linear relationship ($y=x$).

The performance of each machine learning model is quantified using the R-squared (R_2) score, which is displayed in the legend alongside the layer count. The plot uses different markers to represent the predicted values from each model, with circles indicating the predictions.

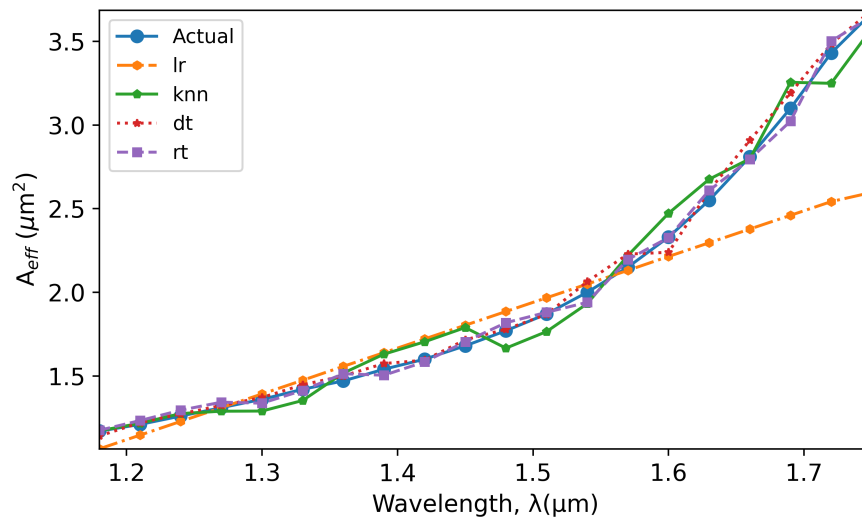


Figure 5.11: Evaluating the correspondence between the simulated a_{eff} and the predicted a_{eff} across multiple algorithms with an unexplored configuration.

Figure 5.11 is a line plot that compares the performance of four different machine learning models in predicting the effective mode area (A_{eff}) as a function of wavelength (λ). The models used are linear regression (LR), k-nearest neighbors (knn), decision tree

(DT), and random forest (rt). The actual A_{eff} values are also plotted for reference. In this plot, the x-axis represents the wavelength (λ) in micrometers (μm), while the y-axis shows the effective mode area (A_{eff}) in square meters (m^2). Each model is represented by a distinct line style and marker specified in the code. The actual A_{eff} values are plotted using solid lines with circle markers. The figure allows for a visual comparison of the accuracy and performance of the different machine learning models in predicting the A_{eff} as a function of wavelength. The closer a model's line is to the actual A_{eff} line, the better its performance. The legend maps the line styles, markers, and corresponding models.

5.2.3 Prediction of Dispersion

The relationship between the predicted and actual dispersion data points of different regression models is shown in Figure 5.12. The dispersion (D) has no linear relationship with all the input parameters. Hence, it has a vast r-square error. KNN gives the r-square value of 0.83, much greater than the linear regression. Besides, the Decision Tree and Random Forest Tree give the highest r-square values of 0.95 and 0.97, respectively.

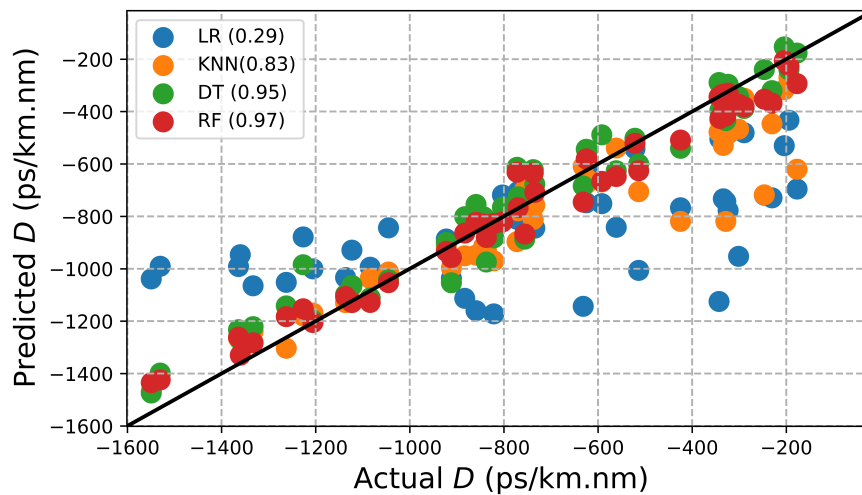


Figure 5.12: The scatter plot of predicted dispersion (D) (y-axis) Vs. Solid dispersion (D) (x-axis) comparing against perfect linear relationship ($y=x$).

Figure 5.13 presents a comparison between four distinct machine learning algorithms in terms of their ability to predict chromatic dispersion (D) as a function of wavelength (λ). The algorithms being compared are linear regression (LR), k-nearest neighbors (knn), decision tree (DT), and random forest (rt). The actual chromatic dispersion values are plotted to serve as a benchmark. In this graphical representation, the x-axis corresponds to the wavelength (λ) measured in micrometers (μm). At the same time, the y-axis dis-

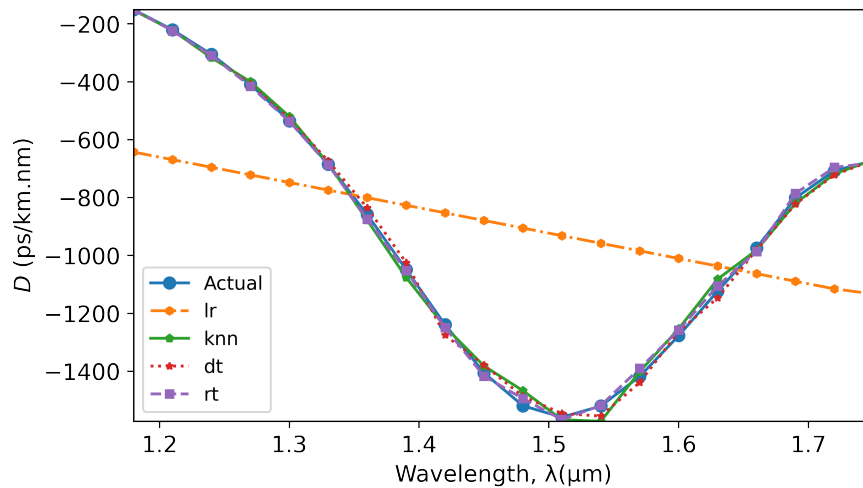


Figure 5.13: Evaluating the correspondence between the simulated dispersion (D) and the predicted dispersion (D) across multiple algorithms with a new configuration.

plays the chromatic dispersion (D) in units of picoseconds per kilometer-nanometer (ps/km.nm). Each algorithm is denoted by a unique line style and marker combination as defined in the code. A solid line with circular markers represents the actual D values. By examining the proximity of each algorithm's line to the line representing the actual D values, one can visually assess the predictive accuracy and performance of the different machine learning models in estimating chromatic dispersion based on wavelength. Including a legend makes it easy to identify the line styles, markers, and corresponding models.

5.2.4 Prediction of Confinement Loss

Confinement loss of the proposed PCF has an almost linear relationship with all input parameters. Hence, the linear regression gives about 96% of the r-square value, shown in Figure 5.14. The KNN couldn't find an exact local approximation in the negative region of confinement loss; it has a smaller r-square value than linear regression. The data points of the Decision Tree are closer to a solid line that gives an r-square value of 0.98. The r-square value for Random Forest Tree is about 99%.

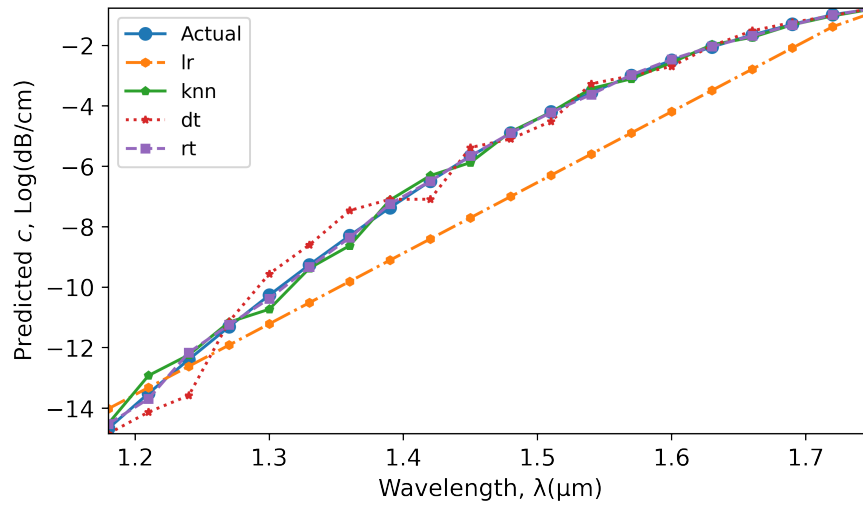


Figure 5.15: Evaluating the correspondence between the simulated and predicted confinement loss across multiple algorithms with a new configuration.

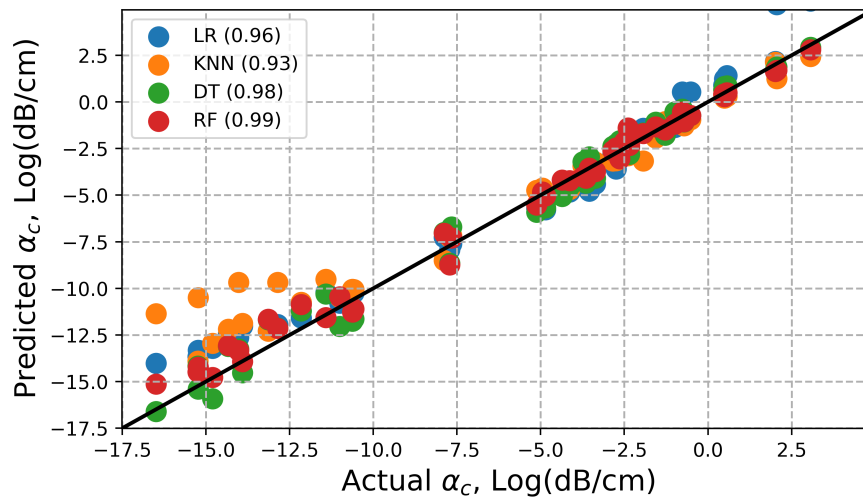


Figure 5.14: The scatter plot of predicted confinement loss (y-axis) Vs. Actual confinement loss (x-axis) compared against perfect linear relationship ($y=x$).

Figure 5.15 visually demonstrates the performance of each machine learning model in predicting confinement loss at various wavelengths. By comparing the data lines, it is possible to assess the accuracy and fitting of each model to the actual confinement loss values. The accuracy described in figure 5.14 is maintained hereafter.

5.2.5 Prediction of V-Parameter

Figure 5.16 shows the predicted vs. actual V-parameter data points. The V_{eff} has an almost linear relationship but is not precisely linear with input features such as wave-

length. The Decision Tree and Random Forest Tree give a 99% r-square value, much more than LR (96%) and KNN (95%).

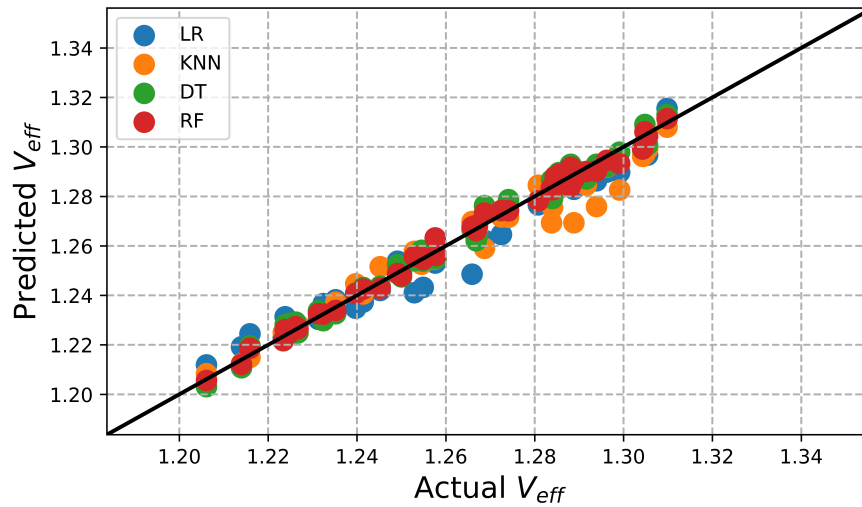


Figure 5.16: The scatter plot of predicted v_{eff} Vs actual v_{eff} comparing against perfect linear relationship ($y=x$).

Figure 5.17 compares four different machine learning algorithms in terms of their ability to predict the V-parameter as a function of wavelength (λ).

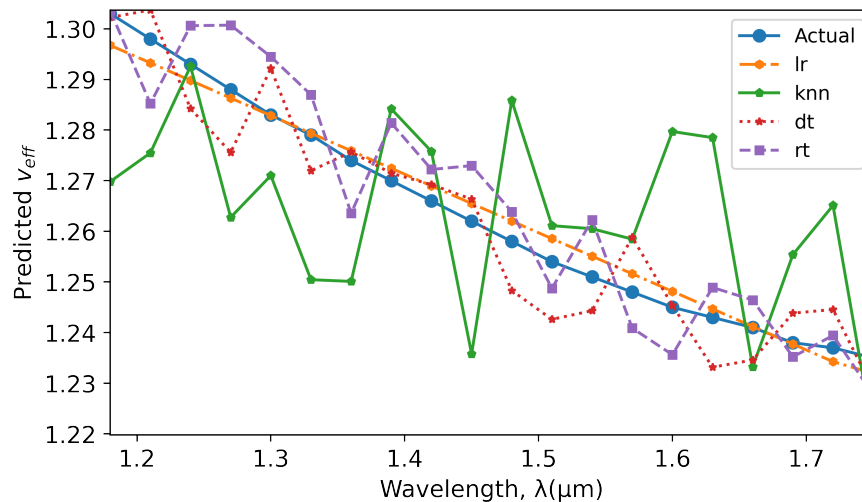


Figure 5.17: Evaluating the correspondence between the simulated and predicted v_{eff} across multiple algorithms with an unexplored configuration.

From the above graphs, the Random Forest Tree performed well with every output parameter and gave an average 98% r-square value. The main reason is that most of the data have a nonlinear trend. Besides, the Decision Tree also performs well, but not

like Random Forest Tree, as Random Forest Tree averages many Decision Trees. And linear regression performs worst as few data have a linear relation with input features.

5.3 Prediction of PCF Optical Properties using Artificial Neural Network

Predicting the optical properties of photonic crystal fibers (PCFs) using artificial neural networks (ANNs) is a promising approach due to the complexity of the PCF structures and the difficulty in solving them analytically. ANNs are machine learning algorithms that can learn complex patterns in data and make predictions based on those patterns. To obtain a better model with higher accuracy, the hyperparameters are tuned to fetch the optimum value.

5.3.1 Layer Tuning of ANN

This study constructs four different neural network models with different numbers of layers and neurons. The first model is a single-layer neural network with 500 neurons. The second model is a two-layer neural network with 500 and 100 neurons, respectively. The third model is a three-layer neural network with 500, 200, and 100 neurons, respectively. The fourth model is a five-layer neural network with 500, 100, 50, 50, and neurons, respectively. Then R-squared error for each of the four models on the test set was calculated. Then trained models are used to make predictions based on the test data. The `r2_score` function from `sci-kit-learn` is used to compute the R-squared error between the predicted and actual values.

5.3.1.1 Prediction of Effective Refractive Index

Figure 5.18 visualizes the performance of Artificial Neural Networks (ANN) with different numbers of hidden layers (1, 2, 3, and 5 layers) in predicting the target variable n_{eff} (effective refractive index). Inset shows the R-squared value obtained with layers. The figure is a scatter plot with the actual n_{eff} values on the x-axis and the predicted n_{eff} values on the y-axis. A diagonal line (in black) represents a perfect prediction where the actual and predicted values are equal. Four sets of scatter points correspond to a different ANN model with varying numbers of hidden layers (1, 2, 3, and 5 layers). The points are represented by circles with different colors and labeled with each model's R-squared (R2) error value. The closer the scatter points are to the diagonal line, the better

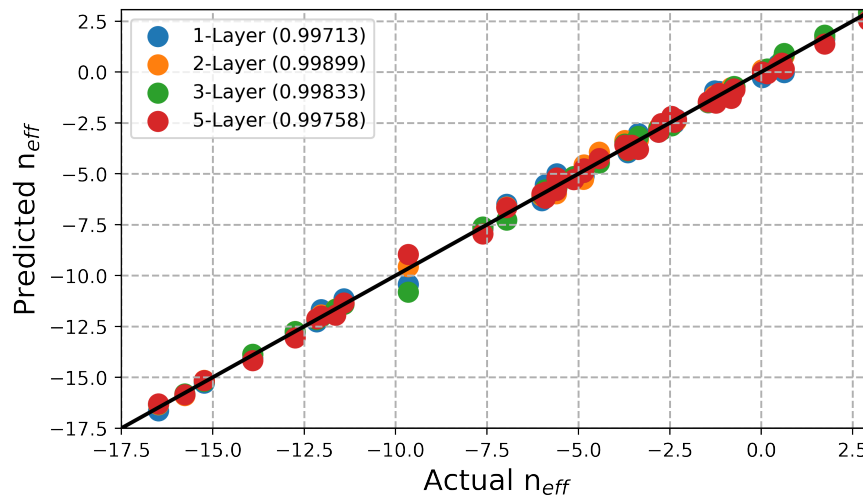


Figure 5.18: The scatter plot comparing predicted n_{eff} (y-axis) and actual n_{eff} (x-axis) for different hidden layers in the ANN against perfect linear relationship ($y=x$).

the model's performance. For n_{eff} parameters of PCF, it can be stated from the figure that the neural network with two hidden layers performs better, giving an R-squared (R²) error value around 0.99899, which is quite significant. All the networks with a specific number of hidden layers perform well, such as architecture with layer 1 giving 0.9971, layer 3 giving 0.99833, and layer 5 with 0.99758 R-squared (R²) error value.

5.3.1.2 Prediction of Effective Mode Area

Figure 5.19 illustrate a scatter plot to assess the performance of four different Artificial Neural Network (ANN) models with varying numbers of hidden layers (1, 2, 3, and 5 layers) in predicting the effective area (A_{eff}) in square meters (m^2). The figure shows that a network with two hidden layers gives a maximum r-squared error of around 0.99975. The inset shows the r-squared error for different numbers of layers.

5.3.1.3 Prediction of Dispersion

Figure 5.20 shows a scatter plot to compare the performance of four Artificial Neural Network (ANN) models, each with a different number of hidden layers (1, 2, 3, and 5 layers), in predicting dispersion (D) values measured in picoseconds per kilometer-nanometer (ps/km.nm). The neural network's performance with two hidden layers is more accurate than others. It gives around 0.99929 r squared value, whereas another network with a different layer gives less than 0.999.

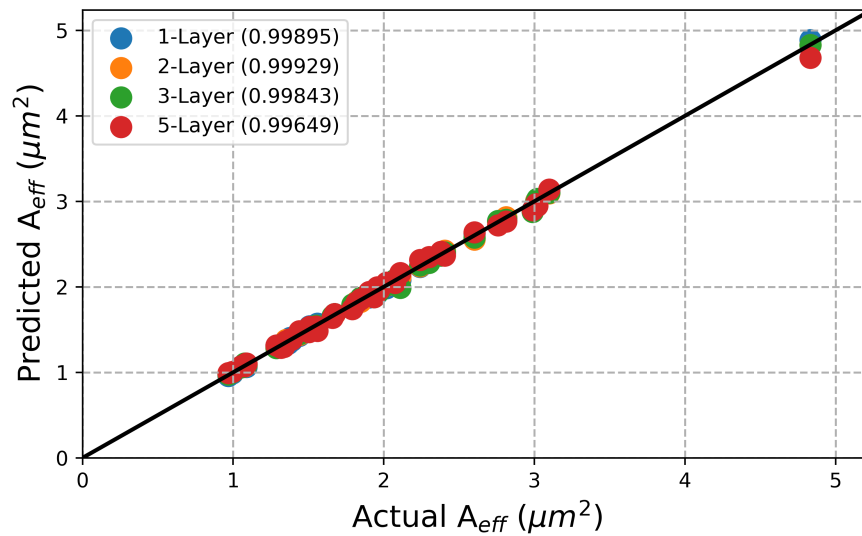


Figure 5.19: The scatter plot comparing predicted a_{eff} (y-axis) and actual a_{eff} (x-axis) for different hidden layers in the ANN against perfect linear relationship ($y=x$).

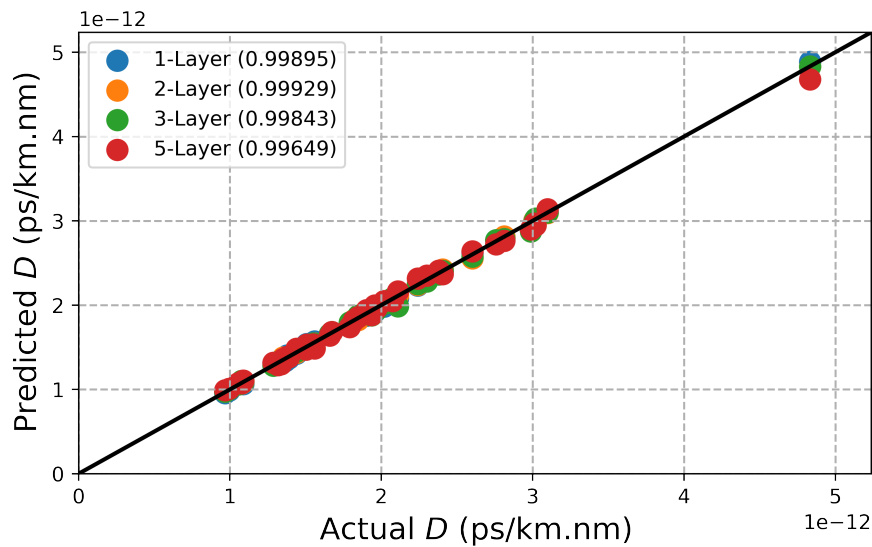


Figure 5.20: The scatter plot comparing predicted dispersion (D) (y-axis) and actual dispersion (D) (x-axis) for different hidden layers in the ANN against perfect linear relationship ($y=x$).

5.3.1.4 Prediction of Confinement Loss

The performance for predicting confinement loss also varies with the number of hidden layers of the neural network. This is clearly illustrated in figure 5.21. But in predicting confinement loss, a neural network with one hidden layer gives more r-square error (0.99891) than all other networks as this optical property of PCF varies smoothly; hence

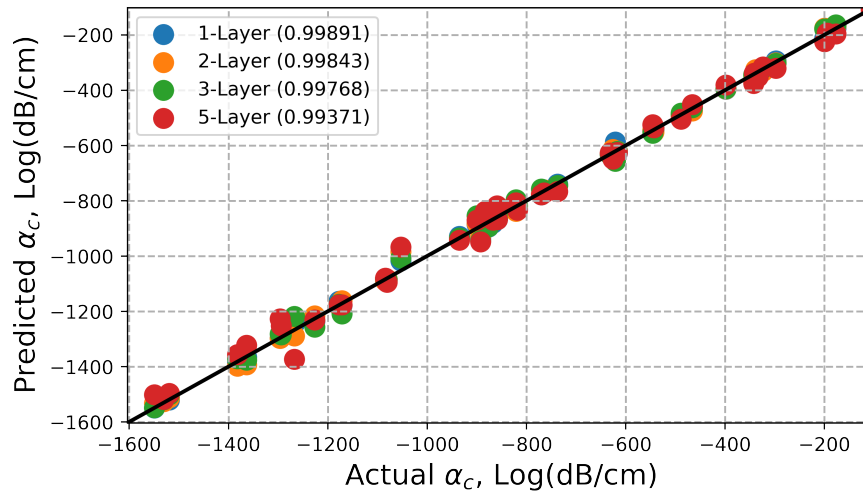


Figure 5.21: The scatter plot comparing predicted confinement loss(α_c) (y-axis) and actual confinement loss(α_c) (x-axis) for different hidden layers in the ANN against perfect linear relationship ($y=x$).

a simple neural network performance is better than a network with multiple layers.

5.3.1.5 Prediction of V-parameter

Figure 5.22 evaluates the predictive capabilities of four distinct ANN models, each having 1, 2, 3, or 5 hidden layers, in estimating the V-parameter of PCF. The figure shows that the neural network with two hidden layers gives a better result, around 0.99975. Another network also gives a close result but is not up to the mark.

In table 5.1, we present a comparison of neural network models with different numbers of layers for various performance metrics. The metrics considered are n_{eff} (effective refractive index), a_{eff} (effective mode area), Dispersion, Conf-Loss (confinement loss), and v_{eff} (v-parameter). Each row represents a neural network model with 1, 2, 3, or 5 layers, and the columns display the corresponding values for each performance metric. To comprehensively understand each model's performance, we calculated the average accuracy for all metrics in the last column. The table illustrates that the 2-layer model achieves the highest average accuracy across the considered metrics, followed by the 3-layer, 1-layer, and 5-layer models. This information can be valuable for choosing the most appropriate model for the given problem to balance computational efficiency and accuracy.

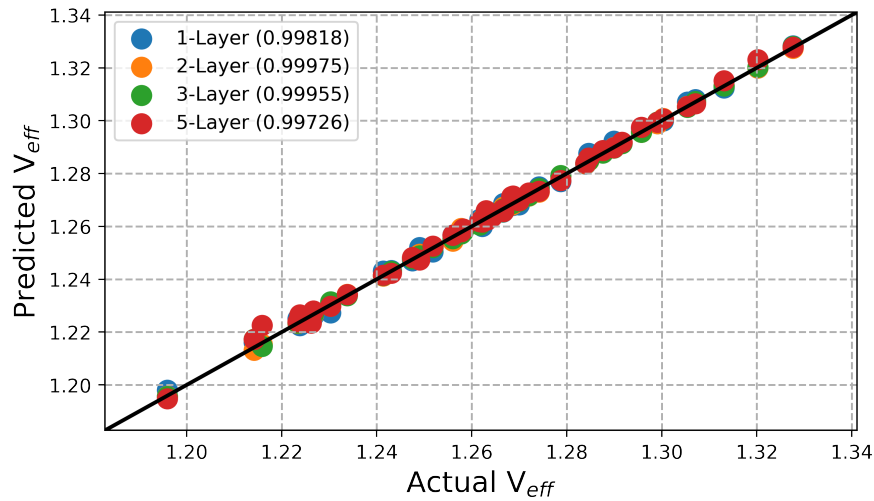


Figure 5.22: The scatter plot comparing predicted v_{eff} (y-axis) and actual v_{eff} (x-axis) for different hidden layers in the ANN against perfect linear relationship ($y=x$).

Table 5.1: Average accuracy in predicting properties with different hidden layers in ANN architecture.

No. of Layers	n_{eff}	a_{eff}	Dispersion	Conf-Loss	v_{eff}	Avg. Accuracy
1-layer	0.99713	0.99881	0.99895	0.99891	0.99818	0.99840
2-layer	0.99899	0.99975	0.99929	0.99843	0.99975	0.99924
3-layer	0.99833	0.99956	0.99843	0.99768	0.99955	0.99871
5-layer	0.99758	0.99722	0.99649	0.99371	0.99726	0.99645

5.3.2 Neuron Tuning of ANN

Figure 5.23 illustrates the relationship between the number of neurons in a two-layer neural network model and its R2 score for predicting five parameters: $X_{N_{eff}}$, A_{eff} , dispersion, conf-loss, and V_{eff} . The x-axis represents the number of neurons in the models, while the y-axis shows the corresponding R2 scores. The models have been trained with different neuron counts, specifically 10, 20, 30, 40, 50, 100, 150, 200, 300, 400, and 500 neurons in the first layer. The plot displays five distinct lines with markers, one for each parameter, and their R2 scores at various neuron counts. Overall, the performance of the models generally improves as the number of neurons increases, with some variations. The figure effectively demonstrates the impact of neuron count on the predictive accuracy of the two-layer neural network models across the five parameters.

The graph shows that the network architecture with 300 neurons gives the same r-squared error for all PCF-optical parameters. As the number of neurons increases, the r-squared error of some variables is reduced and increases for other properties. So it is wise to choose 300 neurons for our best ANN model.

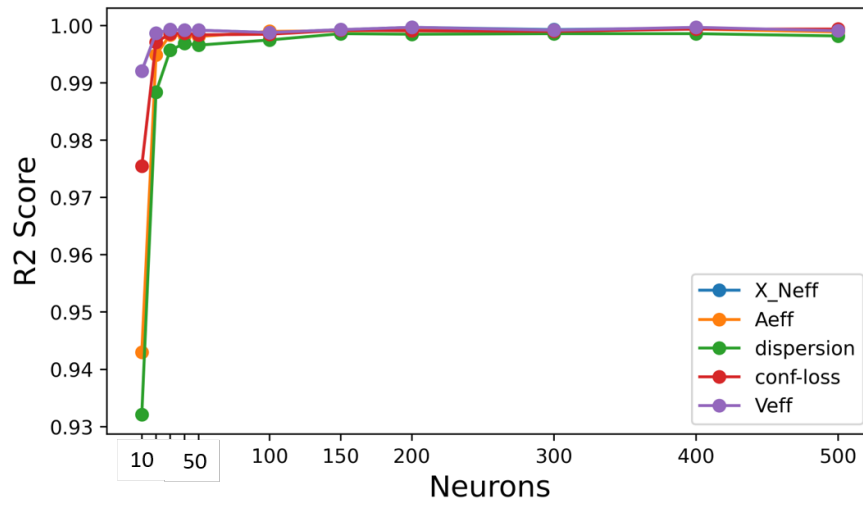


Figure 5.23: R-squared error for different neuron numbers for all optical properties of PCF.

Table 5.2: Average Accuracy of Different Neuron Counts

Neurons	n_{eff}	A_{eff}	Dispersion	Conf-Loss	V_{eff}	Avg. Accuracy
10	0.9921	0.943	0.9321	0.9755	0.9921	0.96696
20	0.9987	0.9949	0.9884	0.9971	0.9987	0.99556
30	0.9993	0.9984	0.9957	0.9986	0.9993	0.99826
40	0.9992	0.9982	0.9969	0.9987	0.9992	0.99824
50	0.9992	0.9981	0.9966	0.9984	0.9992	0.99830
100	0.9988	0.999	0.9975	0.9985	0.9988	0.99852
150	0.9993	0.9991	0.9986	0.9992	0.9993	0.99910
200	0.9997	0.9992	0.9985	0.9991	0.9997	0.99924
300	0.9999	0.9999	0.9995	0.9999	0.9999	0.99982
400	0.9996	0.9994	0.9986	0.9994	0.9997	0.99934
500	0.9991	0.9989	0.9982	0.9994	0.9991	0.99894

In this Table 5.2, we present the results of an experiment investigating the impact of varying the number of neurons in a neural network on the prediction accuracy of different parameters: n_{eff} , a_{eff} , Dispersion, Conf-Loss, and v_{eff} . The table has six rows, each corresponding to a different number of neurons: 10, 20, 30, 40, 50, and 300. Each row is assigned a unique color for easy identification. The table shows the prediction accuracy obtained for each parameter using a neural network with a specified number of neurons. An extra column on the right calculates the average accuracy across all parameters for each neuron count. Upon analyzing the table, it is evident that the neural network with 300 neurons provides the best average accuracy across all parameters. This suggests that increasing the number of neurons up to 300 improves prediction performance. However, further increases in neuron count may not yield significant im-

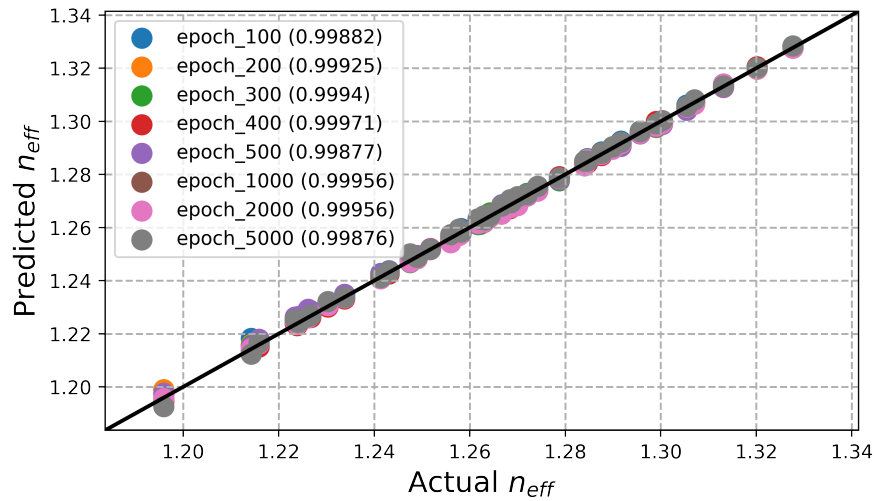


Figure 5.24: The scatter plot comparing predicted n_{eff} (y-axis) and actual n_{eff} (x-axis) for different epochs in the ANN against perfect linear relationship ($y=x$).

provements and could result in overfitting or increased computational complexity.

5.3.3 Epoch Tuning of ANN

Epoch tuning of artificial neural networks (ANN) involves selecting the optimal number of epochs, or training iterations, to use when training the model. The number of epochs is an important hyperparameter that can affect the accuracy and performance of the ANN.

5.3.3.1 Prediction of Effective Refractive Index

Figure 5.24 shows a scatter plot that compares the performance of neural network models trained with different numbers of epochs in predicting the effective refractive index (n_{eff}) values. The x-axis represents the actual n_{eff} values, while the y-axis shows the predicted n_{eff} values. The models have been trained for 100, 200, 300, 400, 500, 1000, 2000, and 5000 epochs, represented as individual scatter plots with distinct markers in the figure. The R² scores are shown in parentheses next to each corresponding label for the models. An error arises for every epoch whenever the effective refractive index is around 1.20. This is because of lesser data points in this area. After learning the behavior of data points, it performs well at the higher refractive index and close to the $y=x$ line.

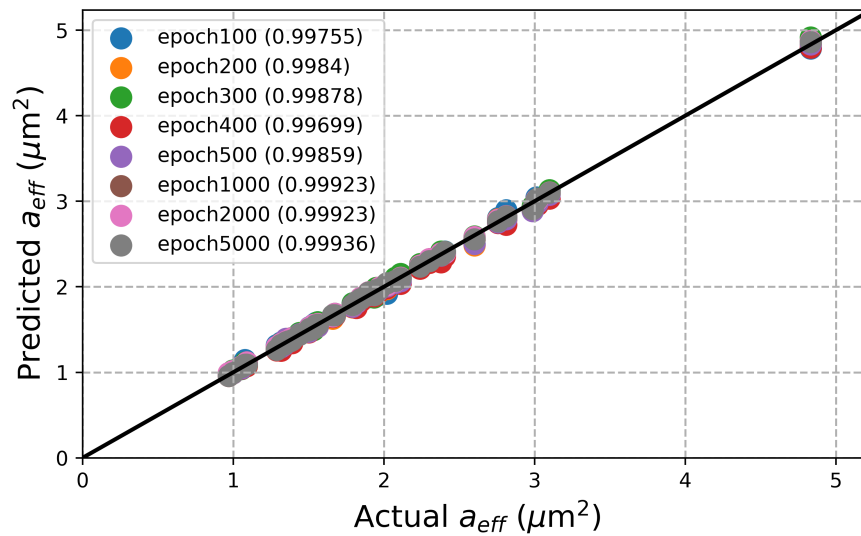


Figure 5.25: The scatter plot comparing predicted a_{eff} (y-axis) and actual a_{eff} (x-axis) for different epochs in the ANN against perfect linear relationship ($y=x$).

5.3.3.2 Prediction of Effective Mode Area

Figure 5.25 is a scatter plot illustrating the predictive performance of neural network models with varying numbers of training epochs for dispersion values. On the x-axis, the actual dispersion values are displayed, while the y-axis represents the predicted dispersion values. The R² score of models increases concerning the epochs. As epochs increase in a sequence from 100, 200, 300, 400, 500, 1000, 2000, to 5000, the R² score increases from 0.99755 to 0.99936. The R² scores for each model are displayed in brackets next to their respective labels. There have been fewer data in the range of $4-5 \times 10^{-12} \text{ m}^2$, the model learns less and gives more significant fluctuation from actual line ($y=x$).

5.3.3.3 Prediction of Dispersion

Figure 5.26 effectively demonstrates the impact of varying training epochs on the neural network models' capability to predict confocal loss values accurately. As the number of training epochs increases, the prediction accuracy improves linearly. The model learns effectively, given that the data covers the entire range of dispersion values. Consequently, increasing the number of epochs enhances the model's performance. The highest R² score, approximately 0.99891, is observed at 5000 epochs, while the lowest R² score, around 0.99526, occurs at 100 epochs, corroborating our earlier observation.

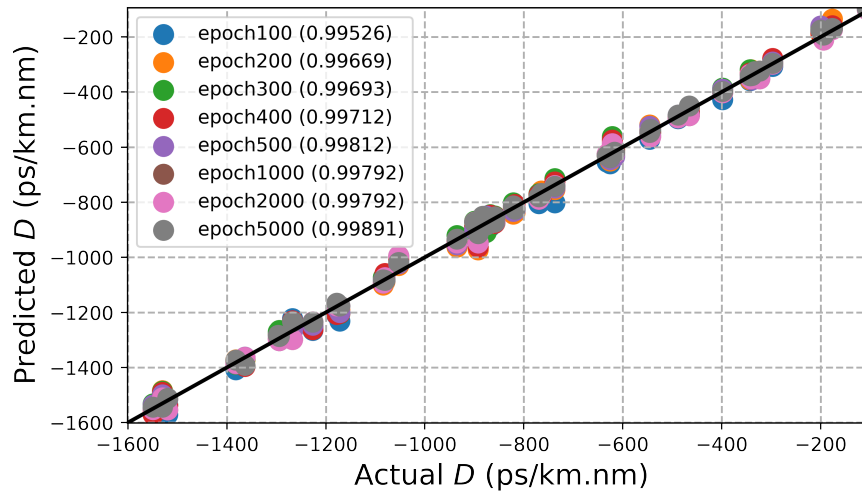


Figure 5.26: The scatter plot comparing predicted dispersion (D) (y-axis) and actual dispersion (D) (x-axis) for different epochs in the ANN against perfect linear relationship ($y=x$).

5.3.3.4 Prediction of Confinement Loss

Figure 5.27 demonstrate the effectiveness of epochs in predicting the optical properties of PCF. As the data points of the dataset widely cover the entire range of confinement evenly, the effect of epochs can be seen figure. The accuracy of the model increases with the number of epochs. The highest R2 score is observed with 5000 epochs. So decreasing the number of epochs also decreases the R2 score.

5.3.3.5 Prediction of V-parameter

Figure 5.28 displays a scatter plot comparing the predicted and actual V-parameter values. The solid black line represents the proper response. There are fewer data points in the range of 1.20 and the upper range from 1.32-1.34, causing the model's performance to decline in these areas. Due to a large amount of data in the middle range, the highest R2 score of 0.99968 is achieved at epoch 400. However, increasing the number of epochs leads to overfitting, decreasing the R2 score with another epic. Considering the various epochs examined, it can be generally concluded that the performance of the neural network model improves as the number of epochs increases. The distribution of data points within the dataset also influences the R2 score. To balance overfitting and underfitting, 5000 epochs have been chosen for constructing the optimal ANN model.

This Table 5.3 presents a comparative analysis of different neural network performance metrics across various epochs. The metrics included are n_{eff} , a_{eff} , Dispersion, Conf-Loss, and v_{eff} . Each table row represents a specific epoch (100, 200, 300, 400, 500,

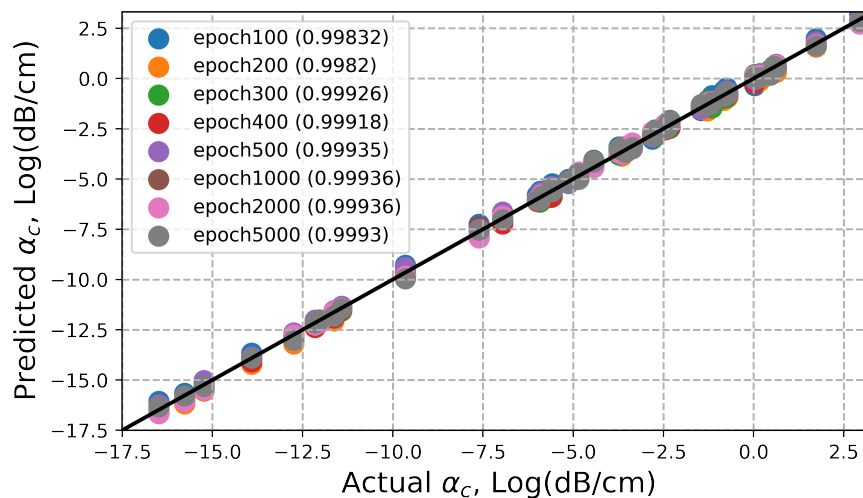


Figure 5.27: The scatter plot comparing predicted confinement loss(α_c) (y-axis) and actual confinement loss(α_c) (x-axis) for different epochs in the ANN against perfect linear relationship ($y=x$).

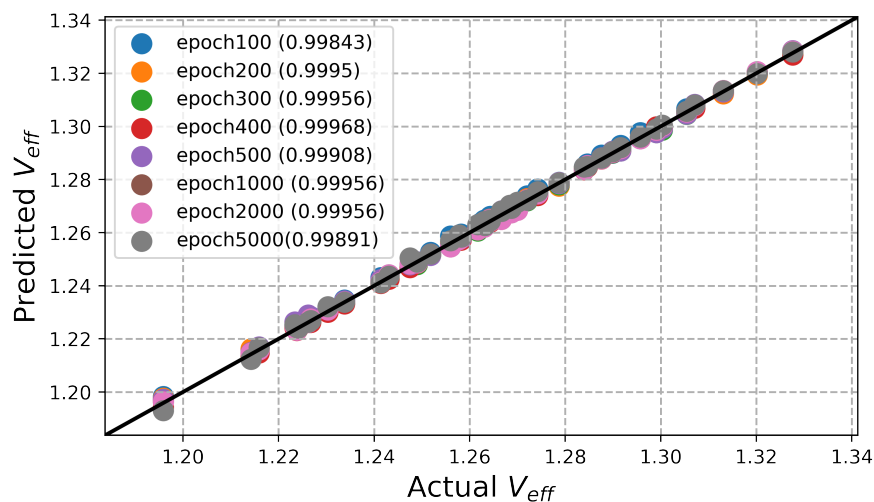


Figure 5.28: The scatter plot comparing predicted v_{eff} (y-axis) and actual v_{eff} (x-axis) for different epochs in the ANN against perfect linear relationship ($y=x$).

Table 5.3: Table of Metrics for Different Epochs

	neff	aeff	Dispersion	Conf-Loss	veff	Avg. Accuracy
Epoch 100	0.99882	0.99755	0.99526	0.99832	0.99843	0.99768
Epoch 200	0.99925	0.9984	0.99669	0.9982	0.9995	0.99841
Epoch 300	0.9994	0.99878	0.99693	0.99926	0.99956	0.99879
Epoch 400	0.99971	0.99699	0.99712	0.99918	0.99968	0.99854
Epoch 500	0.99877	0.99859	0.99812	0.99935	0.99908	0.99878
Epoch 1000	0.99956	0.99923	0.99792	0.99936	0.99956	0.99913
Epoch 2000	0.99756	0.9923	0.99792	0.99936	0.99956	0.99734
Epoch 5000	0.99876	0.99936	0.99891	0.9993	0.99891	0.99905

1000, 2000, and 5000), while each column presents the values for the respective performance metrics at that epoch. An additional column, "Avg. Accuracy," has been included to provide the average accuracy of all five metrics for each epoch. The table provides a comprehensive overview of the neural network's performance at different stages of training, allowing us to easily compare and evaluate the evolution of these metrics as the training progresses. This information can help understand how the network's performance changes over time and identify the optimal number of epochs for a specific problem.

5.3.4 Best Artificial Neural Network Model performance

The previous section of this chapter recommends tuning the hyperparameters of the ANN. Various parameters' influence on predicting optical properties' accuracy has been examined. The number of hidden layers varied from 2 to 5, with the highest R2 score obtained using two hidden layers. The neuron count for the first layer was optimized to 300 to achieve a balanced performance concerning all variables. The number of epochs was analyzed to obtain the highest R2 score. While more epochs result in higher accuracy, overfitting may occur; thus, 5000 epochs were considered a balanced choice. The optimal artificial neural network for this specific task was constructed based on these considerations for predicting optical properties. The network was then tested using a dataset that had not been previously provided.

5.3.4.1 Prediction of Effective Refractive Index

Figure 5.29 compares the actual values of the effective refractive index (n_{eff}) with the values predicted by the best neural network model. The plot has the wavelength (λ) on the x-axis and the effective refractive index (n_{eff}) on the y-axis. The actual values

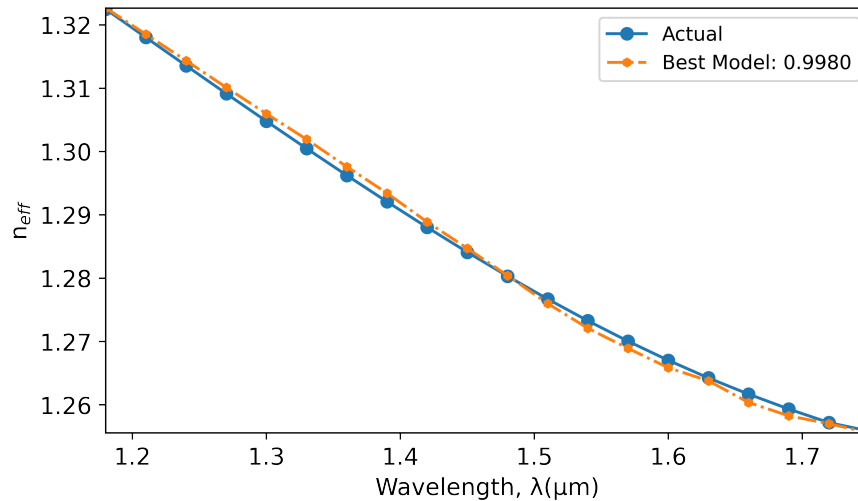


Figure 5.29: Evaluating the correspondence between the simulated n_{eff} and the predicted n_{eff} using best ANN model with an unexplored configuration.

are represented by solid markers connected by a solid line, while the best model's predictions are represented by hexagonal markers connected by a dashed line. The best model's R-square score, which measures how well the model's predictions fit the actual data, is 0.9980. This high score indicates that the model has accurately predicted the effective refractive index across the wavelength range. The plot visually supports this high accuracy, as the predicted values are close to the actual values across the entire wavelength range.

5.3.4.2 Prediction of Effective Mode Area

Figure 5.30 visually compares the actual effective mode area (A_{eff}) values with the predictions made by the best-performing neural network model for a range of wavelengths (λ). The x-axis represents the wavelength (in micrometers), while the y-axis represents the effective mode area (in square meters). The prediction accuracy for wavelengths ranges 1.6-1.7 μm is lower because the data points in this range are more scattered and exhibit weaker correlations. This graph depicts the data points as solid markers connected by a continuous line. On the other hand, the predictions from the best model are shown as hexagonal markers connected by a dashed line. The high R^2 score of 0.99796 signifies that the model's predictions align closely with the actual data, evident from the visual similarity between the two lines in the plot.

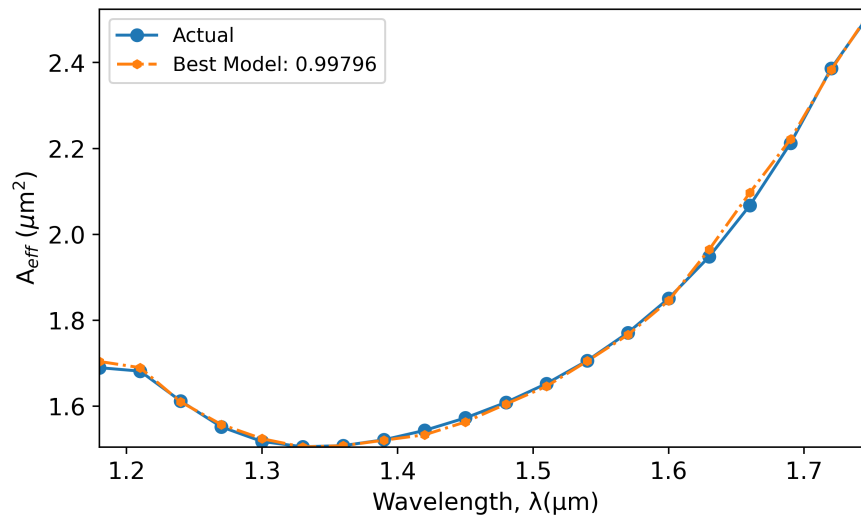


Figure 5.30: Evaluating the correspondence between the simulated a_{eff} and the predicted a_{eff} using best ANN model with an unexplored configuration.

5.3.4.3 Prediction of Dispersion

Figure 5.31 compares the actual chromatic dispersion (D) values to the predictions made by the best-performing neural network model across a range of wavelengths (λ). The x-axis represents the wavelength in micrometers (μm), while the y-axis represents the chromatic dispersion in picoseconds per kilometer-nanometer ($\text{ps}/(\text{km}\cdot\text{nm})$). The dispersion dataset has a cluster of data around $-1600 \text{ ps}/(\text{km}\cdot\text{nm})$. The ANN model's accuracy decreases when predicting dispersion values higher than $-1000 \text{ ps}/(\text{km}\cdot\text{nm})$ in the negative range. While the ANN model can accurately follow the actual values when the dispersion decreases, it struggles to achieve the same accuracy when the values increase from the negative maximum. The R-square score of 0.9965 indicates that the model's predictions agree with the actual data, as seen from the visual similarity of the two lines in the graph.

5.3.4.4 Prediction of Confinement loss

Figure 5.32 displays a comparison between the actual values and the best model's predictions concerning the relationship between wavelength (λ) and the logarithm of confinement loss (α_c) in dB/cm . The x-axis denotes the wavelength in micrometers (μm), spanning from 1.18 to 1.75 μm , while the y-axis represents the logarithm of confinement loss in dB/cm . The 'Best Model' curve, characterized by hexagonal markers and a dashed-dot line, illustrates the predictions made by the best model, boasting an accuracy of 0.9989. The model's training is suboptimal for wavelengths greater than 1.5

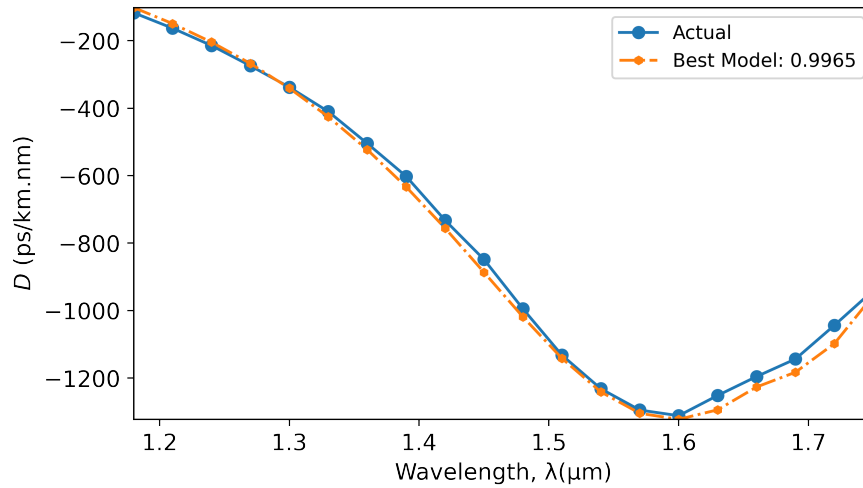


Figure 5.31: Evaluating the correspondence between the simulated dispersion (D) and the predicted dispersion (D) using the best ANN model with an unexplored configuration.

μm . This can be attributed to the irregular distribution of confinement data in the -2 to -6 dB/cm range.

5.3.4.5 Prediction of V-parameter

Figure 5.33 presents a comparison between the actual values and the best model's predictions for the relationship between wavelength (λ) and effective refractive index (v_{eff}). The x-axis represents the wavelength in micrometers (μm), ranging from 1.18 to 1.75 μm , while the y-axis displays the effective refractive index (v_{eff}).

A solid line with circular markers depicts the actual values, while a dashed-dot line with hexagonal markers represents the best model's predictions. The best model is associated with an accuracy of 0.9980. The plot demonstrates that the model's predictions closely follow the values across the entire wavelength range.

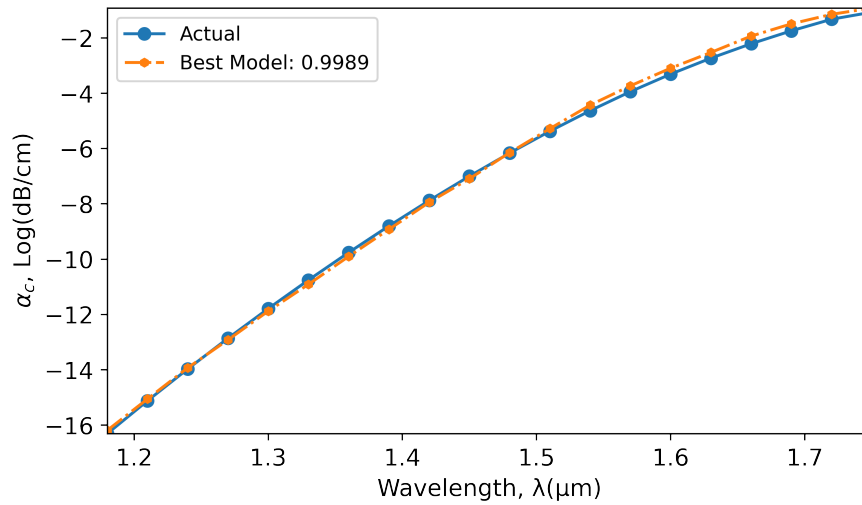


Figure 5.32: Evaluating the correspondence between the simulated confinement loss (α_c) and the predicted confinement loss (α_c) using best ANN model with an unexplored configuration.

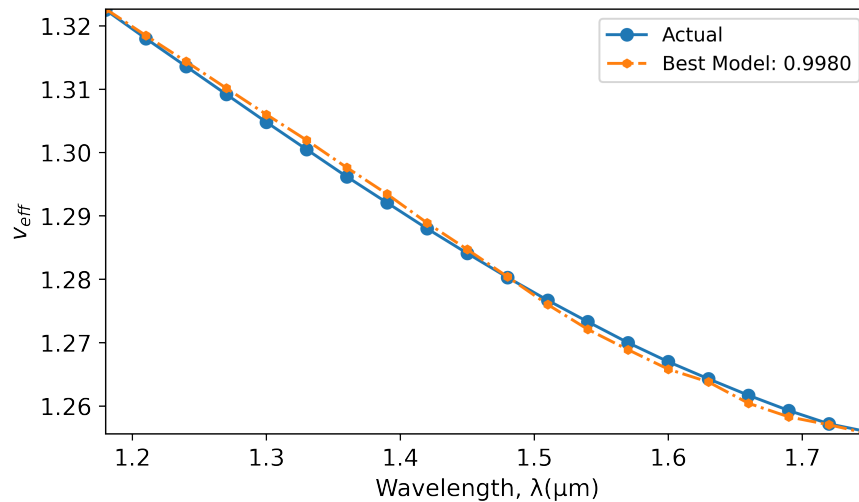


Figure 5.33: Evaluating the correspondence between the simulated v_{eff} and the predicted v_{eff} using best ANN model with an unexplored configuration.

5.3.5 Computational Time

Computation time is one of our evaluation metrics. The computing device has an Intel Core i5 12th generation processor with 8 GB of RAM and a 500 MB SSD. No graphics unit is used. Simulating a single optical property in COMSOL Multiphysics takes an average of 21 seconds in a normal mesh. The time taken increases dramatically as the mesh size increases. In a previous study, the training time of the ANN model was 20 seconds, and the testing time was five milliseconds[12]. Another study found that the

time taken for training and testing the ANN model is about 19 seconds and five milliseconds, respectively[13]. But using all of the proposed machine learning algorithms at a time, the training and testing are reduced to about 282 milliseconds and 30 milliseconds, respectively. An individual machine learning model's training and testing time is much less than the ANN as it requires fewer parameters and simpler operations. Thus, it saves us precious time by simulating with fewer computing resources. The proposed ANN model takes greater time than computation time is one of our evaluation metrics. The computing device has an Intel Core i5 12th generation processor () with 8 GB of RAM and a 500 MB SSD. No graphics unit is used. Simulating a single optical property in COMSOL Multiphysics takes an average of 21 seconds in a normal mesh. The time taken increases dramatically as the mesh size increases. In a previous study, the training time of the ANN model was 20 seconds, and the testing time was five milliseconds[12]. Another study found that the time taken for training and testing the ANN model is about 19 seconds and five milliseconds, respectively[13]. But using all of the proposed machine learning algorithms at a time, the training and testing are reduced to about 282 milliseconds and 30 milliseconds, respectively. An individual machine learning model's training and testing time is much less than the ANN as it requires fewer parameters and simpler operations. Thus, it saves us precious time by simulating with fewer computing resources. The ANN model takes around 15 seconds in training and five milliseconds in the testing phase.

Table 5.4: Comparison of computational time among simulations, previous method and proposed method

Simulation Details	Time Taken	
COMSOL Multiphysics (Normal Mesh)	21 Seconds	
COMSOL Multiphysics (Finer Mesh)	1 minute 27 seconds	
COMSOL Multiphysics (Extreme Fine Mesh)	2 minutes 33 seconds	
Models Details	Training Time	Testing Time
ANN model with 3 layers and 150 nodes[12] [56]	20 seconds	5 milli-seconds
ANN model with 2 layers and 130 nodes [57]	19 seconds	5 milli-seconds
Proposed all ML models at a time	282 milli-seconds	< 1 milli-seconds
Proposed ANN model with 2 layers and 300 nodes	15 seconds	5 milli-seconds

Table 5.4 compares computational time among simulations in a conventional way, the previously proposed ANN model, and proposed Machine Learning (ML) models and the ANN model.

5.4 Chapter Summary

In the results section, we presented the outcomes of our investigation on the optical properties prediction of negative dispersion-compensating photonic crystal fiber using machine learning. We demonstrated the effectiveness of our chosen machine learning algorithm in accurately predicting the dispersion properties of PCFs with varying cladding air hole dimensions and core sizes. By comparing the predicted values with those obtained through traditional simulation methods, we highlighted the significant reduction in computation time and resource utilization achieved through our machine learning approach. Moreover, our analysis revealed the impact of different cladding air hole dimensions and core sizes on the negative dispersion and other optical properties of the PCFs. This understanding allowed us to identify optimal design parameters that result in enhanced performance for various applications, such as dispersion compensation and supercontinuum generation in optical communication systems. Overall, our results confirmed the potential of machine learning algorithms in the efficient prediction and optimization of optical properties in negative dispersion-compensating photonic crystal fibers, providing valuable insights for the design and development of advanced optical communication systems.

Chapter 6

Conclusions

6.1 Conclusions

In this research, we have introduced an innovative photonic crystal fiber (PCF) design featuring one core hole and 152 cladding holes to attain a high negative dispersion value for dispersion compensation. Employing the full vector analysis method with Perfectly Matched Layer (PML) and examining the relative change of dispersion concerning the diameter of various cladding holes, we have conducted a thorough analysis. Our numerical results reveal that the proposed PCF achieves a minimum dispersion of approximately -1582.21 ps/(nm-km) within the 1.34 to 1.7 μm wavelength optical communication window, with a 0.8415 μm pitch in a linear manner. Increasing the size of air holes leads to higher dispersion up to -2065.2 ps/(nm-km), although it is not consistent across the entire wavelength window. The fabrication process is simplified due to the presence of circular air channels throughout the PCF. Owing to the high negative dispersion and low confinement loss, the proposed PCF is suitable for real-time optical communication systems.

Furthermore, we have implemented machine learning approaches to predict the optical properties of negative dispersion-compensating PCF. The computational time required for the proposed approaches is significantly less than conventional numerical simulations and previous ANN prediction models. Basic machine learning models demonstrate negligible training time in milliseconds, and testing time is comparable to real-time simulations with less than a one-millisecond delay. While the accuracy of predicting unknown parameters with given input features is sufficient, it is not as strong as the ANN model. The proposed ANN model, on the other hand, takes approximately 15 seconds for training and 5 milliseconds for testing. It offers the best average accuracy

at the cost of slightly higher computational time compared to basic models (Linear regression, KNN, Decision Tree, Random Forest). Depending on the application area, a trade-off between computational time and accuracy can be made. These machine learning techniques hold the potential for real-time scenarios with minimal computing resources and adequate accuracy in optical fiber communication. our soul contributions are:

- (i) We have developed a novel photonic crystal fiber (PCF) design with one core hole and 152 cladding holes, achieving a high negative dispersion value for dispersion compensation, making it suitable for real-time optical communication systems.
- (ii) Our thorough analysis using the full vector analysis method with PML has allowed us to understand the impact of cladding hole diameters on dispersion, resulting in a minimum dispersion of approximately -1582.21 ps/(nm-km) within the 1.34 to 1.7 μm wavelength optical communication window.
- (iii) We have successfully implemented machine learning approaches, including an ANN model, to predict the optical properties of negative dispersion-compensating photonic crystal fibers, providing a balance between computational time and accuracy, holding the potential for real-time scenarios with minimal computing resources in optical fiber communication.

6.2 Future Works

The future scope of this research encompasses several promising avenues for exploration and expansion. Some potential directions for future work include tuning machine learning parameters and extending the approach to solid-core or mixed PCF types with different air-hole orientations. Additionally, the methods developed in this study can be applied to biosensor or other applicable PCF structures to predict their optical characteristics. Further research can also aim to predict a wider range of optical properties, develop better designs with highly negative dispersion, and investigate the characteristics of other photonic devices, such as waveguides. By pursuing these avenues, future research can contribute to the development of more efficient and versatile optical communication systems and photonic devices.

References

- [1] J. C. Knight, J. Broeng, T. A. Birks, and P. S. J. Russell, "Photonic band gap guidance in optical fibers," *Science*, vol. 282, no. 5393, pp. 1476–1478, 1998.
- [2] T. Matsui, J. Zhou, K. Nakajima, and I. Sankawa, "Dispersion-flattened photonic crystal fiber with large effective area and low confinement loss," *Journal of Lightwave Technology*, vol. 23, no. 12, pp. 4178–4183, 2005.
- [3] C.-P. Yu and H.-C. Chang, "Applications of the finite difference mode solution method to photonic crystal structures," *Optical and Quantum Electronics*, vol. 36, pp. 145–163, 2004.
- [4] A. Cucinotta, S. Selleri, L. Vincetti, and M. Zoboli, "Holey fiber analysis through the finite-element method," *IEEE Photonics Technology Letters*, vol. 14, no. 11, pp. 1530–1532, 2002.
- [5] C. D. Poole, J. M. Wiesenfeld, D. J. Digiovanni, and A. M. Vengsarkar, "Optical fiber-based dispersion compensation using higher order modes near cutoff," *Journal of Lightwave Technology*, vol. 12, no. 10, pp. 1746–1758, 1994.
- [6] S. Ghalmi, S. Ramachandran, E. Monberg, Z. Wang, M. Yan, F. Dimarcello, W. Reed, P. Wisk, and J. Fleming, "Low-loss, all-fibre higher-order-mode dispersion compensators for lumped or multi-span compensation," *Electronics Letters*, vol. 38, no. 24, p. 1, 2002.
- [7] D. Garthe, R. Epworth, W. Lee, A. Hadjifotiou, C. Chew, T. Bricheno, A. Fielding, H. Rourke, S. Baker, K. Byron *et al.*, "Adjustable dispersion equaliser for 10 and 20 gbit/s over distances up to 160 km," *Electronics Letters*, vol. 30, no. 25, pp. 2159–2160, 1994.
- [8] J. Dugan, "All-optical fiber-based 1550 nm dispersion compensation in a 10 gb/s, 150 km transmission experiment over 1310 nm optimized fiber," in *Technical Digest of Optical Fiber Commun. Conf., San Jose, CA, Feb. 1992*, 1992.

- [9] E. Agrell, M. Karlsson, A. Chraplyvy, D. J. Richardson, P. M. Krummrich, P. Winzer, K. Roberts, J. K. Fischer, S. J. Savory, B. J. Eggleton *et al.*, “Roadmap of optical communications,” *Journal of Optics*, vol. 18, no. 6, p. 063002, 2016.
- [10] P. J. Winzer, D. T. Neilson, and A. R. Chraplyvy, “Fiber-optic transmission and networking: the previous 20 and the next 20 years,” *Optics express*, vol. 26, no. 18, pp. 24 190–24 239, 2018.
- [11] S. Tabassum, D. K. Sing, and M. Hassan, “Low confinement loss solid core rectangular photonic crystal fiber,” in *Optical and Wireless Technologies: Proceedings of OWT 2018*. Springer, 2020, pp. 271–277.
- [12] B. K. Paul, K. Ahmed, M. T. Rani, K. S. Pradeep, and F. A. Al-Zahrani, “Ultra-high negative dispersion compensating modified square shape photonic crystal fiber for optical broadband communication,” *Alexandria Engineering Journal*, vol. 61, no. 4, pp. 2799–2806, 2022.
- [13] M. De, R. K. Gangwar, and V. K. Singh, “Designing of highly birefringence, dispersion shifted decagonal photonic crystal fiber with low confinement loss,” *Photonics and Nanostructures-Fundamentals and Applications*, vol. 26, pp. 15–23, 2017.
- [14] S. Rana, A. S. Rakin, M. R. Hasan, M. S. Reza, R. Leonhardt, D. Abbott, and H. Subbaraman, “Low loss and flat dispersion kagome photonic crystal fiber in the terahertz regime,” *Optics Communications*, vol. 410, pp. 452–456, 2018.
- [15] W. Cai, E. Liu, B. Feng, H. Liu, Z. Wang, W. Xiao, T. Liang, S. Wang, J. Liu, and J. Liu, “Dispersion properties of a photonic quasi-crystal fiber with double cladding air holes,” *Optik*, vol. 127, no. 10, pp. 4438–4442, 2016.
- [16] R. Hao, Z. Li, G. Sun, L. Niu, and Y. Sun, “Analysis on photonic crystal fibers with circular air holes in elliptical configuration,” *Optical Fiber Technology*, vol. 19, no. 5, pp. 363–368, 2013.
- [17] Y. Zhu, H. Du, and R. Bise, “Design of solid-core microstructured optical fiber with steering-wheel air cladding for optimal evanescent-field sensing,” *Optics Express*, vol. 14, no. 8, pp. 3541–3546, 2006.
- [18] B. K. Paul, M. S. Islam, K. Ahmed, and S. Asaduzzaman, “Alcohol sensing over o+ e+ s+ c+ l+ u transmission band based on porous cored octagonal photonic crystal fiber,” *Photonic Sensors*, vol. 7, no. 2, pp. 123–130, 2017.

- [19] N. A. Mortensen, M. D. Nielsen, J. R. Folkenberg, C. Jakobsen, and H. R. Simonson, "Photonic crystal fiber with a hybrid honeycomb cladding," *Optics Express*, vol. 12, no. 3, pp. 468–472, 2004.
- [20] W. Su, S. Lou, H. Zou, and B. Han, "Design of a highly nonlinear twin bow-tie polymer photonic quasi-crystal fiber with high birefringence," *Infrared Physics & Technology*, vol. 63, pp. 62–68, 2014.
- [21] K. Ahmed, B. K. Paul, B. Vasudevan, A. N. Z. Rashed, R. Maheswar, I. Amiri, and P. Yupapin, "Design of d-shaped elliptical core photonic crystal fiber for blood plasma cell sensing application," *Results in Physics*, vol. 12, pp. 2021–2025, 2019.
- [22] M. F. Azman, W. R. Wong, M. H. Mhd. Abd. Cader, R. A. Aoni, G. A. Mahdiraji, and F. R. Mahamd Adikan, "Twin-core sunflower-type photonic quasicrystal fibers incorporated gold, silver, and copper microwire: an ultrashort and broad bandwidth polarization splitter," *Optical and Quantum Electronics*, vol. 51, pp. 1–17, 2019.
- [23] E. Chillce, C. M. d. B. Cordeiro, L. Barbosa, and C. B. Cruz, "Tellurite photonic crystal fiber made by a stack-and-draw technique," *Journal of Non-Crystalline Solids*, vol. 352, no. 32-35, pp. 3423–3428, 2006.
- [24] A. Ghanbari, A. Kashaninia, A. Sadr, and H. Saghaei, "Supercontinuum generation for optical coherence tomography using magnesium fluoride photonic crystal fiber," *Optik*, vol. 140, pp. 545–554, 2017.
- [25] X. Jiang, N. Y. Joly, M. A. Finger, F. Babic, M. Pang, R. Sopalla, M. H. Frosz, S. Poulain, M. Poulain, V. Cardin *et al.*, "Supercontinuum generation in zblan glass photonic crystal fiber with six nanobore cores," *Optics Letters*, vol. 41, no. 18, pp. 4245–4248, 2016.
- [26] M. Koshiba, "Wavelength division multiplexing and demultiplexing with photonic crystal waveguide couplers," *journal of Lightwave Technology*, vol. 19, no. 12, p. 1970, 2001.
- [27] M. N. Hossen, M. Ferdous, K. Ahmed, M. A. Khalek, S. Chakma, and B. K. Paul, "Single polarization photonic crystal fiber filter based on surface plasmon resonance," *Frontiers of Optoelectronics*, vol. 12, pp. 157–164, 2019.
- [28] P. Roy, P. Leproux, S. Février, D. Pagnoux, J.-L. Auguste, J.-M. Blondy, S. Hilaire, L. Lavoute, R. Jamier, A. Desfarges-Berthelemot *et al.*, "Photonic crystal fibres for lasers and amplifiers," *Comptes Rendus Physique*, vol. 7, no. 2, pp. 224–232, 2006.

- [29] A. Betlej, S. Suntsov, K. Makris, L. Jankovic, D. Christodoulides, G. Stegeman, J. Fini, R. Bise, and D. DiGiovanni, "All-optical switching and multifrequency generation in a dual-core photonic crystal fiber," *Optics Letters*, vol. 31, no. 10, pp. 1480–1482, 2006.
- [30] J. M. Dudley, G. Genty, and S. Coen, "Supercontinuum generation in photonic crystal fiber," *Reviews of Modern Physics*, vol. 78, no. 4, p. 1135, 2006.
- [31] D. Pristiniski and H. Du, "Solid-core photonic crystal fiber as a raman spectroscopy platform with a silica core as an internal reference," *Optics Letters*, vol. 31, no. 22, pp. 3246–3248, 2006.
- [32] S. Y. Ryu, H. Y. Choi, J. Na, E. Choi, G.-H. Yang, and B. H. Lee, "Optical coherence tomography implemented by photonic crystal fiber," *Optical and Quantum Electronics*, vol. 37, pp. 1191–1198, 2005.
- [33] Y. Liu, J. Yan, and G. Han, "Engineering chromatic dispersion and effective nonlinearity in a dual-slot waveguide," *Applied Optics*, vol. 53, no. 27, pp. 6302–6306, 2014.
- [34] D. Tee, M. A. Bakar, N. Tamchek, and F. M. Adikan, "Photonic crystal fiber for residual dispersion compensation over e+s+c+l+u wavelength bands," *IEEE Photonics Journal*, vol. 5, no. 3, pp. 7 200 607–7 200 607, 2013.
- [35] I. H. Malitson, "Interspecimen comparison of the refractive index of fused silica," *Josa*, vol. 55, no. 10, pp. 1205–1209, 1965.
- [36] S. K. Biswas, R. Arfin, Z. B. Zahir, A. B. Habib, R. Khan, M. R. Islam, S. A. B. Amir, and A. U. Alam, "Ultrahigh negative dispersion compensating hexagonal photonic crystal fiber with large nonlinearity," in *Micro-structured and Specialty Optical Fibres VII*, vol. 11773. SPIE, 2021, pp. 191–198.
- [37] M. S. Habib, R. Ahmad, M. S. Habib, and S. Razzak, "Maintaining single polarization and dispersion compensation with modified rectangular microstructure optical fiber," *Optik*, vol. 125, no. 15, pp. 4030–4034, 2014.
- [38] R. Saha, M. M. Hossain, M. E. Rahaman, and H. S. Mondal, "Design and analysis of high birefringence and nonlinearity with small confinement loss photonic crystal fiber," *Frontiers of Optoelectronics*, vol. 12, pp. 165–173, 2019.
- [39] M. Hasan, M. S. Habib, M. S. Habib, and S. A. Razzak, "Highly nonlinear and highly birefringent dispersion compensating photonic crystal fiber," *Optical Fiber Technology*, vol. 20, no. 1, pp. 32–38, 2014.

- [40] M. R. Hasan, M. A. Islam, A. A. Rifat, and M. I. Hasan, "A single-mode highly birefringent dispersion-compensating photonic crystal fiber using hybrid cladding," *Journal of Modern Optics*, vol. 64, no. 3, pp. 218–225, 2017.
- [41] M. S. Habib, M. S. Habib, S. A. Razzak, and M. A. Hossain, "Proposal for highly birefringent broadband dispersion compensating octagonal photonic crystal fiber," *Optical Fiber Technology*, vol. 19, no. 5, pp. 461–467, 2013.
- [42] S. G. Johnson and J. D. Joannopoulos, "Block-iterative frequency-domain methods for maxwell's equations in a planewave basis," *Optics Express*, vol. 8, no. 3, pp. 173–190, 2001.
- [43] S. Shi, C. Chen, and D. W. Prather, "Plane-wave expansion method for calculating band structure of photonic crystal slabs with perfectly matched layers," *JOSA A*, vol. 21, no. 9, pp. 1769–1775, 2004.
- [44] R. A. Norton and R. Scheichl, "Planewave expansion methods for photonic crystal fibres," *Applied Numerical Mathematics*, vol. 63, pp. 88–104, 2013.
- [45] N. Borhani, E. Kakkava, C. Moser, and D. Psaltis, "Learning to see through multimode fibers," *Optica*, vol. 5, no. 8, pp. 960–966, 2018.
- [46] J. Baxter, A. Calà Lesina, J.-M. Guay, A. Weck, P. Berini, and L. Ramunno, "Plasmonic colours predicted by deep learning," *Scientific reports*, vol. 9, no. 1, p. 8074, 2019.
- [47] W. Ma, F. Cheng, and Y. Liu, "Deep-learning-enabled on-demand design of chiral metamaterials," *ACS nano*, vol. 12, no. 6, pp. 6326–6334, 2018.
- [48] A. Tittl, A. John-Herpin, A. Leitis, E. R. Arvelo, and H. Altug, "Metasurface-based molecular biosensing aided by artificial intelligence," *Angewandte Chemie International Edition*, vol. 58, no. 42, pp. 14 810–14 822, 2019.
- [49] C. C. Nadell, B. Huang, J. M. Malof, and W. J. Padilla, "Deep learning for accelerated all-dielectric metasurface design," *Optics Express*, vol. 27, no. 20, pp. 27 523–27 535, 2019.
- [50] F. Musumeci, C. Rottondi, A. Nag, I. Macaluso, D. Zibar, M. Ruffini, and M. Tornatore, "An overview on application of machine learning techniques in optical networks," *IEEE Communications Surveys & Tutorials*, vol. 21, no. 2, pp. 1383–1408, 2018.

- [51] B. Karanov, M. Chagnon, F. Thouin, T. A. Eriksson, H. Bülow, D. Lavery, P. Bayvel, and L. Schmalen, “End-to-end deep learning of optical fiber communications,” *Journal of Lightwave Technology*, vol. 36, no. 20, pp. 4843–4855, 2018.
- [52] Y. Kiarashinejad, S. Abdollahramezani, M. Zandehshahvar, O. Hemmatyar, and A. Adibi, “Deep learning reveals underlying physics of light–matter interactions in nanophotonic devices,” *Advanced Theory and Simulations*, vol. 2, no. 9, p. 1900088, 2019.
- [53] Y. Kiarashinejad, M. Zandehshahvar, S. Abdollahramezani, O. Hemmatyar, R. Pourabolghasem, and A. Adibi, “Knowledge discovery in nanophotonics using geometric deep learning,” *Advanced Intelligent Systems*, vol. 2, no. 2, p. 1900132, 2020.
- [54] A. da Silva Ferreira, G. N. Malheiros-Silveira, and H. E. Hernández-Figueroa, “Computing optical properties of photonic crystals by using multilayer perceptron and extreme learning machine,” *Journal of Lightwave Technology*, vol. 36, no. 18, pp. 4066–4073, 2018.
- [55] T. Asano and S. Noda, “Optimization of photonic crystal nanocavities based on deep learning,” *Optics Express*, vol. 26, no. 25, pp. 32 704–32 717, 2018.
- [56] S. Chugh, A. Gulistan, S. Ghosh, and B. Rahman, “Machine learning approach for computing optical properties of a photonic crystal fiber,” *Optics Express*, vol. 27, no. 25, pp. 36 414–36 425, 2019.
- [57] H. Kumar, T. Jain, M. Sharma, and K. Kishor, “Neural network approach for faster optical properties predictions for different pcf designs,” in *Journal of Physics: Conference Series*, vol. 2070, no. 1. IOP Publishing, 2021, p. 012001.
- [58] T. Das, M. N. Hossen, S. M. Rahman, T. Parvin, K. Ahmed, and F. M. Bui, “Prepcf_ml: Prediction of photonic crystal fiber parameters using machine learning algorithms,” in *2022 Second International Conference on Advances in Electrical, Computing, Communication and Sustainable Technologies (ICAECT)*. IEEE, 2022, pp. 1–5.
- [59] H. Li, H. Chen, Y. Li, Q. Chen, X. Fan, S. Li, and M. Ma, “Prediction of the optical properties in photonic crystal fiber using support vector machine based on radial basis functions,” *Optik*, vol. 275, p. 170603, 2023.
- [60] A. K. Vyas and H. S. Dhiman, “Predication of negative dispersion for photonic crystal fiber using extreme learning machine,” *Journal of Optical Communications*, 2021.

- [61] F. Zolla, G. Renversez, A. Nicolet, B. Kuhlmeiy, S. R. Guenneau, and D. Felbacq, *Foundations of photonic crystal fibres*. World Scientific, 2005.
- [62] A. Bjarklev, J. Broeng, and A. S. Bjarklev, *Photonic crystal fibres*. Springer Science & Business Media, 2003.
- [63] B. Troia, A. Paolicelli, F. De Leonardis, and V. M. Passaro, “Photonic crystals for optical sensing: A review,” *Advances in Photonic Crystals*, pp. 241–295, 2013.
- [64] J.-P. Berenger, “A perfectly matched layer for the absorption of electromagnetic waves,” *Journal of Computational Physics*, vol. 114, no. 2, pp. 185–200, 1994.
- [65] J. Cohen, P. Cohen, S. G. West, and L. S. Aiken, *Applied multiple regression/correlation analysis for the behavioral sciences*. Routledge, 2013.
- [66] L. Hilary, “The historical development of the gauss linear model,” *Biometrika*, vol. 54, no. 1/2, pp. 1–24, 1967.
- [67] N. R. Draper and H. Smith, *Applied regression analysis*. John Wiley & Sons, 1998, vol. 326.
- [68] F. Camastra and A. Vinciarelli, *Machine learning for audio, image and video analysis: theory and applications*. Springer, 2015.
- [69] D. Von Winterfeldt and W. Edwards, “Decision analysis and behavioral research,” 1993.
- [70] Y. Singh and A. S. Chauhan, “Neural networks in data mining,” *Journal of Theoretical & Applied Information Technology*, vol. 5, no. 1, 2009.
- [71] S. Lau, “A walkthrough of convolutional neural network—hyperparameter tuning,” *Medium. Retrieved*, vol. 23, 2019.
- [72] A. Brahme, *Comprehensive biomedical physics*. Newnes, 2014.
- [73] V. Nair and G. E. Hinton, “Rectified linear units improve restricted boltzmann machines,” in *Proceedings of the 27th international conference on machine learning (ICML-10)*, 2010, pp. 807–814.
- [74] J. Han and C. Moraga, “The influence of the sigmoid function parameters on the speed of backpropagation learning,” in *From Natural to Artificial Neural Computation: International Workshop on Artificial Neural Networks Malaga-Torremolinos, Spain, June 7–9, 1995 Proceedings 3*. Springer, 1995, pp. 195–201.

- [75] W.-H. Steeb, *Nonlinear Workbook, The: Chaos, Fractals, Cellular Automata, Neural Networks, Genetic Algorithms, Fuzzy Logic With C++, Java, Symbolic++ And Reduce Programs*. World Scientific Publishing Company, 1999.
- [76] D. Ciregan, U. Meier, and J. Schmidhuber, “Multi-column deep neural networks for image classification,” in *2012 IEEE conference on computer vision and pattern recognition*. IEEE, 2012, pp. 3642–3649.
- [77] S. Alshahrani and E. Kapetanios, “Are deep learning approaches suitable for natural language processing?” in *Natural Language Processing and Information Systems: 21st International Conference on Applications of Natural Language to Information Systems, NLDB 2016, Salford, UK, June 22-24, 2016, Proceedings 21*. Springer, 2016, pp. 343–349.
- [78] O. B. Sezer, M. U. Gudelek, and A. M. Ozbayoglu, “Financial time series forecasting with deep learning: A systematic literature review: 2005–2019,” *Applied Soft Computing*, vol. 90, p. 106181, 2020.
- [79] P. Ramachandran, B. Zoph, and Q. V. Le, “Searching for activation functions,” *arXiv preprint arXiv:1710.05941*, 2017.
- [80] L. Hardesty, “Explained: neural networks,” *MIT News*, vol. 14, 2017.